ELECTROMAGNETIC GENERATION OF ACOUSTIC WAVES IN METALS; APPLICATIONS TO ULTRASONIC MEASUREMENTS

by

KENNETH RUSSELL LYALL

B.Sc., University of British Columbia, 1961
M.Sc., University of British Columbia, 1965

A DISSERTATION SUBMITTED IN PARTIAL FULFILLMENT
OF THE REQUIREMENTS FOR THE DEGREE OF
DOCTOR OF PHILOSOPHY

in the

Department of Physics

SIMON FRASER UNIVERSITY
June 1970

APPROVAL

Name: Kenneth Russell Lyall

Degree: Doctor of Philosophy

Title of Thesis: Electromagnetic Generation of Acoustic Waves in Metals; Applications to Ultrasonic Measurements

Examining Committee:

J. F. Cochran
Senior Supervisor

R. H. Enns
Examining Committee

D. J. Huntley
Examining Committee

E. A. Stern
External Examiner
Professor of Physics
University of Washington
Seattle, Washington

Date approved: 8 JUNE, 1970

ABSTRACT

The generation of radio-frequency acoustic waves within the skin layer of a metal in the presence of a static magnetic field has been studied in single-crystal plates of pure gallium. Acoustic resonances generated in this manner were detected as singularities in the surface impedance at those frequencies which satisfy the boundary conditions for the existence of standing sound waves in the plate. The amplitude, line-shape, and magnetic field dependence of these singularities are in quantitative agreement with the predictions of the phenomenological model of Turner, Lyall, and Cochran. This theory is applicable to all real metals, under certain conditions of frequency and magnetic field, and its results are discussed in relation to those detailed calculations which assume that the metal consists of a free-electron gas in an isotropic, positively-charged background.

The measurements were obtained using a radio-frequency bridge which is capable of measuring changes in the phase and amplitude of the surface impedance of a metal plate, with an amplitude uncertainty of ± 3%, and a phase-angle uncertainty of 1.5 degrees. This apparatus was calibrated at helium temperatures, and at frequencies between 5 MHz and 10 MHz.

Using the continuous-wave resonance technique, the velocities of ultrasound in single crystals of gallium were measured at 4.2°K, 77°K, and 273°K. From these measurements, the nine elastic constants of gallium were calculated. The Debye temperature calculated from the 4.2°K elastic constants, 328 ± 3.3°K, is in agreement with the value of 324.7 ± 2°K previously obtained from low-temperature specific heat data by Phillips.

The electromagnetic generation of acoustic waves is considered as a technique to obtain further information relating to the ultrasonic properties of metals. In particular, three types of measurements are discussed:

1. quantum oscillations in the ultrasonic attenuation and velocity;
2. small changes in the ultrasonic velocity;
3. absolute ultrasonic attenuation.

In each instance, data obtained using gallium single crystals are presented.

A description of an experiment in which the radio-frequency bridge was used to measure the normal and superconducting skin depths in polycrystalline plates of pure indium is included as an appendix.

TABLE OF CONTENTS

Page

LIST OF TABLES

LIST OF FIGURES

Figure Page

ACKNOWLEDGMENTS

I am fortunate to have enjoyed the enthusiastic supervision of Professor John Cochran, whose ideas, encouragement, and guidance have stimulated this research from its beginning. Thanks also to Messrs. Frank Wick and Walter Gloor for their invaluable technical help; to Miss Pat Goldberg for some of the gallium crystals; to Mr. Bob Turner, among other colleagues, for many helpful discussions; and to Mrs. Elsie Waite for typing the thesis. And finally to Barbara, who has made this endeavor both possible and worthwhile.

CHAPTER 1. INTRODUCTION

1.1 Historical perspective

Acoustic waves may be generated in a metal when an electromagnetic field is incident on its surface in the presence of a steady magnetic field. The existence of this phenomenon has been well-known for many years, and its origin has been correctly identified with the Lorentz force of the magnetic field acting on the rf current carriers in the metal. In 1939, for example, Randall, Ross, and Zener (1) used this "electromagnetic drive" to excite kilohertz-frequency longitudinal vibrations in brass rods. During the last three years there has been a revived interest in this effect, as is evidenced by the chronological bibliography given in Appendix I. Experimentally, the phenomenon presents a convenient source of phonons, with frequencies from kilohertz to gigahertz. Theoretically, an analysis of the electromagnetic generation of acoustic waves involves a treatment of the interaction between the electromagnetic and acoustic excitations in a metal.

At sufficiently large magnetic fields in an infinite uncompensated metal, lightly-damped, circularly-polarized electromagnetic waves called helicons may propagate in a direction parallel to the magnetic field (2). The electromagnetic-acoustic interaction was first investigated in terms of the coupling between these helicons and transverse acoustic waves, by Skobov and Kaner (3), Langenberg and Bok (4), and Quinn and Rodriguez (5). These workers considered the transport equations of the ions and of the electrons, coupled by their mutual electromagnetic interactions in an infinite metal. The resulting dispersion equation for the electon-ion system shows that the helicon-phonon coupling is strongest when the frequency and magnetic field are such that the linear acoustic dispersion curve and the quadratic helicon dispersion curve intersect, *i.e.*, in the regime where the acoustic and helicon phase velocities coincide. All of the above workers recognized the possibility of using electromagnetic excitation to generate transverse phonons (and vice versa) in this branch-crossing region. The predicted helicon-phonon interaction was first observed experimentally by Grimes and Buchsbaum (6) in potassium at a frequency of 30 MHz, and at fields between 50 and 100 kG.

In 1966-67 Gantmakher and Dolgopolov (7) and Larsen and Saermark (8) reported the observation of acoustic resonances in the surface impedance of metallic plates which were placed in a radio-frequency electromagnetic field, with a static magnetic field applied normally to the plate. This effect was observed in a field-frequency region far from that of the helicon-acoustic dispersion curve intersection. Following these experiments, Houck, *et.al.* (9) showed experimentally and theoretically that coupling between electromagnetic and transverse acoustic modes can occur near the surface of a metal in the presence of a perpendicular magnetic field, independently of helicon propagation. The exact form of this result, for free electrons, was given by Quinn (10), and the details of the derivation will be reproduced in the theoretical chapter of this thesis. The experiments of Houck, et.al. were extended by Betjamann and coworkers (11), who generated both longitudinal and transverse acoustic waves in metal rods, using different polarizations of radio-frequency excitation relative to the static magnetic field. Meredith, et.al. (12) presented further experimental results obtained with a magnetic field parallel, and perpendicular to the surface, and showed theoretically that the generation of longitudinal acoustic waves is to be expected when the magnetic field lies in the plane of the surface.(*)

More recently, Turner, Lyall and Cochran (17) have shown that for conditions of frequency and magnetic field which are appropriate to most of the experiments mentioned above, the electromagnetic generation of acoustic waves at the surface of a metal may be quantitatively predicted by means of a purely phenomenological argument. These authors have considered the geometry which is approximated in the common experimental

---

(*) In these theoretical treatments, no momentum transfer from the electrons to the lattice at the surface is considered. At frequencies above 1 GHz, however, the diffuse nature of the surface scattering apparently provides an important driving force on the lattice (13), and strong electromagnetic-acoustic coupling exists in the absence of a static magnetic field. This case, which will not be discussed further in this thesis, has been investigated experimentally by Abeles (14) and by Weisbarth (15), and theoretically by Abeles (14), Southgate (13), and Cohen (16).

configuration of a metal plate contained in an rf solenoid (7,8,18), and have calculated the effect of the generated acoustic waves on the surface impedance of the plate (*). The phenomenological argument does not rely on any microscopic model of the metal, but is valid for all real metals in the limit where the radio-frequency electric currents are confined to a distance near the surface that is small compared to the wavelength of sound.

While this theory yielded expressions which could easily be compared with empirical results, none of the experiments discussed above produced a quantitative measurement of the conversion efficiency of electromagnetic to acoustic energy. Presented in this thesis are quantitative results, obtained using single crystalline plates of pure gallium, which are in agreement with the predictions of the physical model of Turner, Lyall and Cochran. Several applications of this effect as a technique to investigate the ultrasonic properties of metals are considered in detail.

1.2 Contributions to this thesis

The contributions to this thesis are best presented within the framework of the remaining chapters:

(*) A complex microscopic theory for this geometry has been given by Kravchenko (19).

Chapter 2

The phenomenological model (17) for the electromagnetic generation of acoustic waves is presented in detail, and its results are compared with the microscopic theories of Quinn (10) and of Kravchenko (19). The different approaches are found to be in agreement, under certain restrictions for the frequency and magnetic field.

Chapter 3

A radio-frequency bridge, designed to measure absolute changes in the surface resistance and surface reactance of metal plates, is described. The bridge is calibrated at 4°K, and at frequencies between 5 MHz and 10 MHz.

Chapter 4

The first quantitative measurements of the electromagnetic generation of acoustic waves in metals are presented. These measurements are of the singularities in the surface resistance and reactance due to acoustic resonances in single-crystal plates of pure gallium. The experimental results are found to be in quantitative agreement with the theoretical predictions of the phenomenological model presented in Chapter 2.

Chapter 5

Assuming that the surface impedance singularities occur at frequencies which yield acoustic velocities equivalent to the ordinary ultrasonic velocities in a bulk metal, the nine elastic constants of gallium at 4.2°K, 77°K and 273°K are calculated. The uncertainty in the measured velocities is estimated to be ± 0.3%. A discussion of this uncertainty, and of the above assumption, is given. The Debye temperature calculated from the 4.2° elastic constants is in good agreement with that obtained from low temperature specific heat measurements (20). The only values of the elastic constants of gallium previously reported are those of Roughton and Nash (21) at 273°K, which are in disagreement with the results presented in this thesis.

Chapter 6

The electromagnetic generation of acoustic waves is considered as a technique to obtain further information related to the ultrasonic properties of metals. In particular, three types of measurements are discussed:

(a) quantum oscillations in the ultrasonic attenuation and velocity;

(b) small changes in the ultrasonic velocity;

(c) absolute ultrasonic attenuation.

In each instance, data obtained using gallium single crystals are presented.

CHAPTER 2. ELECTROMAGNETIC GENERATION OF ACOUSTIC WAVES - THEORY

2.1 Introduction

In this chapter, the theoretical basis for the electromagnetic generation of acoustic waves in a metal in the presence of a magnetic field is presented. A phenomenological model (17) is discussed in detail in section 2, and the limits of its applicability are examined. This model assumes that the acoustic wave generation is due entirely to the Lorentz force of the magnetic field acting on the current carriers in the skin depth of the metal. Expressions are derived for the acoustic resonance singularities which appear in the frequency spectrum of the surface impedance of an infinite metal plate which is immersed in a uniform radio-frequency magnetic field. In section 3 the microscopic treatments of Quinn (10) and Kravchenko (19) are considered. The theory of Quinn, which has also been discussed by Meredith, et.al. (12), is reproduced in some detail, as an example of this approach. It is shown that for ordinary metals at low megahertz frequencies and magnetic fields of the order of 10^4 gauss, the Quinn and Kravchenko results may be reduced to expressions that can easily be obtained by means of the simple physical argument of section 2.

2.2 Phenomenological model

2.2.1 Semi-infinite metal

Consider the geometry of Fig. 2-1. An electromagnetic plane wave of angular frequency ω, linearly polarized with the magnetic vector along the y-axis, is incident normally on the surface of a semi-infinite metal. A skin current density, $\vec{j}_s(z)$, flows within a distance Δ of the surface and shields the interior of the metal from the external electromagnetic field. A static magnetic field $\vec{B}_0$ is applied to the metal, at an arbitrary angle to the surface.

The Lorentz force density acting on the current carriers in the skin layer is (*)

$$\vec{F}(z) = \frac{1}{c}\left(\vec{J}_s(z) \times \vec{B}_0\right) \qquad \text{dyne-cm}^{-3}, \qquad [1]$$

and, if the spatial distribution of $\vec{j}_s(z)$ may be approximated by a Dirac delta-function $\delta(z)$ at the surface, we can write:

$$\vec{F}(z) = \frac{1}{c}\left(\vec{I}_0 \times \vec{B}_0\right)\delta(z) \qquad \text{dyne-cm}^{-3}, \qquad [2]$$

where

$$\vec{I}_0 = \int_0^\infty \vec{J}_s(z)\, dz \qquad \text{statamp-cm}^{-1}. \qquad [3]$$

According to Maxwell's equations, the rf magnetic field that

(*) Throughout this thesis we use the Gaussian (cgs) system of units.

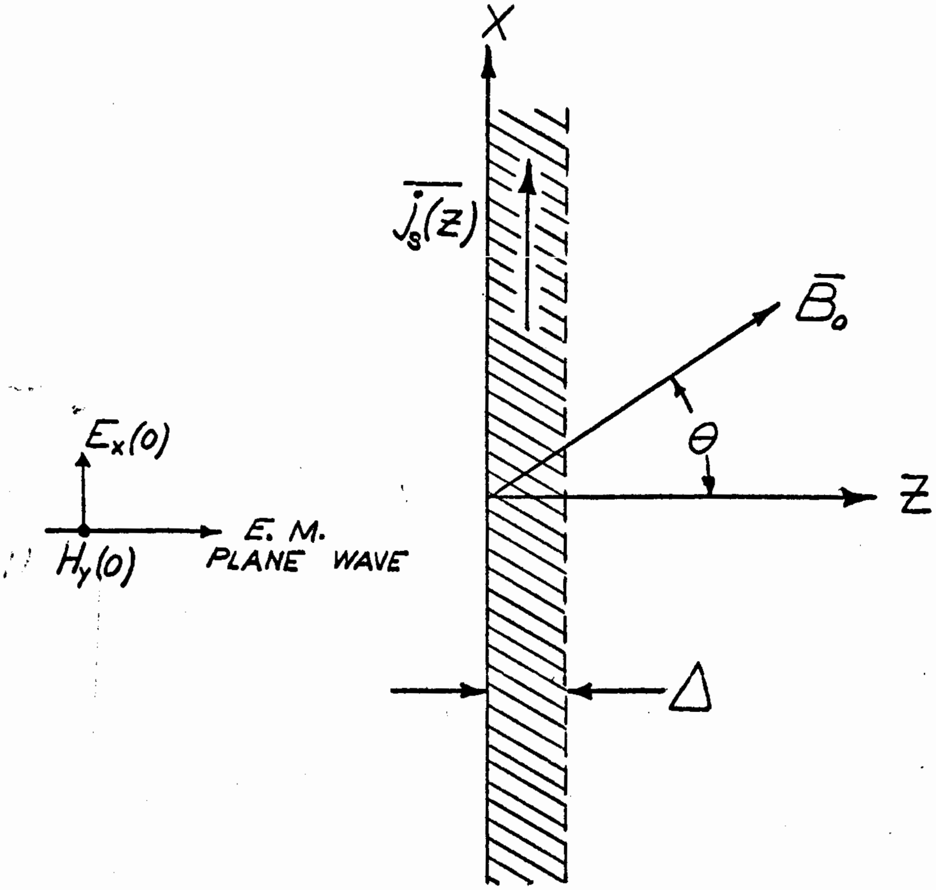

FIG. 2-1. GEOMETRY USED TO DISCUSS THE GENERATION OF AN ACOUSTIC WAVE AT THE SURFACE OF A METAL.

is applied to the surface of a semi-infinite metal is attenuated as one moves into the metal. The interior rf magnetic field, which approaches zero at depths larger than $\sim \Delta$, is the sum of the magnetic field applied to the surface and that due to the current flowing in the surface layer, Δ. It is clear, then, that the magnitude and direction of the integrated surface current $\vec{I}_0$ is fixed by the rf magnetic field applied to the surface. The relation which results from Maxwell's equation is

$$I_0 = \frac{c}{4\pi} H(0) \quad \text{statamp-cm}^{-1}, \qquad [4]$$

where we have neglected the displacement current in comparison to the conduction current in the metal. This general result shows that the direction and magnitude of the integrated surface current are determined solely by the geometry of the experiment, and are not dependent upon the static field, $\vec{B}_0$. The Lorentz force acting on the electrons must therefore be balanced by an equal and opposite force due to interactions with the lattice. From this physical argument we conclude that the Lorentz force on the electrons is communicated to the lattice, and that it provides the driving mechanism for the generation of acoustic waves in the metal. If the acoustic wavelength is much larger than Δ, it is clear that the exact distribution of force on the lattice over the distance Δ is unimportant, and [2] can be used to calculate the amplitude and phase of the acoustic wave which is generated. If and only if the plate normal lies along a high symmetry axis in the crystal, pure acoustic modes will propagate in this direction. These waves will be longitudinal when $\vec{B}_0$ lies in the plane of the specimen and transverse when $\vec{B}_0$ lies in the plane defined by the rf current and the surface normal; in all other cases, both longitudinal and transverse waves will be generated.

The equation of motion for the lattice may now be written, assuming that only the driving force [2] is important. For an elastically isotropic material, neglecting acoustic damping:

$$\frac{d^2\vec{\xi}(z)}{dt^2} = S_\ell^2\, \vec{\nabla}(\vec{\nabla}\cdot\vec{\xi}(z)) - S_t^2\, \vec{\nabla}\times(\vec{\nabla}\times\vec{\xi}(z)) + \frac{\vec{I}_0\times\vec{B}_0}{\rho c}\,\delta(z), \qquad [5]$$

where S_ℓ and S_t are the acoustic velocities for longitudinal and transverse waves, ρ is the density of the metal, and $\vec{\xi}(z)$ is the displacement of the lattice from its equilibrium position.

2.2.2 Unbounded metal plate

This phenomenological approach for a semi-infinite metal may easily be extended to the case of a metal plate of thickness d, and of infinite extent. We assume that the plate is immersed in a spatially uniform rf magnetic field. This is approximated experimentally by placing a metal plate within a long rf solenoid, whose axis lies in the plane of the plate. The rf electric fields at the plate surfaces $z = 0$ and $z = d$ are then $E_x(0) = -E_x(d)$. This result may be understood as follows: by symmetry, the electric fields at the two surfaces must be equal in magnitude, and in order to screen the externally applied rf magnetic field from the interior of the plate, the skin currents at the two surfaces must be equal in magnitude but opposite in direction. Consequently, $E_x(0) = -E_x(d)$. For simplicity, we also assume that the static magnetic field is applied in the plane perpendicular to the coil axis, at an angle θ to the plate normal (Fig. 2-1). With this geometry, if the metal is isotropic, or if the y-axis coincides with a principle axis of the sound velocity tensor, pure transverse acoustic waves are generated in the plate. The Lorentz force density is given by:

$$F_y(z) = -\frac{I_0 B_0}{c} \cos\theta \left[\delta(z) - \delta(z-d)\right] \quad \text{dyne-cm}^{-3} \qquad [6]$$

The acoustic equation of motion may then be written

$$\frac{d^2 \xi_y(z)}{dt^2} = S_t^2 \frac{d^2 \xi_y(z)}{dz^2} - \gamma \frac{d\xi_y(z)}{dt} - \frac{I_0 B_0 \cos\theta}{\rho c}\left[\delta(z) - \delta(z-d)\right], \qquad [7]$$

where all acoustic attenuation mechanisms in the metal have been represented by a damping force density,

$$F_D = -\gamma\rho \frac{d\xi_y}{dt} \quad \text{dyne-cm}^{-3}. \qquad [8]$$

The acoustic amplitude attenuation coefficient is given by $\alpha = \gamma/(2S_t)$ cm^{-1}. Changes of the ultrasonic attenuation (and velocity) as a function of magnetic field strength are of course not included in this treatment.

Equation [7] can be solved by means of the Fourier cosine series. Let

$$\xi_y(z) = \sum_{m=1}^{\infty} A_m \cos\frac{m\pi z}{d},$$

where m is an integer. Then, assuming an $e^{-i\omega t}$ time variation for $\xi_y(z)$,

$$\sum_{m=1}^{\infty} \left[\omega^2 - \left(\frac{m\pi S_t}{d}\right)^2 + i\omega\gamma\right] A_m \cos\frac{m\pi z}{d} = \frac{I_0 B_0 \cos\theta}{\rho c}\left[\delta(z) - \delta(z-d)\right].$$

Multiplying by $\cos(n\pi z/d)$, and integrating from 0 to d:

$$\left[\omega^2 - \left(\frac{n\pi S_t}{d}\right)^2 + i\omega\gamma\right] A_n \frac{d}{2} = \frac{I_0 B_0 \cos\theta}{\rho c}\left[1 - \cos n\pi\right]$$

$$\therefore A_n = \frac{2 I_0 B_0 \cos\theta}{c d \rho} \frac{(1-\cos n\pi)}{(\omega^2 - \omega_n^2 + i\omega\gamma)}$$

where $\omega_n = n\pi S_t/d$, and the solution for the ion displacement is

$$\xi_y(z,t) = \frac{2 I_0 B_0 \cos\theta}{c d \rho}\left\{\sum_{n=1}^{\infty} \frac{(1-\cos n\pi)(\cos\frac{\omega_n z}{S_t})}{(\omega^2 - \omega_n^2 + i\omega\gamma)}\right\} e^{-i\omega t}. \qquad [9]$$

We now consider the singularities in the surface impedance, or skin depth, which are associated with the acoustic resonances in the plate described by [9]. This requires a calculation of the electric field that is set up within the metal, due to the passage of the acoustic wave and the presence of $\vec{B}_0$. For this calculation, we assume that the ion currents due to the acoustic wave are completely screened by the electrons, <u>i.e.</u>, no net currents flow within the metal, apart from the skin current. The total current in the interior of the metal is the sum of the ion current, $\vec{j}_i(z) = n_0 e\dot{\vec{\xi}}(z)$, and the electron current, $\vec{j}_e(z) = -n_0 e\vec{v}(z)$, where n_0 is the density of conduction electrons, with charge (-e), and $\vec{v}$ is the electron velocity. The assumption of total screening, then, may be written

$$\vec{v} = \dot{\vec{\xi}}\,.$$

The validity of this assumption will be considered in section 2.2.3.

The electrons are moving in the presence of a magnetic field, and hence they experience a Lorentz force,

$$\vec{F}(z) = -\frac{e\,\dot{\vec{\xi}}(z) \times \vec{B}_0}{c}\,.$$

Because of the assumption of complete screening, this force must be balanced by a force due to an electric field which is set up in the metal;

$$\Delta\vec{E}(z) = -\frac{\dot{\vec{\xi}}(z) \times \vec{B}_0}{c} . \qquad [10]$$

In the geometry which has been assumed, the x-component of this electric field at the surfaces of the plate,

$$\Delta E_x(0) = -\frac{\dot{\xi}_y(0)\, B_0 \cos\theta}{c} , \qquad [11]$$

will alter the surface impedance Z, which is the quantity that is measured in our experiments. The surface impedance is determined by the total electric field at the surface,

$$Z = \frac{E_x(0) + \Delta E_x(0)}{I_0} = Z_0 + \Delta Z , \qquad [12]$$

where Z_0 is the surface impedance in the absence of acoustic waves, and ΔZ is the acoustic contribution. Finally, equations [9], [11], and [12] may be combined to yield the acoustic contribution to the surface impedance of one face of an infinite metal plate: (*)

$$\Delta Z = \left(\frac{2i\omega}{\rho d}\right) \frac{B_0^2 \cos^2\theta}{c^2} \sum_{n=1}^{\infty} \frac{(1-\cos n\pi)}{(\omega^2-\omega_n^2+i\omega\gamma)} = \Delta R - i\Delta X . \qquad [13]$$

R and X are the surface resistance and reactance. Using

(*) Hereafter, when we refer to changes in the surface impedance, or skin depth of a plate, we mean the contribution from only one side. The total change, accounting for both faces, will be twice this value.

the formal definition for the complex skin depth in a semi-infinite metal,

$$\delta = \frac{1}{H(0)}\int_0^{\infty} H(z)\,dz = -\frac{c^2}{4\pi i\omega}Z = \delta_X + i\delta_R\,, \qquad [14]$$

we can rewrite equation [13], for the acoustic contribution to the skin depth;

$$\Delta\delta = -\frac{B_0^2\cos^2\theta}{2\pi\rho d}\sum_{n=1}^{\infty}\frac{(1-\cos n\pi)}{(\omega^2-\omega_n^2+i\omega\gamma)}\,. \qquad [15]$$

These expressions have been derived for $\vec{B}_0$ perpendicular to the rf coil axis ($\vec{B}_0$ in the plane of Fig. 2-1), and in this case, the generated acoustic waves are transverse. When the magnetic field lies in the plane of the plate, longitudinal waves are generated. The derived expressions are then identical to [13] and [15], but θ is the angle between $\vec{B}_0$ and the rf skin current. When the magnetic field lies in neither of these two planes, both transverse and longitudinal waves are generated, and two terms must be included in the above expressions.

2.2.3 Validity of the electron screening assumption

To complete the discussion of the phenomenological model, we must examine the validity of the assumptions that have been made in the above derivation. We first consider, for simplicity, transverse waves propagating parallel to $\vec{B}_0$ in the interior of the metal. The propagation vector is in the z-direction, and the lattice displacement is along y. In arriving at expression [10] for the transverse electric field, $\Delta E_x(z)$, which is set up in the metal, it was assumed as a first approximation that the total transverse current $j_x(z)$ was zero. There is such a current required, however, to generate the rf field, $\Delta E_x(z)$. The magnitude of this current can be calculated from Maxwell's equations and equation [10]:

$$\frac{d^2(\Delta E_x(z))}{dz^2} = -\frac{4\pi i\omega j_x(z)}{c^2} \qquad [16]$$

$$j_x(z) = \frac{cq^2\xi_y(z)B_0}{4\pi} .$$

$\vec{q}$ is the wave vector of the electromagnetic excitation in the metal. It is this rf Hall current which in turn interacts with $\vec{B}_0$ to produce a force proportional to B_0^2 in the y-direction which gives rise to a slight change in the elastic constants, and hence a change in the sound velocity in the metal (*).

The ratio of $j_x(z)$ to the ion current $j_i(z) = n_0 e\dot{\xi}_y(z)$ is

$$\left|\frac{j_x(z)}{j_i(z)}\right| = \left(\frac{c}{S_t}\right)^2 \frac{\omega}{4\pi}\left(\frac{B_0}{n_0 ec}\right) , \qquad [17]$$

and our assumption that the total currents in the metal are negligible requires this term to be much less than unity.

(*) See section 6.2.

For a typical metal having $n_0 = 10^{23}$ (*) electrons/cm^3, and $S_t = 3 \times 10^5$ cm-sec^{-1},

$$\left(\frac{c}{S_t}\right)^2 \frac{\omega}{4\pi}\left(\frac{B_0}{n_0 ec}\right) \cong 5 \times 10^{-16} \; \omega B_0 \quad .$$

At frequencies up to 10 MHz and fields to 20 kG, as in our experiments, this term is small, and the rf Hall current may be neglected.

The value of $j_x(z)$ given by [16] can now be used in a second approximation to demonstrate that the next order term $\Delta E_x'(z)$, which must be added to $\Delta E_x(z)$ in equation [10], is small:

$$|\Delta E_x'(z)| = \frac{|j_x(z)|}{\sigma_{eff}} \; ,$$

and

$$\frac{|\Delta E_x'(z)|}{|\Delta E_x(z)|} = 8\pi^2\left(\frac{\delta_{eff}}{\lambda_s}\right)^2 , \qquad [18]$$

where σ_{eff} is the appropriate conductivity in the presence of a magnetic field, and $\delta^2_{eff} = c^2/(8\pi\omega\sigma_{eff})$. Thus [10] is the correct expression for the transverse electric field that arises due to the passage of the acoustic wave, if the wavelength of sound is much larger than the parameter δ_{eff}, which

---

(*) Note that $n_0 = Nz$, where N is the ion number density, and z is the ion valence. n_0 is not the effective number of charge carriers which is obtained from the Hall constant.

can be closely identified with the skin depth of the metal. This condition is similar to the one which supports the delta-function approximation of equation [2]. For a typical metal at a frequency of 5 MHz, with $\sigma_0 = 10^5\ \Omega^{-1}\ \mathrm{cm}^{-1} = 9 \times 10^{16}$ e.s.u. at $T = 300°K$, $S_t = 3 \times 10^5$ cm-sec^{-1}, $\delta_0/\lambda_s \cong 0.06$, and this factor will be reduced as much as 10^2 at helium temperatures. A similar argument and result apply to the transverse current which is set up when longitudinal waves are propagating perpendicular to the magnetic field.

The components of total current along the directions of ion displacement have been considered in reference (17).(*) It is demonstrated there that (1) for transverse waves this current is small if $\Delta/\lambda_s << 1$, where Δ is a measure of the depth of penetration of the surface currents into the metal, and (2) that longitudinal screening is effectively complete for all longitudinal modes which can propagate in the metal. The first of these results is easily understood qualitatively, since the ordinary skin depth provides a measure of the shortest transverse wavelength which may be screened by the electrons. The second result follows because the electrons must move with the lattice to maintain local charge neutrality in the metal.

(*) Note that reference (17) contains a misprint: on page 2300, column 2, line 23, "shorter" should read "longer".

It may be concluded, then, that the validity of the phenomenological theory of the generation of acoustic waves at the surface of a metal is subject to two conditions:

1. $\left(\frac{c}{S_t}\right)^2 \frac{\omega}{4\pi}\left(\frac{B_0}{n_0 ec}\right) \ll 1$. [19]

2. $\frac{\Delta}{\lambda_s} \ll 1$. [20]

This model predicts the size and shape of the singularities which appear in the surface impedance of a metal plate as a result of acoustic resonances which are generated in the plate. It does not, of course, give the magnetic field dependence of the acoustic velocity and attenuation, for which a full analysis of the coupled ion and electron transport equations is required.

2.3 Microscopic theory

2.3.1 Semi-infinite metal, free electrons

As an example of the microscopic approach to the electromagnetic-acoustic coupling problem in a metal, we outline in this section the formulation given by Quinn (10). This theory is based on a model used by Cohen, Harrison, and Harrison (22), and by Rodriguez (23): the metal consists of a free-electron gas embedded in an isotropic background of positive ions which is able to support longitudinal and shear acoustic waves. We refer again to Fig. 2-1, where an electromagnetic wave with time variation $e^{-i\omega t}$ (*) is incident normally on the surface of the metal, which occupies the half-space, $z > 0$. The static magnetic field $\vec{B}_0$ is assumed to lie perpendicularly to the surface. For this geometry, and for frequencies much less than the plasma frequency, only the transverse rf fields $E_{x,y}(z)$ and $H_{x,y}(z)$ need be considered in the metal, and the circular polarization notation will be used throughout this section, e.g.:

$$\begin{aligned} E_\pm(z) &= E_x(z) \pm i E_y(z) , \\ H_\pm(z) &= H_x(z) \pm i H_y(z) , \quad \text{etc.} \end{aligned} \qquad [21]$$

The problem to be solved is to calculate the response of the ion displacements, $\vec{\xi}(z)$, to the applied rf electromagnetic field as a function of $\vec{B}_0$. The physics of this problem is completely described by Maxwell's equations, and by the transport equations of the ions and of the electrons, in the presence of acoustic wave propagation in the metal.

Maxwell's two equations,

$$\operatorname{curl} \vec{H}(z) = \frac{4\pi}{c} \vec{J}(z) + \frac{1}{c} \frac{d\vec{D}(z)}{dt}$$

and

$$\operatorname{curl} \vec{E}(z) = -\frac{1}{c} \frac{d\vec{B}(z)}{dt}$$

(*) Quinn (10) and Meredith, et.al. (12) assume a time variation $e^{i\omega t}$ for the fields, and therefore the signs of their results differ from those presented here.

may be written in the circular polarization notation for the metal:

$$\frac{dH_\pm(z)}{dz} = \mp \frac{4\pi i}{c} J_\pm(z) \mp \frac{\omega}{c} E_\pm(z)$$

and

$$\frac{dE_\pm(z)}{dz} = \pm \frac{\omega}{c} H_\pm(z).$$

The presence of the metal surface can easily be accommodated if it is assumed that the electrons are specularly reflected from the boundary (24). In this case, an electron after reflection follows a path which is the mirror image of the trajectory that it would have followed, had it been allowed to continue into the other ($z < 0$) half-space. Because of this, the electromagnetic problem may be considered in an infinite medium, if the electric fields and currents are extended to negative values of z:

$$E_\pm(-z) = E_\pm(z) \qquad \text{and} \qquad J_\pm(-z) = J_\pm(z) \tag{22}$$

and if a fictitious surface current sheet,

$$j_{0\pm}(z) = \pm \frac{ic}{2\pi} H_\pm(0) \quad \delta(z) \tag{23}$$

is introduced, where $\delta(z)$ is the Dirac delta-function. The current sheet $j_{0\pm}(z)$ is required to produce the correct boundary conditions for the electric field; the magnitude and direction of $j_{0\pm}(z)$ are determined by the discontinuity in $dE_\pm(0)/dz$, and hence in $H_\pm(0)$, which exists in the infinite metal problem.

Maxwell's equations can now be written for the infinite metal: $$\frac{d^2E_\pm(z)}{dz^2} + \frac{\omega^2}{c^2}E_\pm(z) = -\frac{4\pi i\omega}{c^2}J_\pm(z) ,$$

where [24]

$$J_\pm(z) = -in_oe\omega\xi_\pm(z) + j_{e_\pm}(z) + j_{o_\pm}(z) .$$

The three contributions to the total current density are the ion, electron, and surface currents, respectively.

When a sound wave propagates through a metal, an equation analagous to Ohm's law relates the electronic current to the electric field: (23)

$$\vec{j}_e = \tilde{\tilde{\sigma}}(\omega,q)\left\{\vec{E} + \frac{i\omega m\vec{\xi}}{e\tau} + \frac{2E_F}{3n_oe(1+i\omega\tau)}\vec{\nabla}n\right\} \qquad [25]$$

where $\tilde{\tilde{\sigma}}(\omega,q)$ is the magnetoconductivity tensor for frequency ω and wave vector $\vec{q}$, τ is the electronic relaxation time, and E_F is the Fermi energy. The three terms on the right side of equation [25] are the conduction current, the collision-drag current, and the diffusion current, respectively (22). The collision-drag current is due to electron collisions with the moving ions. The diffusion current arises because the passage of the acoustic wave may disturb the electron density, n, from its equilibrium value, n_0.

Finally, the isotropic equation of motion for one ion in the presence of a static magnetic field, $\vec{B}_0$, is (23):

$$\left.\begin{aligned} M\frac{d^2\vec{\xi}(z)}{dt^2} &= MS_\ell^2\vec{\nabla}(\vec{\nabla}\cdot\vec{\xi}(z)) - MS_t^2\vec{\nabla}\times(\vec{\nabla}\times\vec{\xi}(z)) + Ze\vec{E}(z) \\ &\quad - \frac{i\omega Ze}{c}(\vec{\xi}\times\vec{B}_o) + \vec{F}_c(z) \qquad , \end{aligned}\right| \qquad [26]$$

$$\vec{F}_c(z) = -\frac{zm}{n_0 e\tau}\left(\vec{j}_e(z) - i n_0 e\omega\vec{\xi}(z)\right), \qquad [26]$$

where z is the number of conduction electrons per atom, and M is the mass of one ion. $\vec{F}_C$ is the collision-drag force which approximates the average increase in ion momentum due to electronic collisions. This collision term vanishes in the case of complete electron screening, when the electron current completely cancels the ion current.

The program is to eliminate $\vec{j}_e$, $\vec{E}$, and $\vec{j}_0$ from equations [23] to [26], and to obtain an expression for the ion displacement $\vec{\xi}(z)$ as a function of the static magnetic field $\vec{B}_0$ and the rf magnetic field $\vec{H}(0)$ which is applied to the metal surface.

Equations [25] and [26] may be written in a simplified form which is appropriate to the geometry $\vec{B}_0 = (0,0,B_0)$ and $\vec{q} = (0,0,q)$. In this case, there is no coupling between the transverse rf fields and the longitudinal component of the ion displacement, ξ_z. Thus only transverse acoustic waves can be generated, and, in the "jellium" model that has been assumed for the metal, the diffusion current term in [25] vanishes. Further, for a free-electron metal with $\vec{B}_0$ lying along the z axis, the magnetoconductivity is:

$$\sigma_\pm(\omega,q) = \sigma_{xx} \mp i\sigma_{xy} = \frac{3\sigma_0}{4}\int_0^\pi \frac{\sin^3\theta \; d\theta}{\left[1 + i(\mp\omega_c\tau + \omega\tau - ql\cos\theta\right]}\;; \qquad [27]$$

where $\sigma_{xx} = \sigma_{yy}$, $\sigma_{xy} = -\sigma_{yx}$, ℓ is the electronic mean free path, and $\sigma_0 = n_0 e^2\tau/m$ is the dc conductivity.

With these simplifications, and the definitions for the Fourier transforms of the fields

$$E_\pm(q) = \frac{1}{2\pi}\int_{-\infty}^{\infty} E_\pm(z)\, e^{-iqz}\, dz = \frac{1}{\pi}\int_0^{\infty} E_\pm(z)\cos qz\; dz, \quad \text{etc.,} \tag{28}$$

we can write the Fourier transforms of equations [23] to [26]:

$$j_{0\pm}(q) = \pm\frac{ic}{4\pi^2}H_\pm(0). \tag{23'}$$

$$j_{e\pm}(q) = -i\sigma_0\beta E_\pm(q) + in_0 e\omega\xi_\pm(q) - j_{0\pm}(q), \tag{24'}$$

where $\beta = \dfrac{c^2q^2}{4\pi\omega\sigma_0}\left(1 - \dfrac{\omega^2}{c^2q^2}\right).$

(Neglecting the displacement current, $\beta \triangleq c^2q^2/(4\pi\omega\sigma_0) = 2\delta_0^2 q^2$).

$$j_{e\pm}(q) = \sigma_\pm E_\pm(q) + \frac{i\omega m}{e\tau}\sigma_\pm\xi_\pm(q). \tag{25'}$$

$$\left(S_t^2 q^2 - \omega^2 \pm \omega\Omega_c\right)\xi_\pm(q) = \frac{zeE_\pm(q)}{M} + \frac{F_{c\pm}(q)}{M}, \qquad [26']$$

where $\Omega_c = zeB_0/(Mc) = zm\omega_c/M$ is the cyclotron frequency of the ions.

Combining equations [24'] and [25'], we obtain an expression for $E_\pm(q)$:

$$E_\pm(q) = \frac{-im\omega}{e\tau}\,\frac{(1-\sigma_0 R_\pm)}{(1+i\sigma_0 R_\pm\beta)}\,\xi_\pm(q) - \frac{R_\pm}{(1+i\sigma_0 R_\pm\beta)}\,j_{0\pm}(q), \qquad [29]$$

where $$R_\pm = \frac{1}{\sigma_\pm}.$$

Substituting this into [26']:

$$\xi_\pm(q) = \frac{ze}{M\sigma_0}\,\frac{(1-R_\pm\sigma_0)}{f(\omega,q)}\,j_{0\pm}(q),$$

$$[30]$$

$$f(\omega,q) = \left\{\left(S_t^2 q^2 - \omega^2 \pm \Omega_c\omega\right)\left(1+i\beta\sigma_0 R_\pm\right) + \frac{izm\omega}{M\tau}\left(1-\sigma_0 R_\pm\right)\left(1+i\beta\right)\right\},$$

which is the result given by Quinn (10).

For excitations such that $q\ell \ll \omega_c\tau$, we may use the local conductivity,

$$\frac{\sigma_\pm}{\sigma_0} = \frac{1}{1-i(\omega\pm\omega_c)\tau}$$

$$\cong \frac{1}{1\mp i\omega_c\tau},$$

if $\omega/\omega_c << 1$. With this approximation, and neglecting the displacement current, the function $f(\omega,q)$ of equation [30] may be written

$$f(\omega,q) = \left\{(S_t^2 q^2 - \omega^2)(1+2\delta_0^2 q^2[i \pm \omega_c \tau]) + \frac{q^2 B_0^2}{4\pi\rho}\right\} \qquad [32]$$

where ρ is the density of the metal. The dispersion relations for the uncoupled acoustic and electromagnetic excitations follow from [32] by setting $f(\omega,q) = 0$, and neglecting the coupling term, $qB_0^2/(4\pi\rho)$:

$$(S_t^2 q^2 - \omega^2) = 0 \qquad \text{(acoustic),} \qquad [33]$$

and

$$\left.\begin{aligned} & (1 + 2\delta_0^2 q^2[i \pm \omega_c \tau]) = 0 \\ \text{or} \qquad & c^2 q^2 = 4\pi i \omega \sigma_{\pm} . \end{aligned}\right] \qquad \text{(electromagnetic).} \qquad [34]$$

The acoustic and electromagnetic excitations are coupled by the last term in [32], which is small if $B_0^2/(4\pi\rho S_t^2) << 1$. The electromagnetic excitation at low fields is simply the surface excitation which at high temperatures is damped out within a distance into the metal of the order of the classical skin depth, $\delta_0 = [c^2/(8\pi\omega\sigma_0)]^{\frac{1}{2}}$. At low temperatures and high magnetic fields, this excitation becomes a lightly damped helicon wave with frequency

$$\omega_H = \pm \frac{c^2 q^2 \omega_c}{\omega_p^2} = \pm \frac{c^2 q^2}{4\pi}\left(\frac{B_0}{n_0 e c}\right) \qquad [35]$$

(this calculation is for an uncompensated free-electron metal, in the regime of local conductivity).

Using [23'] and [32], equation [30] may be written:

$$\xi_\pm(q) = \frac{B_0 H_\pm(0)}{4\pi^2 \rho \omega^2 \phi(\lambda)}, \qquad [36]$$

where $\phi(\lambda) = (1-\lambda)(1-a\lambda) - b\lambda,$

$$\lambda = \frac{S_t^2 q^2}{\omega^2},$$

$$a = -\frac{\omega}{4\pi\sigma_0}\frac{c^2}{S_t^2}(i \pm \omega_c \tau),$$

$$b = \frac{B_0^2}{4\pi\rho S_t^2}.$$

The inverse Fourier transform of [36],

$$\xi_\pm(z) = \int_{-\infty}^{\infty} \frac{B_0 H_\pm(0)}{4\pi^2 \rho \omega^2 \phi(\lambda)} e^{iqz}\, dq,$$

gives the real-space ion displacement as a function of the rf magnetic field applied at the surface, and of the perpendicular static magnetic field. This integration is discussed by Meredith, et.al. (12), and the solution for the acoustic wave is:

$$\xi_{\pm}(z) = \frac{i B_0 H_{\pm}(0) \exp[i(1-\alpha)^{1/2} \omega z/S_t]}{4\pi \rho S_t \omega [1 - a + (1+a)\alpha](1-\alpha)^{1/2}} \qquad [37]$$

where $\alpha = b/(1-a)$.

Equation [37] is greatly simplified in regimes where $b \ll 1$ and $a \ll 1$. We consider these approximations separately:

(i) The condition $b \ll 1$ (*) is satisfied for most metals in magnetic fields up to at least 10^4 G. For a metal having $\rho = 5$ g-cm^{-3}, $S_t = 3\times10^5$ cm-sec^{-1}, in a field of 10^4 G, $B_0^2/(4\pi\rho S_t^2) \cong 1.8 \times 10^{-5}$.

(ii) $|\text{Im } a| = \omega c^2/(4\pi\sigma_0 S_t^2) = 2q^2\delta_0^2$. Thus $|\text{Im } a| \ll 1$ is essentially the condition that the acoustic wavelength in the metal is much larger than the claasical skin depth.

(iii) $|\text{Re } a| = \omega/(4\pi\sigma_0)(c^2/S_t^2)\omega_c\tau = \omega/(4\pi)(c^2/S_t^2)B_0/(n_0 ec)$.

(*) b is the parameter which determines the strength of the coupling between the helicon and acoustic modes in the interaction region $(\omega\omega_c c^2/(\omega_p^2 S_t^2) = 1$ where the helicon and acoustic phase velocities coincide (6).

> It was demonstrated in the previous section that the condition $|\mathrm{Re}\ a| \ll 1$ must be satisfied if the electrons are tightly tied to the ions.

Thus the condition $a \ll 1$ is the free-electron analogue of the two conditions [19] and [20] which were used in the development of the phenomenological model, and which are satisfied in typical metals at low megahertz frequencies in fields up to 20 kG.

It can easily be shown that in the limit $a \ll 1$ and $b \ll 1$, the expression [36] is the same as that derived in the previous section. Equation [5] may be rewritten, for this perpendicular field geometry, in the form:

$$\left(\omega^2 + S_t^2 \nabla^2\right)\xi_\pm(z) = \pm \frac{i I_{0\pm} B_0}{\rho c}\,\delta(z).$$

Extending $I_{0\pm}(z) = I_{0\pm}\delta(z)$ evenly to negative values of z, and taking the Fourier transforms over all space:

$$\xi_\pm(q) = \frac{B_0 H_\pm(0)}{4\pi^2 \rho \omega^2 \phi(\lambda)}$$

where

$$\phi(\lambda) = \left(1 - \frac{S_t^2 q^2}{\omega^2}\right).$$

This result is identical to [36], for $a = b = 0$.

2.3.2 Unbounded metal plate, free electrons

Expressions have been obtained by Kravchenko (19) for the acoustic resonance singularities in the surface impedance of a metal plate, using a complex derivation for free electrons. This derivation is based on a different formulation of the ionic and electronic transport equations (25, 3) than is Quinn's treatment of a semi-infinite metal (10), which is outlined above. With the same approximations that were applied in that case, Kravchenko's result may be rewritten using our notation (from equation 5.17 of reference (19)) (*):

$$\Delta R_n = \frac{4B_0^2}{\rho c^2 \gamma d}\left\{\frac{1}{1+\left[\frac{2(\omega-\omega_n)}{\gamma}\right]^2}\right\}, \qquad [38]$$

valid in the vicinity of an acoustic resonance, $[(\omega-\omega_n)/\omega] << 1$, for a perpendicular magnetic field. For comparison, we rewrite the real part of equation [13], keeping only the nth term:

$$\Delta R_n = \frac{4B_0^2 \cos^2\theta}{\rho c^2 \gamma d\left[1+\left(\frac{\omega^2-\omega_n^2}{\omega\gamma}\right)^2\right]} . \qquad [39]$$

(*) Expression 5.17 of Kravchenko's paper actually yields an expression for ΔR_n which is larger by a factor of 2 than [38]. This is because Kravchenko considers the surface impedance of the plate, which is double the surface impedance of one surface, the object referred to throughout this thesis.

But
$$\frac{\omega^2-\omega_n^2}{\omega\gamma} = \frac{(\omega-\omega_n)(\omega+\omega_n)}{\omega\gamma}$$

$$\cong \frac{2(\omega-\omega_n)}{\gamma} \quad if \quad \frac{(\omega-\omega_n)}{\omega_n} \ll 1 \,,$$

and the Kravchenko result is the same as the expression derived by Turner, Lyall and Cochran using more direct and general arguments.

It is of interest to calculate the amplitude, $\xi_0(0)$, of the lattice displacement which is generated at the surface of a semi-infinite metal. From equation [37], with $a \ll 1$ and $b \ll 1$:

$$\xi_0(0) = \frac{B_0 H(0)}{4\pi\rho S_t \omega} \,.$$

Substituting into this equation the parameters $B_0 = 10$ kG, $\omega = 2\pi(5 \times 10^6)$ sec^{-1}, $H(0) = 0.02$ G, $S_t = 2.75 \times 10^5$ cm-sec^{-1}(*) and $\rho_{4.2°K} = 5.98$ g-cm^{-3}, which are appropriate to our gallium experiments:

$$\xi_0(0) \cong 3 \times 10^{-13} \text{ cm.}$$

This displacement may be compared to the deformation of approximately 2×10^{-10} cm which is produced in a piezoelectric quartz crystal by an applied potential of 1 V (26). Thus the

---

(*) This is the 4.2°K velocity of a transverse wave propagating along the gallium a-axis, and polarized along the c-axis (see Table 5-3).

conversion efficiency of electromagnetic-to-acoustic generation of acoustic waves at a metal surface is relatively small, and in general, the use of higher-power pulse methods, or of acoustic resonators, will be necessary in order to produce effects which are large enough to be observed in the laboratory. The acoustic contribution to the skin depth of an electromagnetically-excited resonating metal plate, however, may be large. At an acoustic resonance characterized by a quality factor $Q = \omega/\gamma = 10^3$, for example, the height of the singularity in the skin depth may be calculated by substituting the above parameters into equation [15]:

$$|\Delta\delta| = \frac{B_0^2 Q}{\pi^2 \rho \omega S_t} = 2.1 \times 10^{-4}\ \mathrm{cm},$$

which represents a change of the order of 100% in the zero-field, 4.2°K skin depth in gallium at 5 MHz (27).

CHAPTER 3. APPARATUS AND TECHNIQUE

3.1 Measurement of the skin depth in a metal plate

Changes in the skin depth of thin metal plates were measured using a two-coil arrangement similar to that shown in Fig. 3-1. The primary and secondary coils are coaxial with the long dimension of the metal plate. If the front and back surfaces of the plate coincide with z = 0 and z = d, then the rf electric and magnetic fields at the surfaces due to the current in the primary coil are approximately

$$\left.\begin{aligned} &E(0) = -E(d) = E_x(0) = E_0 e^{-i\omega t} \\ \text{and}\quad &H(0) = H(d) = H_y(0) = H_0 e^{-i\omega t} \end{aligned}\right] \qquad [1]$$

We have assumed that the free-space wavelengths are much larger than the coil dimensions, that the primary coil is much longer than the specimen, and that end-effects due to the finite specimen may be neglected.

If the detector circuit presents a large impedance to the secondary coil, no secondary current is allowed to flow, and changes in the phase and amplitude of the secondary voltage are very simply related to changes in the complex skin depth (or in the surface impedance) of the plate. The change in the secondary potential is

$$\Delta e_2 = -\frac{1}{c}\frac{d(\Delta\Phi)}{dt} \text{ esu}, \qquad [2]$$

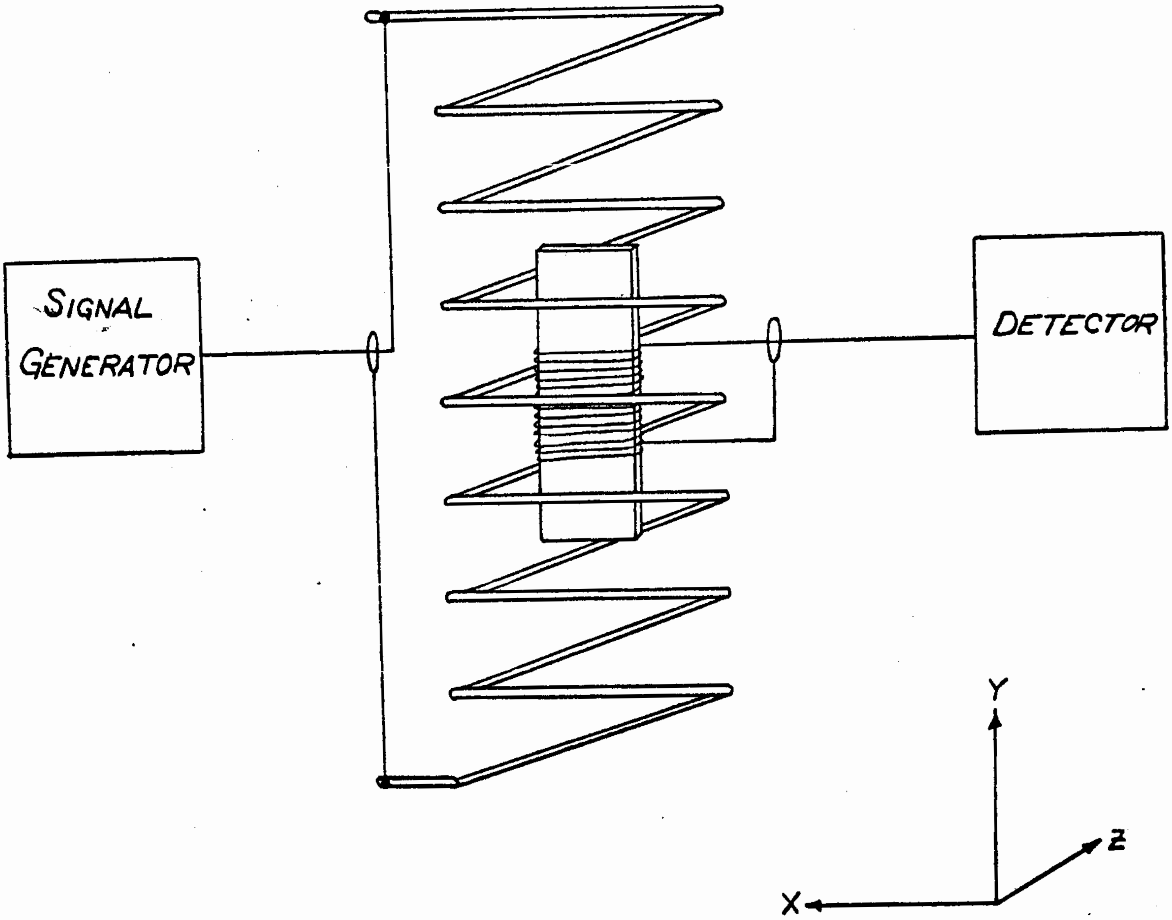

FIG. 3-1. TWO-COIL GEOMETRY FOR SKIN-DEPTH MEASUREMENTS.

where $\Delta\Phi$ is the change in the rf magnetic flux which is contained in the metal. This flux may be described in terms of the complex skin depth, δ. For an electromagnetic field $H_y(0)$, $E_x(0)$, incident on the surface of a semi-infinite ($z > 0$) metal,

$$\delta = \frac{1}{H_y(0)} \int_0^\infty H_y(z)\,dz = \delta_X + i\delta_R \quad \text{cm}, \tag{3}$$

where δ_X and δ_R are the reactive and resistive components, proportional to the flux in the metal which is in-phase, and out-of-phase, respectively, with $H_y(0)$. If $\Delta\delta \ll d$, and if W is the x-dimension of the plate,

$$\Delta e_2 = \frac{i\omega}{c}\left[2H_y(0)\,\Delta\delta(W+d)\right] \quad \text{esu}. \tag{4}$$

$H_y(0)$ may be obtained from the number of turns per centimeter n_1 of the primary coil, and the primary current i_1. Approximately,

$$H_y(0) = \frac{4\pi n_1 i_1}{c} \quad \text{gauss, } i_1 \text{ in esu}. \tag{5}$$

According to [4], the output voltage e_2 responds linearly to changes in the reactive and resistive skin depths of the metal plate, provided that these changes are small enough to have negligible effect on the primary current, and therefore on the fields at the surfaces. This requirement is equivalent to the condition

$$2(W+d)|\Delta\delta| \ll A_1 , \tag{6}$$

where A_1 is the cross-sectional area of the primary coil. In our experiments $A_1 \cong 3\ \mathrm{cm}^2$ and $(W+d) \cong 0.3$ cm, and the above condition was satisfied for any changes which were observed in the skin depth of the specimen.

In the more general situation where the detector presents an impedance, Z_D, to the secondary coil (Fig. 3-2), an analysis of the transformer leads again to a linear relationship between Δe_2 and $\Delta\delta$. The current in the secondary coil is

$$i_2 = -\frac{i_1 Z_M}{Z_D + Z_2} , \tag{7}$$

where $Z_2 = R_2 + i\omega L_2$. Equation [7] defines the mutual impedance Z_M between the two coils. Z_M will include a resistive component if the coils surround a resistive metal specimen. The measured change in the secondary voltage is

$$\Delta e_2 = Z_D \Delta i_2 \cong Z_D \left\{ \frac{-i_1}{(Z_D+Z_2)} \Delta Z_M + \frac{i_1 Z_M}{(Z_D+Z_2)^2} \Delta Z_2 - \frac{Z_M}{(Z_D+Z_2)} \Delta i_1 \right\} , \tag{8}$$

where ΔZ_M, ΔZ_2, and Δi_1 are all dependent upon the skin-depth change, $\Delta\delta$. A numerical consideration of the parameters of the specimen holder (#14, see Fig. 3-3) and of the detection apparatus indicates that $\Delta e_2 \propto \Delta\delta$ to within 2% for changes in the skin depth of less than 2×10^{-3} cm, at frequencies below 10 MHz (*).

(*) This upper limit, $\Delta\delta = 2 \times 10^{-3}$ cm, may be compared with the following values for the reactive skin depths at 7 MHz:

pure gallium (single crystals, anisotropic)	$(.791\text{-}1.79) \times 10^{-4}$ cm (27)
pure indium (polycrystal)	1.69×10^{-4} cm (Appendix C)
indium - 3% tin alloy	1.03×10^{-3} cm (Appendix B)

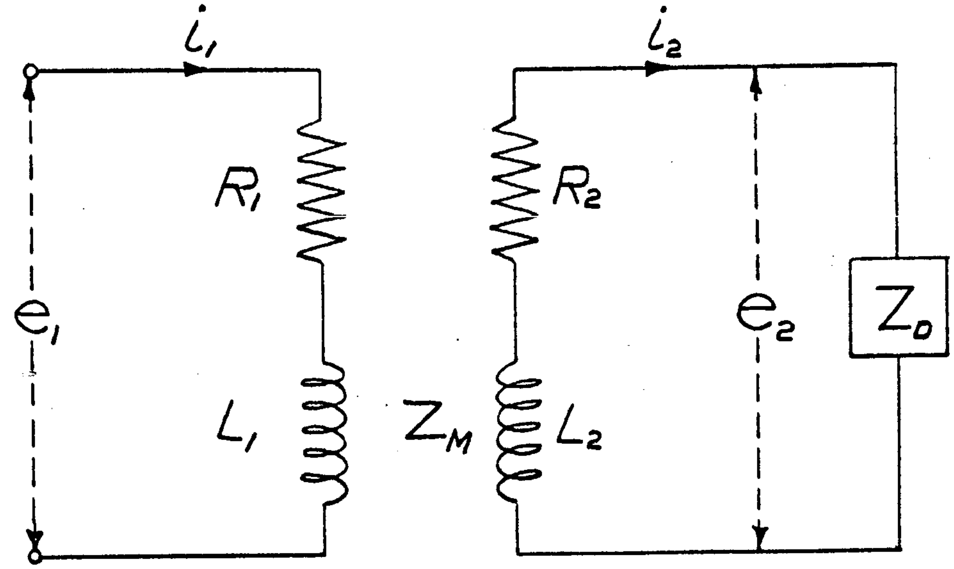

FIG. 3-2. EQUIVALENT CIRCUIT OF MEASUREMENT APPARATUS.

In addition, because of the fringing of the field lines at the ends of the short secondary coil, the secondary current will cause the direction of $\vec{H}(0)$ to deviate slightly from the axial direction. For the parameters of this experiment, however, the field due to the secondary coil is at most a few percent of that provided by the primary coil, and it is estimated that the effect of this field distortion on the measurements is negligible. Numerous empirical checks of the linearity of the system, including several measurements of the skin-depth changes in a metal plate using different specimen holders and detector circuits, substantiate the above conclusions.(*)

In all of the experiments, a constant-voltage rf signal with an amplitude of approximately 1 V was applied to the primary coil. This voltage, the maximum obtainable from the signal generator, produced an rf magnetic field amplitude of approximately 0.02 G at the specimen surface. The smallest detectable change in the skin depth is limited by noise originating in the wide-band signal amplifiers. At liquid

---

(*) In particular, two distinct configurations of the detection apparatus were used in the experiments. The signal from the secondary coil was fed either directly to a signal adder (~50Ω), or to the input of a high-input-impedance amplifier (1 MΩ, 22 pf). The former configuration is illustrated in Fig. 3-4, and a detector input impedance of 50Ω was used in the above calculation of the upper limit for linear skin-depth measurements.

helium temperatures a change $\Delta\delta = 1.0 \times 10^{-7}$ cm can be detected at 7 MHz with a measurement time constant of 1 sec and without using modulation (derivative measurement) techniques. This figure corresponds to a noise level of $\sim 3 \times 10^{-8}$ V (*); combined with the upper limit, $\Delta\delta = 2 \times 10^{-3}$cm, it gives a dynamic range of more than 80 db for the system, providing that the detection apparatus itself is linear over this range.

An absolute measurement of skin-depth changes requires a precise knowledge of the conversion factor

$$K = \frac{\Delta\delta}{\Delta e_2}, \qquad [9]$$

where both $\Delta\delta$ and Δe_2 are complex quantities. Since the geometry does not lend itself to an accurate calculation, the conversion factor was determined empirically, by measuring the skin-depth change at the superconducting transition of an indium - 3% tin alloy plate. The details of this calibration procedure may be found in a later section of this chapter.

3.2 Specimen holders

Virtually all of the data reported in this thesis were obtained using one or other of the two specimen holders

---

(*) The thermal noise generated over this frequency bandwidth in a 50 - Ω resistor at 300°K is $\sim 5 \times 10^{-10}$ V.

(#14 and #16) which are shown schematically in Fig. 3-3(a) and (b). L_1, N_1, and L_2, N_2, are the lengths and number of turns of the primary and secondary coils, respectively. In each holder the primary coil was wound from AWG 24 copper magnet wire on a frame constructed of epoxied fiber-board ("Celoron"). The secondary coil, also of AWG 24 copper wire, was wound on a slightly-tapered brass plate a little larger than the specimen. The coil was then carefully epoxied (*) into place within the Celoron frame, and the brass plate, which was lightly greased before epoxying, was removed. This technique ensured a fairly large filling factor for the specimen in the secondary coil. Alignment of this coil in the apparatus was well within 1° of the horizontal and vertical axes (see Fig. 3-3), verified by low-temperature measurements of the gallium skin depth, which is very sensitive to the direction of a strong magnetic field with respect to the metal surface. The copper coils were soldered to miniature-coaxial-cable leads (†), using bismuth-cadmium solder, whose superconducting transition temperature is less than 0.56°K (28).

(*) Fast-drying Eccobond PDQ epoxy obtained from Emerson and Cuming, Inc., Canton, Mass..

(†) Microdot microminiature low-noise cable (250-3839) consists of silver-plated copper conductors, and Teflon dielectric. It is therefore non-magnetic, unlike many other miniature cables, and shows no mechanical failure at low temperatures. Microdot, Inc., 220 Pasadena Ave., South Pasadena, Calif..

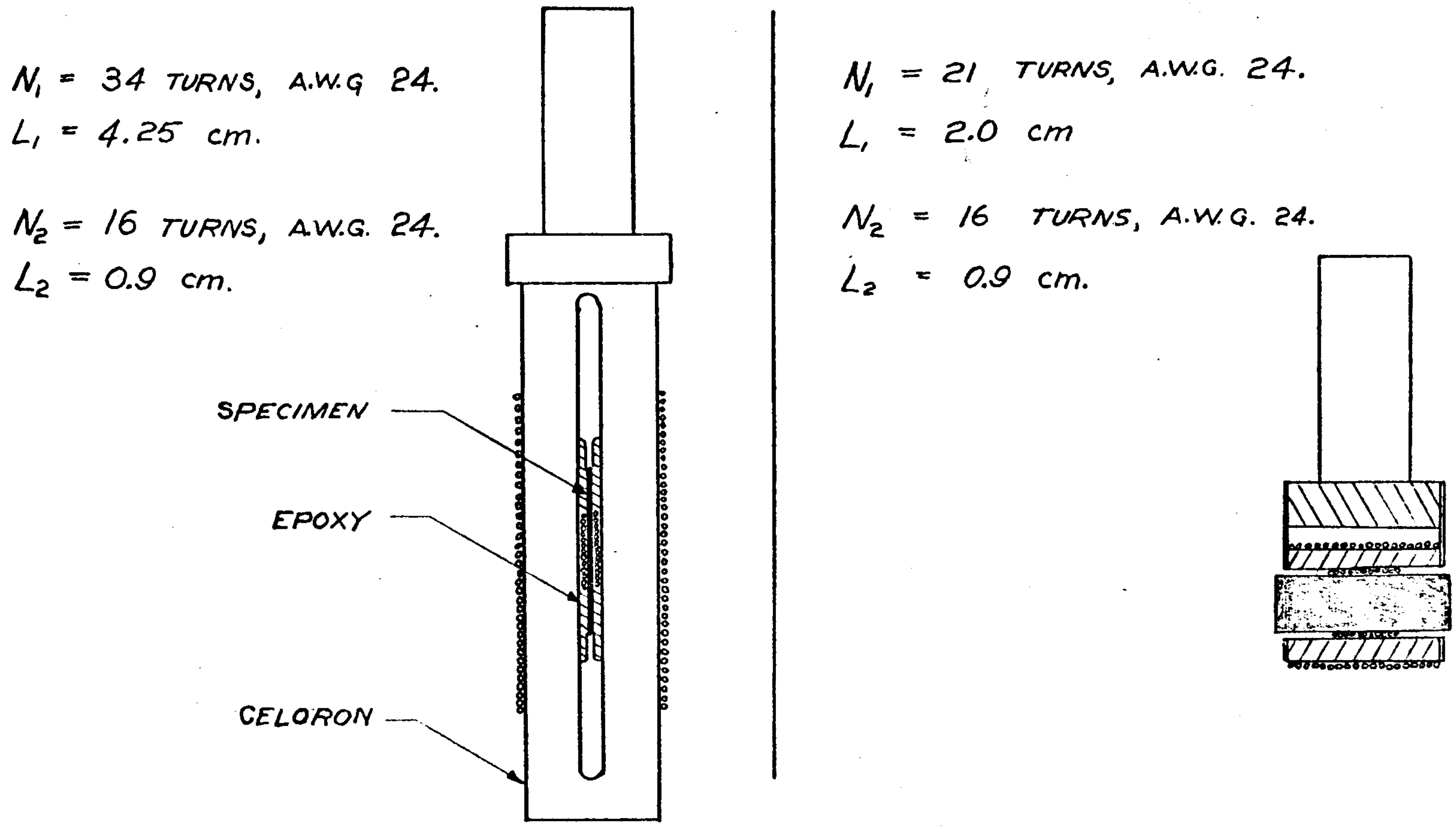

(a) HOLDER #14

(b) HOLDER #16

(FULL SCALE)

FIG. 3-3. SPECIMEN HOLDERS.

The entire specimen holder was enclosed in a brass can, which could be evacuated, or filled with an exchange gas.

Several early specimen holders were constructed in one piece from a casting epoxy (*), but this technique was abandoned when it was discovered that the epoxy has a magnetic susceptibility which varies with magnetic field. In experiments in which a swept magnetic field was applied, the epoxy contributed an inconveniently large background signal. As the field was swept from 0 to 2 kG, this background signal from the epoxy was equivalent to a change in the skin depth of the specimen of $\sim 2 \times 10^{-5}$ cm. It is rather surprising that this effect has not been reported before, as Stycast 2850-GT epoxy is widely used in low temperature research because of its exceptional mechanical properties, and the matching of its thermal expansion coefficient with that of copper (29, 30). No similar background signal was observed from the Celoron and PDQ epoxy holders described above.

3.3 Detection apparatus

The voltage signal from the secondary coil was detected using the apparatus shown in block diagram form in Fig. 3-4. A similar detection system has been described by Hansen, _et. al_. (31). The purpose of the apparatus is to measure the

---

(*) Stycast 2850-GT epoxy, obtained from Emerson and Cuming Inc., Canton, Mass.

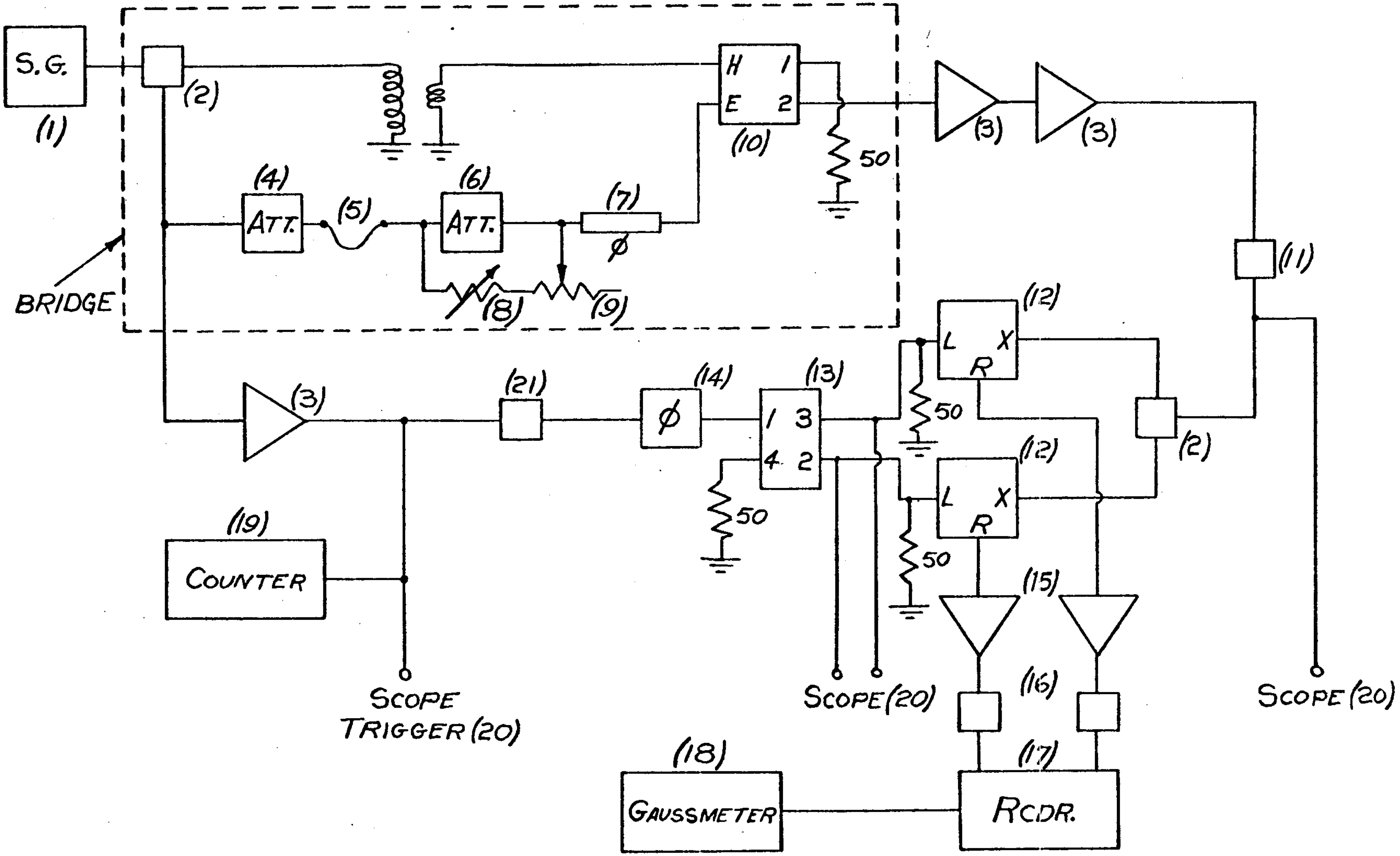

FIG. 3-4. BLOCK DIAGRAM OF MEASUREMENT APPARATUS.

TABLE 3-1. COMPONENTS OF THE RF DETECTION APPARATUS

(1) Constant amplitude signal generator (191) (.35 to 100 MHz; max. 2.5 V output into 50Ω)

Tektronics Instruments, Beaverton, Oregon.

(2) 50-Ω divider (MC101)

Ad-Yu Electronics, Passaic, N.J..

(3) Wide-band amplifier (1121) (5 Hz to 17 MHz; gain .2x to 100x)

Tektronics Instruments, Beaverton, Oregon.

(4) 0 to 90db, 10db-step, 50-Ω attenuator (74600-K)

Standard Telephone and Cables, Newport, Mon., England

(5) Length of 50-Ω coaxial cable (coarse phase shift).

(6) 0 to 10.9db, 0.1db-step, 50-Ω attenuator (TCB-50A)

Telonic Industries, Beach Grove, Indiana.

(7) Variable-length, 50-Ω line (874-LTL) (fine phase shift)

General Radio, West Concord, Mass..

(8) Nine 39-Ω, ¼-watt metal film resistors in series, switched.

(9) 50-Ω, 22-turn, trimming potentiometer (55-R50) (fine attenuator)

Beckman (Helipot Division), Fullerton, Calif..

(10) 50-Ω hybrid junction (CHT-10) (signal adder)

Merrimac Research and Development, West Caldwell, N. J..

(Table 3-1 continued on next page)

(11) 93-Ω - 50-Ω matching pad (011-058)

Tektronics Instruments, Beaverton, Oregon.

(12) Diode mixers (10514A) (phase-sensitive detectors)

Hewlett Packard, Palo Alto, Calif..

(13) Quadrature hybrid (QH-1-7) (fixed 0° and 90° phase shifts)

Merrimac Research and Development, West Caldwell, N. J..

(14) 0 to .075μs delay line (559a2)

Ad-Yu Electronics, Passaic, N. J..

(15) dc amplifier with variable gain and time constant, employing operational amplifiers (P65A/U)

Philbrick Researches, Dedham, Mass..

(16) dc voltage offset; 10-turn potentiometer supplied from mercury cells.

(17) Two-pen X-Y recorder (2FAM)

Hewlett Packard, Palo Alto, Calif..

(18) Hall-effect gaussmeter (620)

Bell, Inc., Columbus, Ohio.

(19) Frequency counter (5246L)

Hewlett Packard, Palo Alto, Calif..

(20) Oscilloscope (547)

Tektronics Instruments, Beaverton, Oregon.

(21) 93-Ω - 25-Ω matching pad (metal film resistors).

amplitude and phase of a small change in rf voltage ($\sim 10^{-8}$ V) which is superimposed on a large rf background ($\sim 10^{-1}$ V). The labelled components of Fig. 3-4 are identified in Table 3-1.

The first part of the detector forms an rf bridge. By adjusting the attenuators and phase shifters ((4), (5), (6), (7), (8), (9) in Fig. 3-4) in the bridge circuit, the background signal from the secondary coil can be reduced by a factor of $\sim 10^{6}$. A small off-balance voltage signal appearing at port 2 of the hybrid junction can then be amplified without the danger of over-driving the rf amplifiers and diode mixers in the detection circuit.

Because of this high degree of balance, the long-term stability of the bridge requires exceptional stability of the variable attenuators and phase shifters. Several components were tried and rejected, and the only continuously variable components found to exhibit this stability were the General Radio variable-length line ((7) in Fig. 3-4), and a simple trimming potentiometer ((9) in Fig. 3-4). The other attenuators in the bridge are of the switch type, and larger phase shifts than are available from the variable-length line are obtained by inserting into the circuit different lengths of 50-Ω coaxial cable ((5) in Fig. 3-4), firmly taped to lucite cylinders.

The off-balance signal from the bridge is divided and fed to the signal ports (X) of two diode mixers ((12) in

Fig. 3-4) which are used as rf phase-sensitive detectors, having a specified frequency range 200 kHz to 500 MHz. The reference ports (L) of these mixers are supplied with two signals differing in phase by 90°, derived from a quadrature hybrid ((13) in Fig. 3-4). A voltage signal applied to port (1) of this component is split equally into two orthogonal signals when the ports are all properly terminated by 50-Ω impedances. The quadrature hybrid has a center frequency of 7 MHz and an octave band width, and represents the primary frequency restriction in our apparatus (*). The high input-impedance amplifier ((3) in Fig. 3-4) is needed in this reference channel primarily as a buffer to ensure that adjustment of the reference phase shifter ((14) in Fig. 3-4) does not change the balance of the bridge. This amplifier is accompanied by a switch attenuator which serves to keep the amplitude of the reference signals fed to the (L) ports of the mixers at a level (.15 V to .30V) such that the mixer conversion efficiency is independent of reference signal amplitude. This is necessary because the reference phase shifter introduces an amplitude wow of approximately 5%, even when propertly terminated, as it is adjusted through its range (190° at 7.0 MHz). The phase shifter is in fact a variable-length loaded transmission line, operated by a sliding contact.

(*) The frequency range 2 to 76 MHz is covered by two broad-band quadrature hybrids which are now available from Merrimac Research and Development, Inc., West Caldwell, N.J..

It therefore does not have infinite resolution, the minimum increments of phase shift being approximately 1.5° at 7 MHz.

The dc outputs from the two mixers pass through identical dc amplifiers ((15) in Fig. 3-4) with variable time constants (.1, 1, 3 sec.) and gains (2, 11, 100x). Finally, after being added to dc offset voltages, they are used to drive a two-pen X-Y recorder. The X-axis of the recorder was driven either from the output of a Hall-effect gaussmeter, or, when frequency sweeps were being made, from the internal time-sweep of the recorder. In the latter experiments, a slow-speed motor and reduction gear unit (*) were used to drive the frequency control shaft of the signal generator. This mechanism, with rotary speeds from 0.001 to 1 revolution per minute, is capable of sweeping the frequency at rates between approximately 5 and 5000 Hz/sec.

The range over which the system may be used to measure phase is limited by the quadrature hybrid to 5 MHz to 10 MHz. Signals have been detected, however, at frequencies from 1 MHz to 15 MHz. For some measurements, the signal amplifiers were tuned (not shown in Fig. 3-4), with a resulting increase in the signal-to-noise ratio of approximately 10. The grounded copper shielding which was found to be necessary in order to obtain reproducible and stable operation of the rf bridge is illustrated in Fig. 3-5. The signal generator

---

(*) Obtained from Insco Corporation, Main Street, Groton, Mass.

was completely enclosed in a grounded copper box, and the coaxial cables to and from the dewar passed through grounded copper tubing. The brass can surrounding the specimen holder was tightly connected to this shield, which was grounded via a "quiet" connection to the earth (*). The low side of the signal (chassis ground) was connected to the copper-box system at only one point, to avoid unstable ground loops. No connection was made to the grounded lead supplied as the third wire in the ac mains. Finally, the ac power input to the signal generator passed through a low-pass L-C filter, (Fig. 3-6), in order to eliminate any rf interference from that source. An informative review of the practical rules of shielding and grounding for instrumentation is given in an article by Morrison (32).

3.4 Calibration

The apparatus was calibrated by measuring the change in the skin depth of an indium - 3% tin alloy at the superconducting transition. Details of the preparation of the alloy specimens, and the results of measurements of their

---

(*) Fig. 3-5 shows the shielding system as it existed during the earlier stages of the experiments. For reasons of convenience, the copper box surrounding the attenuators, phase shifters, and signal adder was later removed, with no noticable depreciation in the behaviour of the bridge. The shield surrounding the signal generator and the specimen coils was present for all experiments.

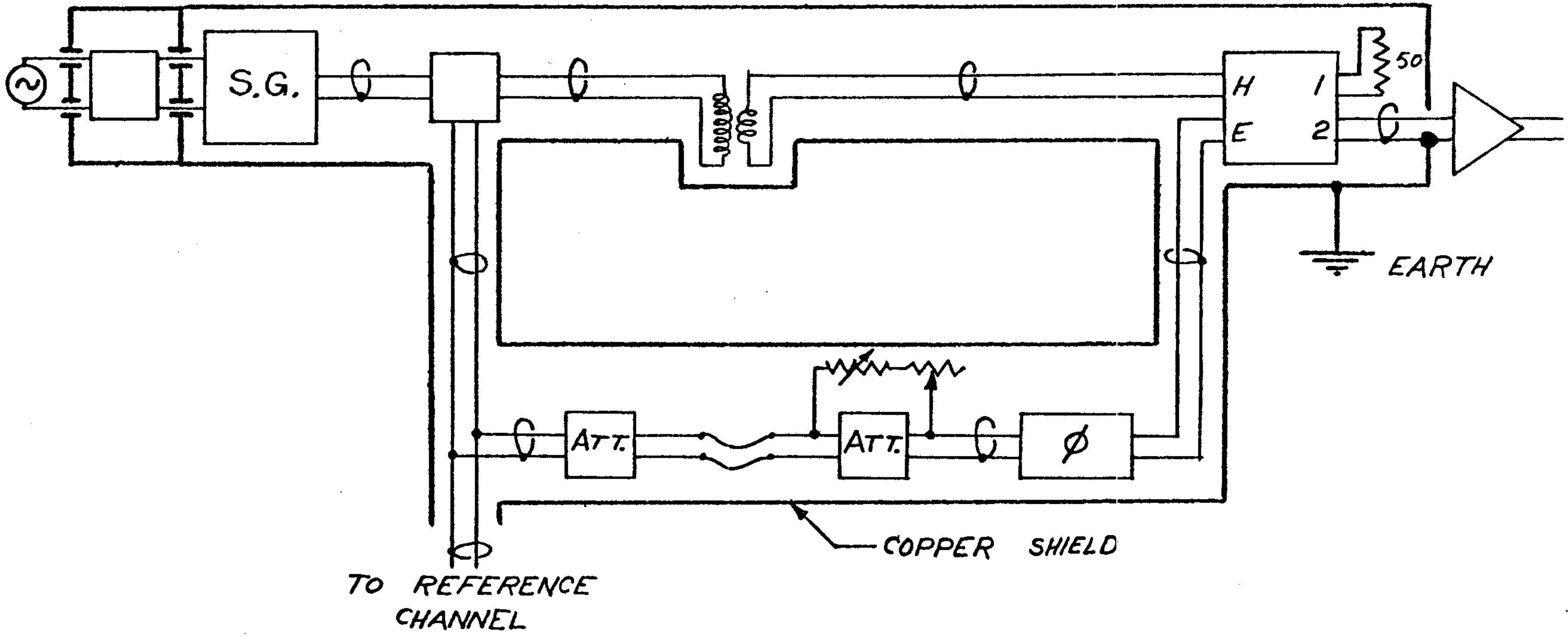

FIG. 3-5. SHIELDING OF RF BRIDGE.

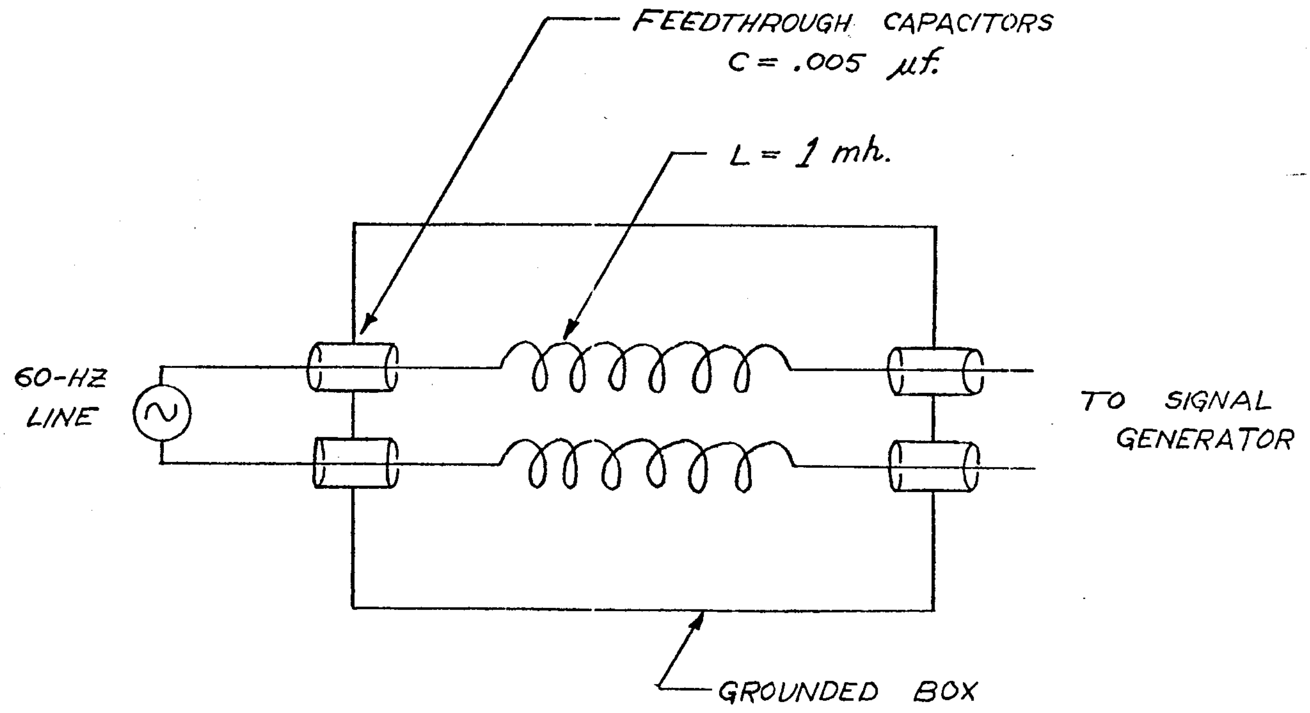

FIG. 3-6. LOW-PASS POWER FILTER FOR SIGNAL GENERATOR.

dc resistivities are presented in Appendix B. It is estimated there that $[|\delta_{C\ell}|/\ell]_{4.2°K,\ 7\ MHz} \cong 48$, where $\delta_{C\ell}$ is the normal-state skin depth calculated from the classical-skin-effect theory (*) using the measured dc resistivity, and ℓ is the electronic mean free path. The alloy thus satisfies the condition $|\delta_{C\ell}| >> \ell$ that is required for the validity of the classical theory, and the calculated value of $\delta_{C\ell}$ was used to calibrate the signal observed at the transition.

The quantity actually measured at the superconducting transition is the change in flux, which is proportional to the difference $(\delta_{C\ell} - \delta_s)$ between the normal and superconducting skin depths in the specimen. We can, however, neglect δ_s in comparison with $\delta_{C\ell}$ at low megahertz frequencies, and the skin-depth change which must correspond to the observed transition is simply

$$\delta_{C\ell} - \delta_s \cong \delta_{C\ell} = \left(\frac{c^2}{8\pi\omega\sigma_0}\right)^{1/2}(1+i) = \left(\delta_x + i\,\delta_R\right)_{C\ell}, \qquad [10]$$

which yields, using the measurements of Appendix B for the 0.26 mm - thick specimen,

---

(*) We define the classical skin depth as $\delta_{C\ell} = \delta_0(1+i) = [c^2/(8\pi\omega\sigma_0)]^{\frac{1}{2}}(1+i)$, in agreement with the generalized definition of the skin depth given by [3]. It should be noted, however, that a commonly used definition is $\delta_0 = [c^2/(2\pi\omega\sigma_0)]^{\frac{1}{2}}$, in which case δ_0 is the distance into the metal at which the rf fields are reduced to a fraction 1/e of their values at the surface.

$$\left(\delta_X\right)_{C\ell} = \left(\delta_R\right)_{C\ell} = 1.03 \times 10^{-3} \quad \text{cm.} \qquad [11]$$

The approximation in [10] is justified empirically. The reactive skin depth in a superconductor, $\delta_s(T)$, changes rapidly with temperature at temperatures just below the transition, and the relative magnitudes of $\delta_{C\ell}$ and $\delta_s(0)$ may be inferred from measurements of the temperature variation of $(\delta_{C\ell} - \delta_s(T))$. An example of this method of obtaining both the normal and superconducting skin depths for pure indium is given in Appendix C. From the absence of any observed temperature variation in $(\delta_{C\ell} - \delta_s(T))$ in the alloy at temperatures below the transition, we are able to affirm that

$$\frac{\delta_s(0)}{\delta_{C\ell}} < 1\% \quad ,$$

and the approximation in [10] is justified. (*)

The superconducting-to-normal transition was induced either by warming the alloy above its critical temperature in zero magnetic field, or by destroying the superconductivity with a small (100 G) field, applied in the plane of the plate.

(*) This result is consistent with the findings of Pippard (33), who reported that $\delta_s(0)$ in a tin - 3% indium alloy was approximately twice as large as the zero-temperature skin depth in pure superconducting tin. If a similar ratio holds for pure indium and our indium - 3% tin alloy, then for this alloy $\delta_s(0)/\delta_{C\ell} = 0.84\%$, and $\delta_s(0)$ may be neglected in comparison to $\delta_{C\ell}$.

The change in the normal-state skin depth associated with a magnetic field of this magnitude was found to be negligible. No evidence of trapped flux in the superconducting alloy was observed when the magnetic field was switched on and off. For fields lying perpendicular to the plate, however, the trapped flux amounted to approximately 5% of the total flux contained in the specimen in the normal state. It is interesting to note that Pippard (34) has investigated flux trapping in a tin - 2.94% indium alloy, and found that for a cylindrical specimen in a transverse field, the proportion of trapped flux varied from 5% to 12% at temperatures between 0.4 T_c and 0.95 T_c.

The superconducting transition of the alloy was used both to align the phase response of the system, and to provide an absolute amplitude calibration. Because in the classical-skin-effect regime the reactive and resistive skin depths of a metal are equal (equation [10]), the reference phase shifter ((14) in Fig. 3-4) was adjusted until the two recorder pens were displaced equally when the alloy passed through the transition. The phase alignment was then such that one recorder pen responded only to resistive changes in the skin depth, and the other only to reactive changes. The size of the recorder displacement was calibrated through equation [10], where σ_0 was obtained from a measurement of the dc resistivity of the alloy at 4.2°K (Appendix B). This calibration procedure was repeated at different frequencies, and a typical graph of the absolute amplitude calibration and the reference phase-shifter dial setting, as functions of frequency, is shown in

Fig. 3-7. At least some of the deviations from linearity in Fig. 3-7 are real, and the measured points have been connected by straight lines. (The error bars in Fig. 3-7 indicate the absolute error; the reproducibility of the measurements corresponds approximately to the size of the circles in the figure). The calibration is valid only for metal plates which are the same size and shape as the alloy specimens used to calibrate the system.

The amplitude equality and phase orthogonality of the two reference signals derived from the quadrature hybrid ((13) in Fig. 3-4) were checked as follows. After aligning the phase response by observing the alloy-transition signal as described above, the phases of the reference signals were changed, using the reference phase shifter, by exactly 90°, measured to within ± 0.5° on an oscilloscope. The superconducting transition was then remeasured. For frequencies between 5 MHz and 10 MHz, these two measurements were found to agree to within ± 1% (see Fig. 3-8). The equivalence of the two channels, each consisting of a diode mixer, dc amplifier, and recorder, was checked by interchanging the signals applied to the (X) ports of the two mixers.

The uncertainty in the absolute amplitude calibration is due largely to the uncertainty in the alloy dc resistivity measurement, and is estimated to be ± 3%. The phase alignment uncertainty is determined by the resolution of the reference phase shifter, and is ± 1.5° at 7 MHz.

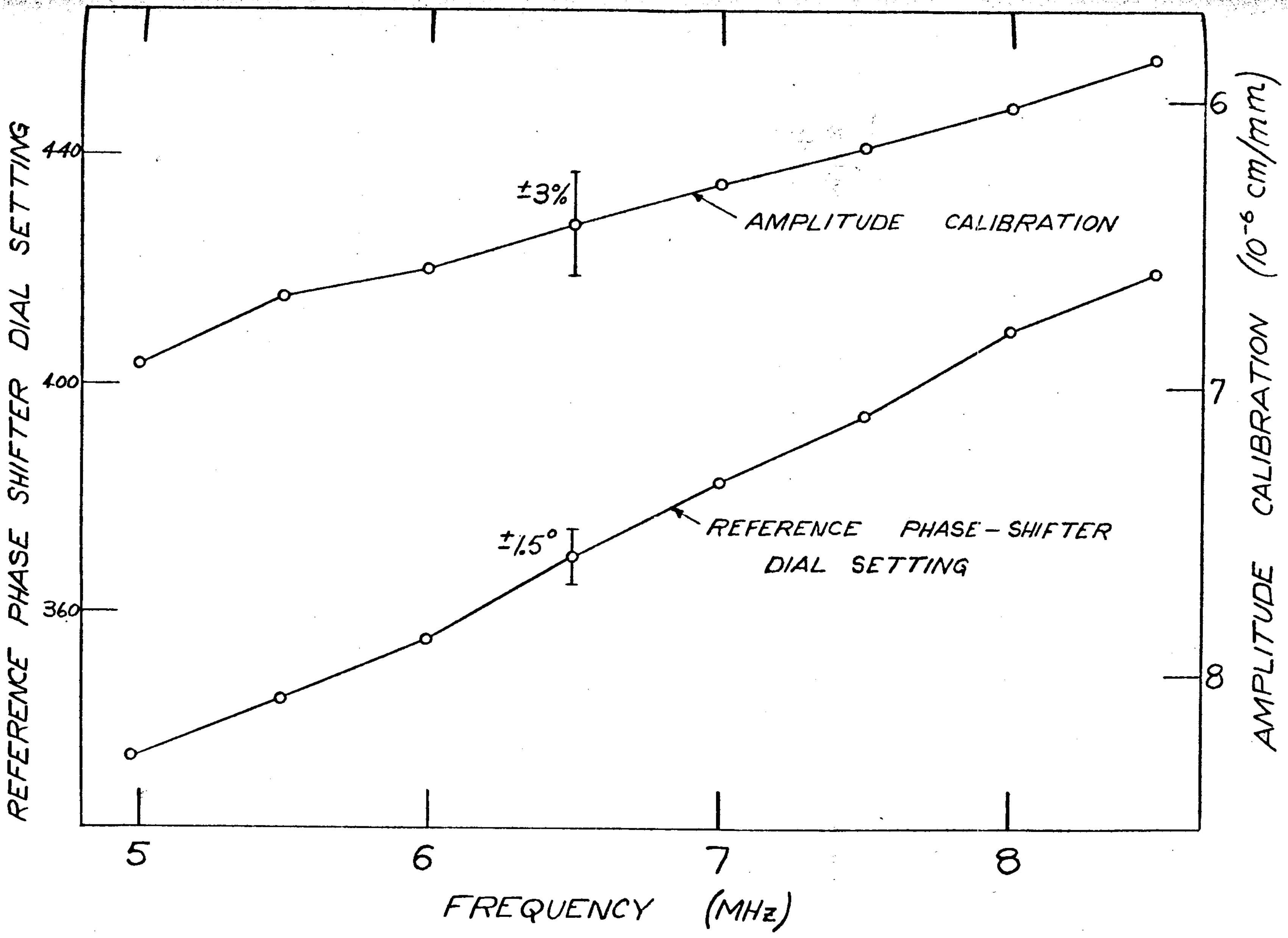

FIG. 3-7. PHASE AND AMPLITUDE CALIBRATIONS AS FUNCTIONS OF FREQUENCY.

An interesting verification of the phase alignment was obtained by measuring the ratio of the reactive and resistive skin depths in plates of pure, polycrystalline indium. According to the anomalous-skin-effect theory, this ratio is $\delta_x/\delta_R = \sqrt{3}$, or $\tan^{-1}(\delta_x/\delta_R) = 60°$. The measured values of $\tan^{-1}(\delta_x/\delta_R)$ ranged between 58.6° and 59.7°, in agreement with the theory to within the estimated error. This experiment, which confirms unambiguously the phase-measuring capability of the system, is described in Appendix C.

We conclude this section by reproducing in Figs. 3-8 to 3-10 several recorder traces obtained using the apparatus.

The signals observed at the superconducting-transition of the indium-tin alloy are shown in Fig. 3-8. The recorder traces (b) and (c) in Fig. 3-8 were obtained with the mixer reference signals rotated by 45° and 90° respectively, from the original phase alignment of Fig. 3-8(a). No electrical noise is discernable on the scale of Fig. 3-8.

Fig. 3-9 shows quantum oscillations (*) in the reactive skin depth which were observed at 1.2° K, with $\vec{B}_0$ lying along the b-axis in gallium. The magnetic field was modulated at a frequency of 33 Hz using a pair of Hemholtz coils, and the derivative $d\delta_x/dB_0$ was obtained by phase-sensitive

---

(*) see section 6.1.

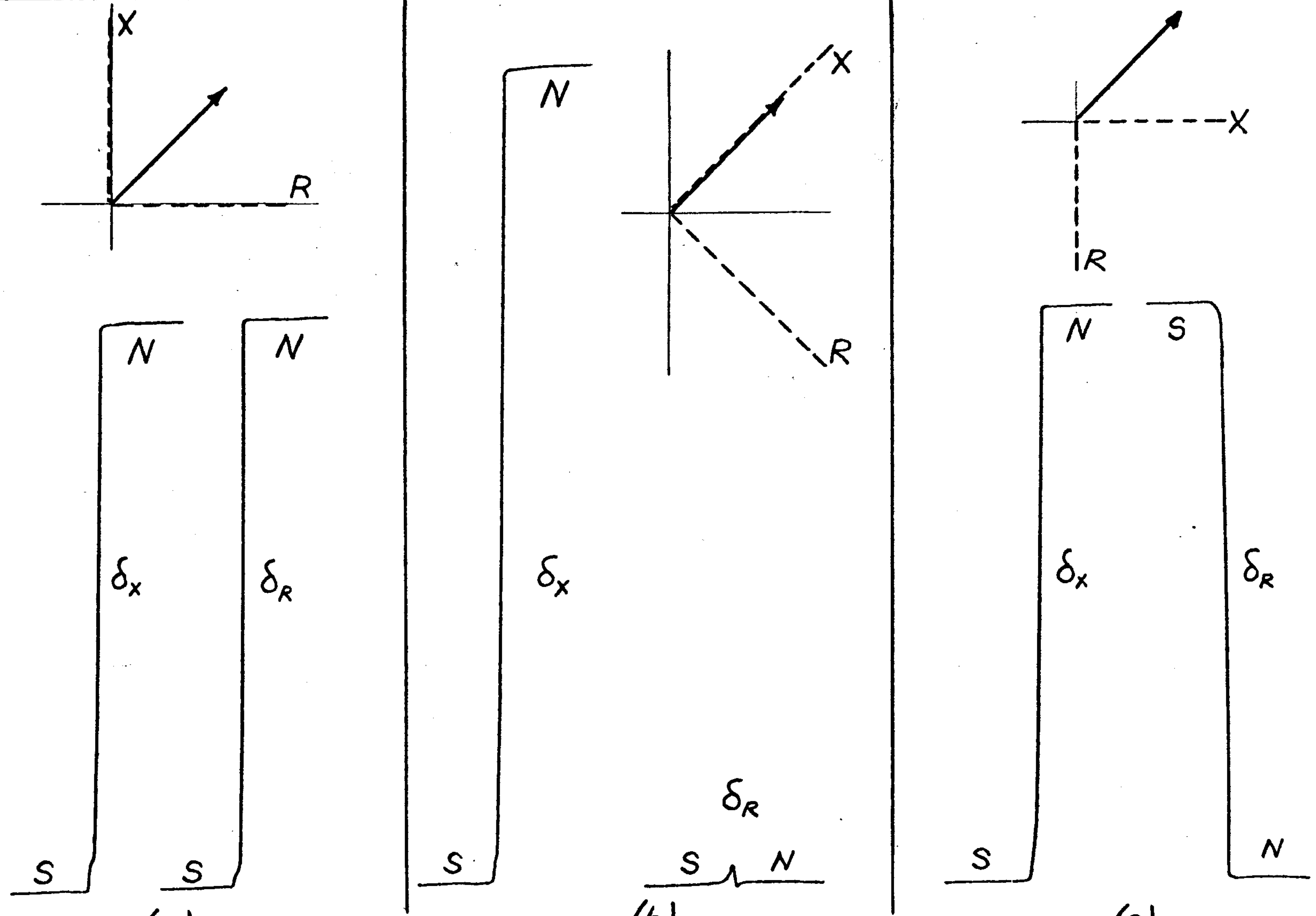

(a) (b) (c)

FIG. 3-8 S-N TRANSITION IN INDIUM - 3% TIN ALLOY PLATE.

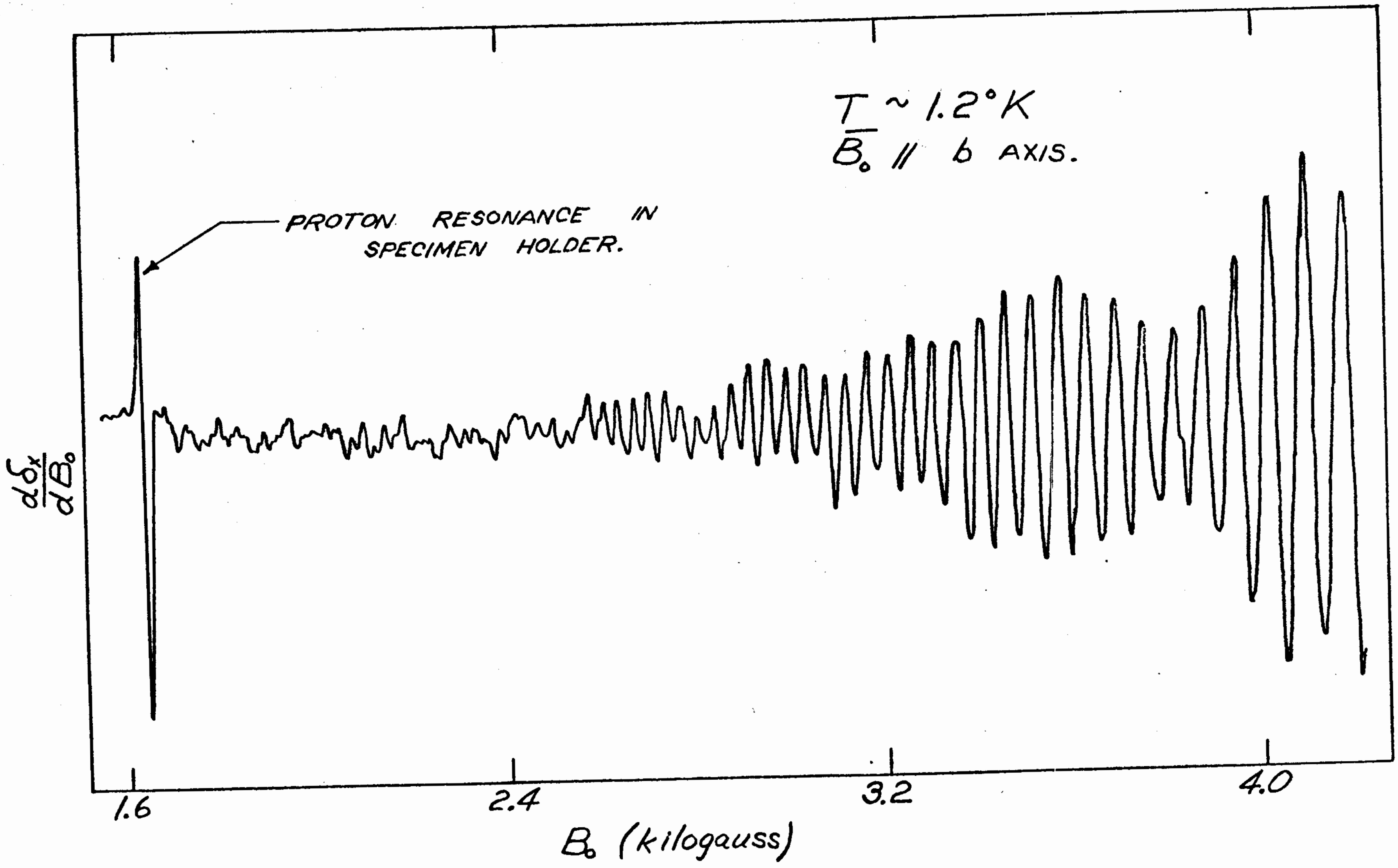

FIG. 3-9. QUANTUM OSCILLATIONS IN THE SKIN DEPTH OF GALLIUM.

detection (*) of the output from the diode mixer ((12) in Fig. 3-4). Also shown in Fig. 3-9 is the proton resonance signal which was observed at all temperatures, and which probably arises from the protons in the Celoron specimen holder. This signal provided a convenient field marker, and also a standard for use in signal-to-noise comparisons during the development of the apparatus. Nuclear magnetic resonance signals in water and in powdered copper, and the electron spin resonance signal in DPPH were also useful for these reasons.

A radio-frequency-size-effect (Gantmakher) resonance (35, 36) in a 0.261 mm-thick single crystal of gallium is shown in Fig. 3-10. This particular resonance was obtained with $\vec{B}_0$ and $\vec{H}(0)$ lying in the plane of the plate, parallel to the gallium c-axis. The a-axis was perpendicular to the surface of the crystal. $\vec{B}_0$ was modulated by a pair of Hemholtz coils at a frequency of 33 Hz, and the derivatives $\frac{d\delta_X}{dB_0}$ and $\frac{d\delta_R}{dB_0}$ were obtained by phase-sensitive detection of the outputs from the two mixers. The two low-frequency phase-sensitive detectors used for this purpose displayed slightly different sensitivities, which explains the difference in amplitude of the resistive and reactive signals shown in Fig. 3-10. For this reason also, the calibration shown is only approximate. The reactive line-shape is very similar to that reported for

---

(*) Using a Princeton Applied Research Model HR-8 Lock-in Amplifier. Princeton Applied Research Corporation, Princeton, N. J..

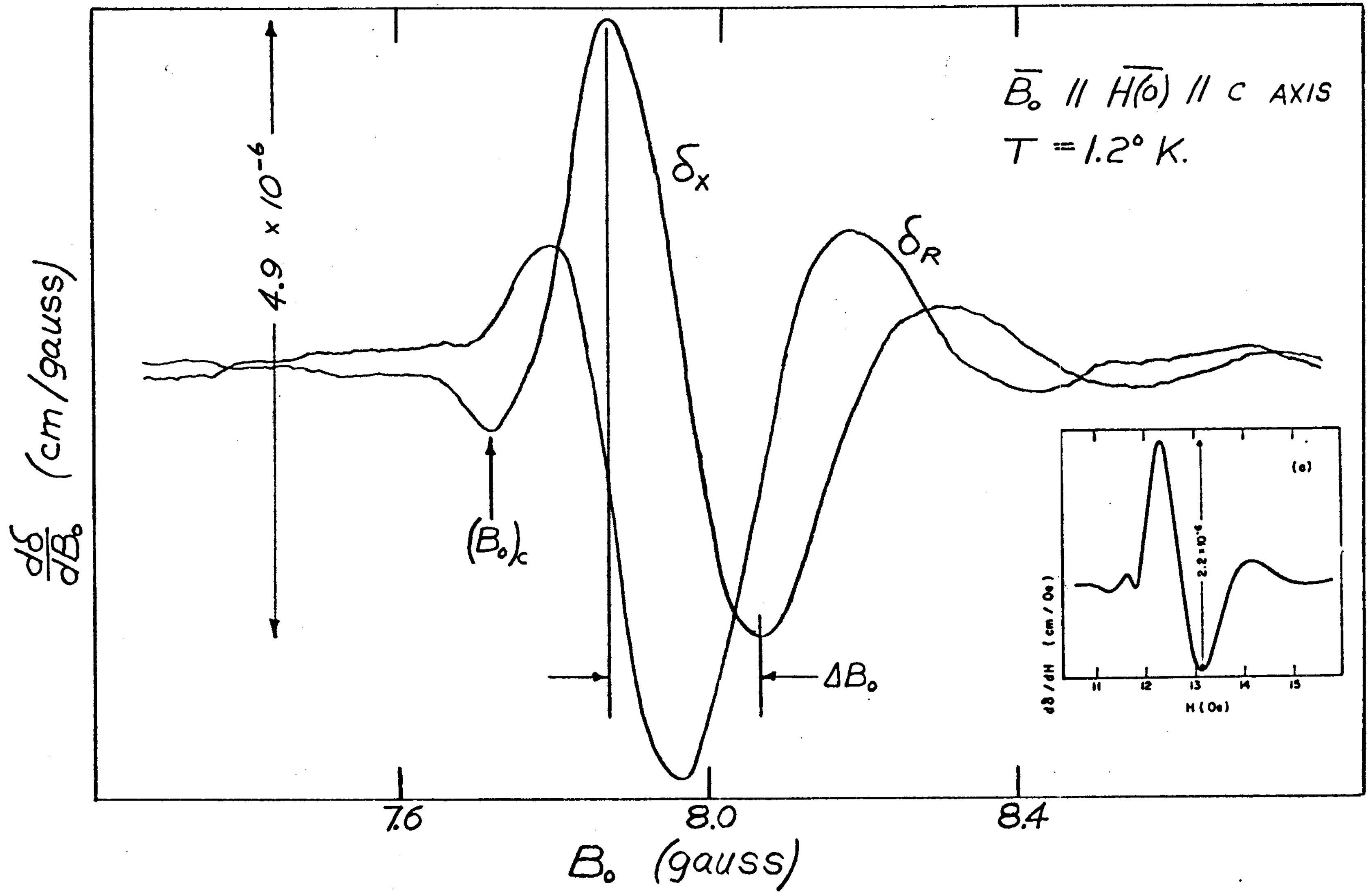

FIG. 3-10. RADIO-FREQUENCY SIZE-EFFECT RESONANCE IN GALLIUM.
INSET: SAME RESONANCE, REPORTED BY HABERLAND, ET. AL. (27).

the same resonance by Haberland, et.al. (27), and their curve is reproduced in the inset of Fig. 3-10. Gabel (37) has also observed this resonance in the rf transmission through a gallium plate, and the three sets of data are compared in Table 3-2. The "cut-off" field $(B_0)_c$ (38) is expected to scale with 1/d, and the line-width $\Delta B_0/(B_0)_c$ to scale with $|\delta|/d$, or $f^{-1/3}/d$, in the anomalous-skin-effect regime (35). These two predictions are confirmed, to within the accuracies of the available data, as is shown in the last two columns of Table 3-2.

3.5 Associated equipment

All results were obtained with the specimen holder surrounded by a brass can, and placed inside a liquid-helium dewar vessel. In the earlier stages of the experiment, glass dewars were used, similar to the one described in reference (39). It was soon found, however, that because of fragile copper-glass seals, these dewars had a useful lifetime of only a few months. A simple metal dewar (Fig. 3-11) was then constructed in the Simon Fraser University science machine shop, and proved to be entirely satisfactory. A charge of liquid helium (2.0 liters) in this dewar lasted for approximately four hours. Temperatures between 4.2°K and 1.2°K were obtained by pumping on the liquid helium bath, using a mechanical pump connected to the cryostat by a six-inch pumping line. A Walker pressure regulator (40) was used to

	f (MHz)	d (mm)	$(B_0)_c$ (G)	$\frac{\Delta B_0}{(B_0)_c}$	$(B_0)_c d$	$\frac{\Delta B_0}{(B_0)_c} f^{1/3} d$
Present Work	7	0.261	7.72	.0259	2.02	.013
Haberland, et.al.(1)	1	0.17	11.75	.074	2.00	.012
Gabel(11)	1.74	0.38	5.35	.028	2.03	.013

TABLE 3-2. RADIO-FREQUENCY-SIZE-EFFECT DATA.

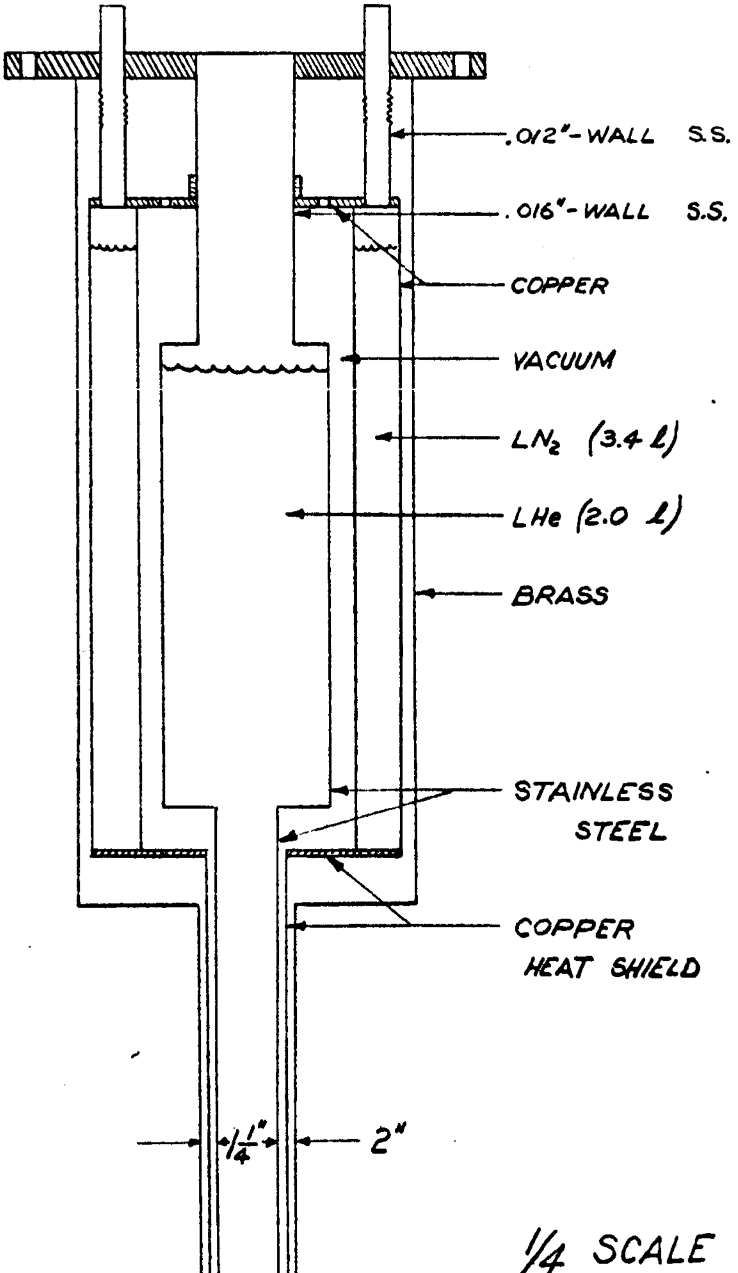

FIG. 3-11. METAL DEWAR VESSEL.

regulate the temperature of the bath. The specimen temperature was obtained by monitoring the resistance of a 1/10-watt, 100-Ω, Allen-Bradley carbon composition resistor which was epoxied onto the specimen holder. A Magnion (*) 12-inch electromagnet, in conjunction with a Magnion FFC-4 current regulator, was used to provide fields up to 14 kG.

3.6 Gallium crystals

Gallium single crystals, in the form of rectangular plates, 2.35 cm by 0.8 cm, and having a thickness of 0.26 mm or 0.80 mm, were grown in lucite molds from 99.9999% - pure metal (†). The crystal-growth procedure has been described in detail by Yaqub and Cochran (41). A sketch of a lucite mold which was used to grow crystals is shown in Fig. 3-12; the mold consists of two ¼" polished lucite plates, bolted together with sheet plastic spacers between. Molten gallium was injected into the carefully cleaned mold using a 1-cc hypodermic syringe. The high-purity gallium was allowed to supercool several degrees below its melting point, 29.8°C, and the mold was then moved so that a projecting meniscus of the liquid metal lightly touched the oriented seed crystal (Fig. 3-13). Solidification started at the moment of contact, proceeded slowly across the crystal, and was complete

---

(*) Magnion, Inc., Burlington, Mass.

(†) Obtained from the Aluminum Company of America, Pittsburgh, Pa.

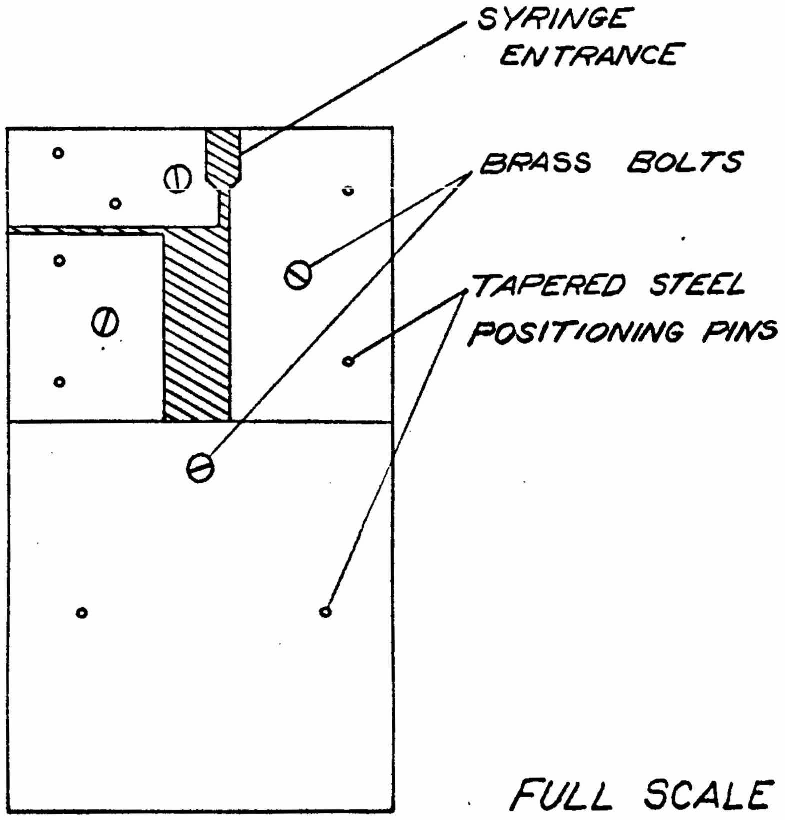

FIG. 3-12. MOLD FOR GALLIUM CRYSTALS.

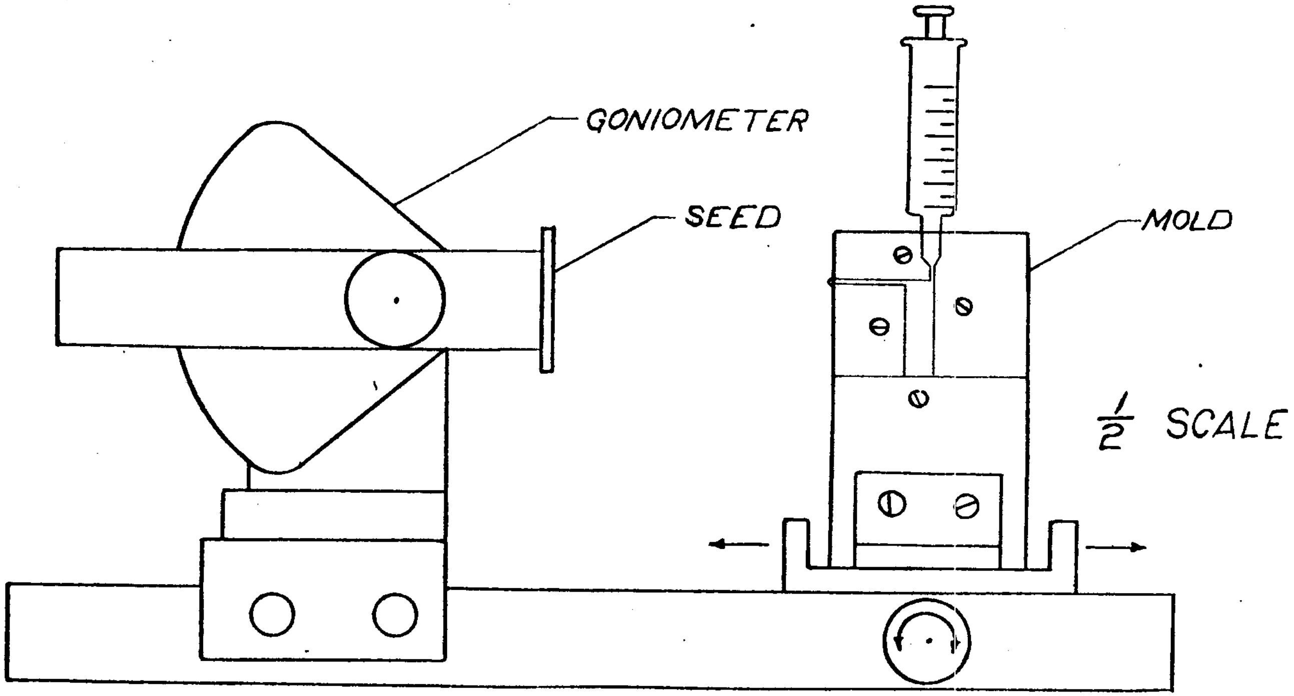

FIG. 3-13. APPARATUS FOR SEEDING GALLIUM CRYSTALS.

approximately 15 minutes after seeding, for a 0.80 mm-thick crystal in room-temperature surroundings. The crystal was easily separated from the lucite mold after soaking for a day in pure isopropyl alcohol, and its surfaces were mirror-smooth reproductions of the polished lucite surfaces.

X-ray back-reflection Laue photographs of the crystals were taken to check that the crystal axes coincided with the rectangular-plate axes to within 1°. Crystals which did not meet this requirement were rejected. Our labelling of the a, b, and c cyrstal axes is in agreement with that of Yaqub and Cochran (41), who present X-ray photographs in their paper to make this labelling unambiguous.

For studies of the electromagnetically-generated acoustic resonance, it was necessary that the two faces of the gallium plates be as nearly parallel as possible, and the thicknesses as well known as possible. Gallium crystals were grown, in the manner described above, whose two faces were parallel to ± 0.00025 cm. Their thickness could be measured to this accuracy by means of a good mechanical micrometer. Only those plates which possessed this degree of parallelism were used to obtain the ultrasonic velocity data which are presented in Chapter 5.

CHAPTER 4. ELECTROMAGNETIC GENERATION OF ACOUSTIC WAVES - EXPERIMENTAL RESULTS

Acoustic resonance singularities have been observed in the skin depths of gallium plates having several crystal orientations, and thicknesses of 0.010 and 0.030 inches. These singularities are seen at the frequencies

$$f_n = \frac{nS}{2d} , \quad n = 1, 3, 5, \ldots \qquad [1]$$

where S is the sound velocity and d is the thickness of the plate. With the external magnetic field directed so as to generate either longitudinal or transverse waves, singularities corresponding to n = 1, 3, and 5 have been studied.

In this chapter we present results which may be compared directly with the theory developed in Chapter 2. We rewrite, for reference, expression [2-15] for the acoustic resonance singularities in the complex skin depth:

$$\Delta\delta = -\frac{B_0^2 \cos^2\theta}{2\pi\rho d} \sum_{n=1}^{\infty} \frac{(1-\cos n\pi)}{(\omega^2 - \omega_n^2) + i\omega\gamma} . \qquad [2\text{-}15]$$

This theory, derived for a free-standing, infinite metal plate, with ideally uniform static and radio-frequency magnetic fields at the surfaces, predicts the excitation of a single transverse or longitudinal mode, for $\vec{B}_0$ in the appropriate plane. These conditions are only approximated, of course, in practice. The rectangular plate must be physically clamped or suspended in the apparatus, and the radio-frequency magnetic field, in particular, is inhomogeneous due to coil end-effects. These conditions have the effect of exciting vibrations other than a single shear- or longitudinal-thickness mode in the plate. In fact, the experimentally observed frequency spectrum of the skin depth in the neighbourhood of a transverse or longitudinal resonance was often found to contain several satellite peaks (*), the number and strength of which depended on the manner in which the sample was suspended within the specimen holder. In an attempt to obtain a single, clean resonance line, many suspension systems were tried, and the one found to be most satisfactory is illustrated in Fig. 4-1. The plate was held lightly by four pressure points on each side, located near its ends.

Extensive data were taken pertaining to the fundamental (n = 1) transverse-wave resonances in two 0.010-inch plates, and the following discussion will be confined mostly to these results. The two specimens (10 A_c-1 and 10 A_c-3) were grown with the b and c crystal axes in the plane of the plates; the rf surface currents flowed along the b-axis, and $\vec{B}_0$ lay in the a - b plane. The frequency spectra of the skin depth obtained using these two plates suspended as shown in Fig. 4-1 consisted almost entirely of the single, transverse-wave

---

(*) A further discussion of these extraneous vibrational modes is included in section 5.3.

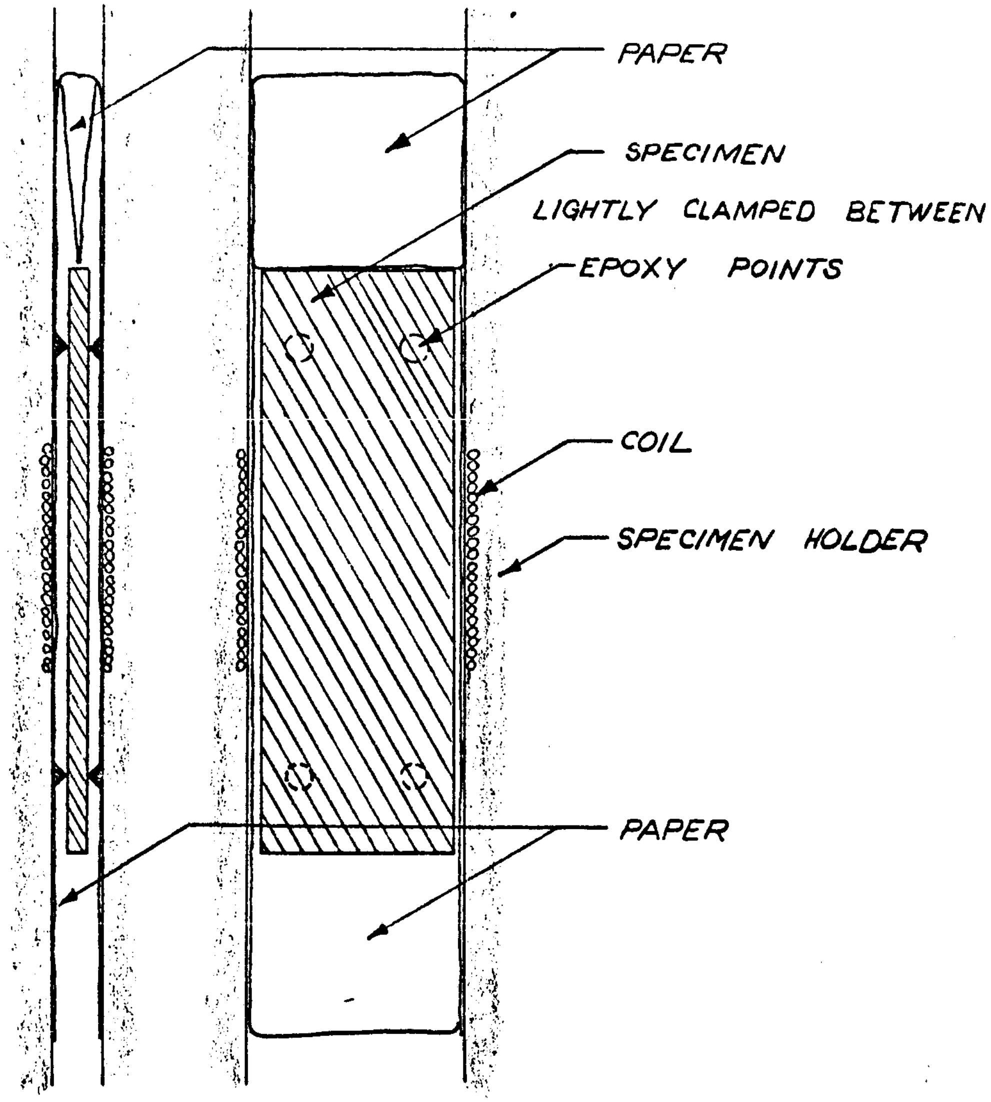

FIG. 4-1. SUSPENSION OF PLATE IN SPECIMEN HOLDER.

resonance line. Measurements were taken at temperatures between 1.2°K and 273°K. We present first the liquid-helium results, since the phase and amplitude calibration of the detection apparatus was known only over this temperature range.

A typical recorder trace showing singularities in the reactive and resistive skin depths is reproduced in Fig. 4-2. Some satellite resonances appear on the high-frequency side of the main peak. The background drift is due to the frequency dependence of the rf bridge balance.

Fig. 4-3 compares an experimentally observed resonance line with the theoretical prediction. The experimental (solid) curve was obtained at 4.2°K using a perpendicular magnetic field of 4 kG. This curve has been obtained from the recorder tracing by subtracting the background drift signal. The theoretical (dashed) curve was calculated from equation [2-15] using $\rho = 5.98$ g-cm^{-3}, $d = 0.26$ mm, and $\omega = 33.783 \times 10^6$ sec^{-1}. The linewidth, γ, in this expression was measured from the experimental curve: $\gamma = (8.1 \pm 0.6) \times 10^3$ sec^{-1}. This singularity in the skin depth represents a skin depth change of the order of 100% (27). Although the experimental accuracy of the ordinate is estimated to be ± 3%, a further error of ± 7% in Fig. 4-3 arises from an uncertainty in the frequency axis, and we regard the agreement with the theory to be satisfactory. It should be noted, however, that most of the observed resonance lines were slightly smaller in amplitude

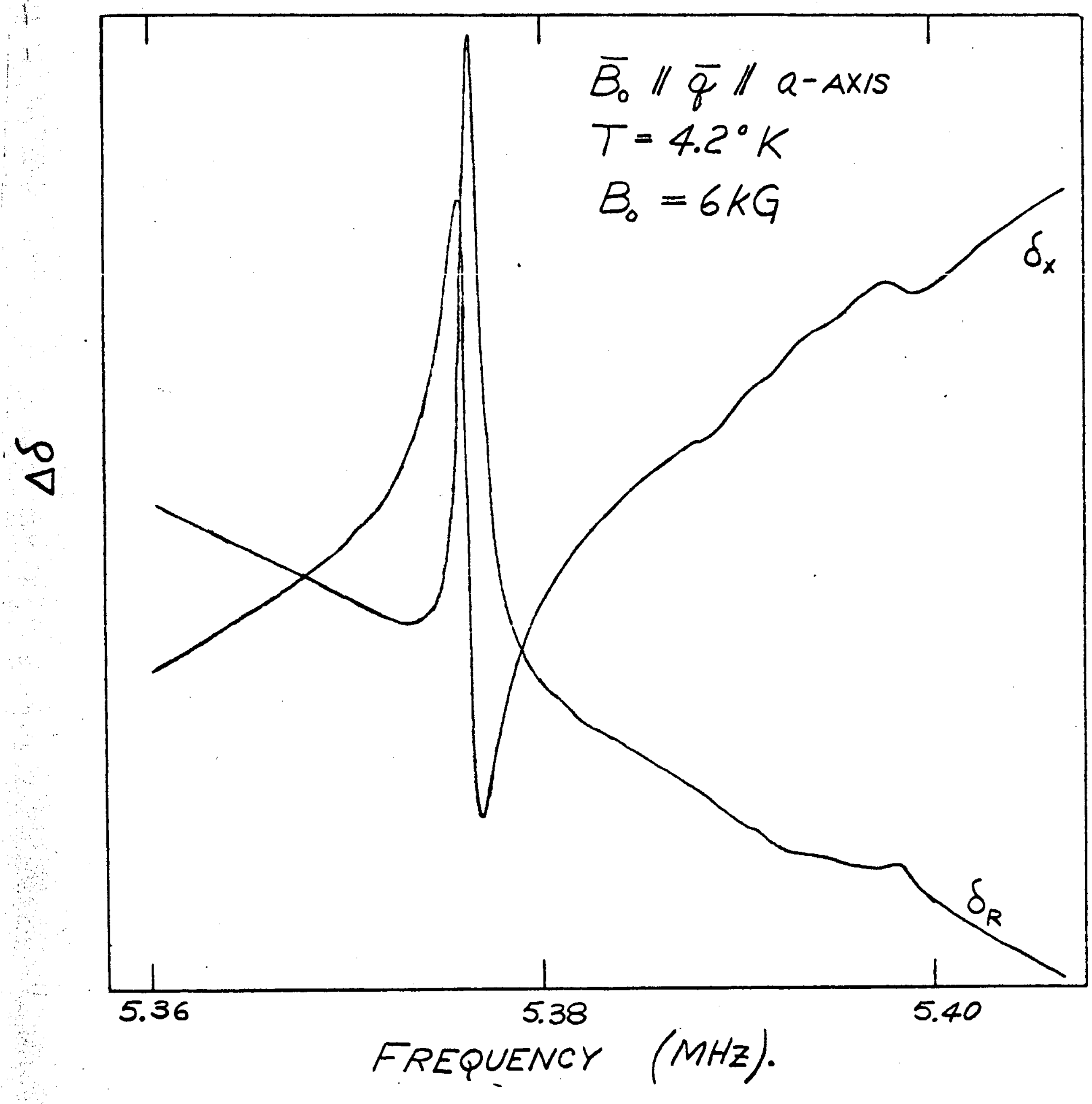

FIG. 4-2. ACOUSTIC SINGULARITIES IN THE REACTIVE AND RESISTIVE SKIN DEPTHS.

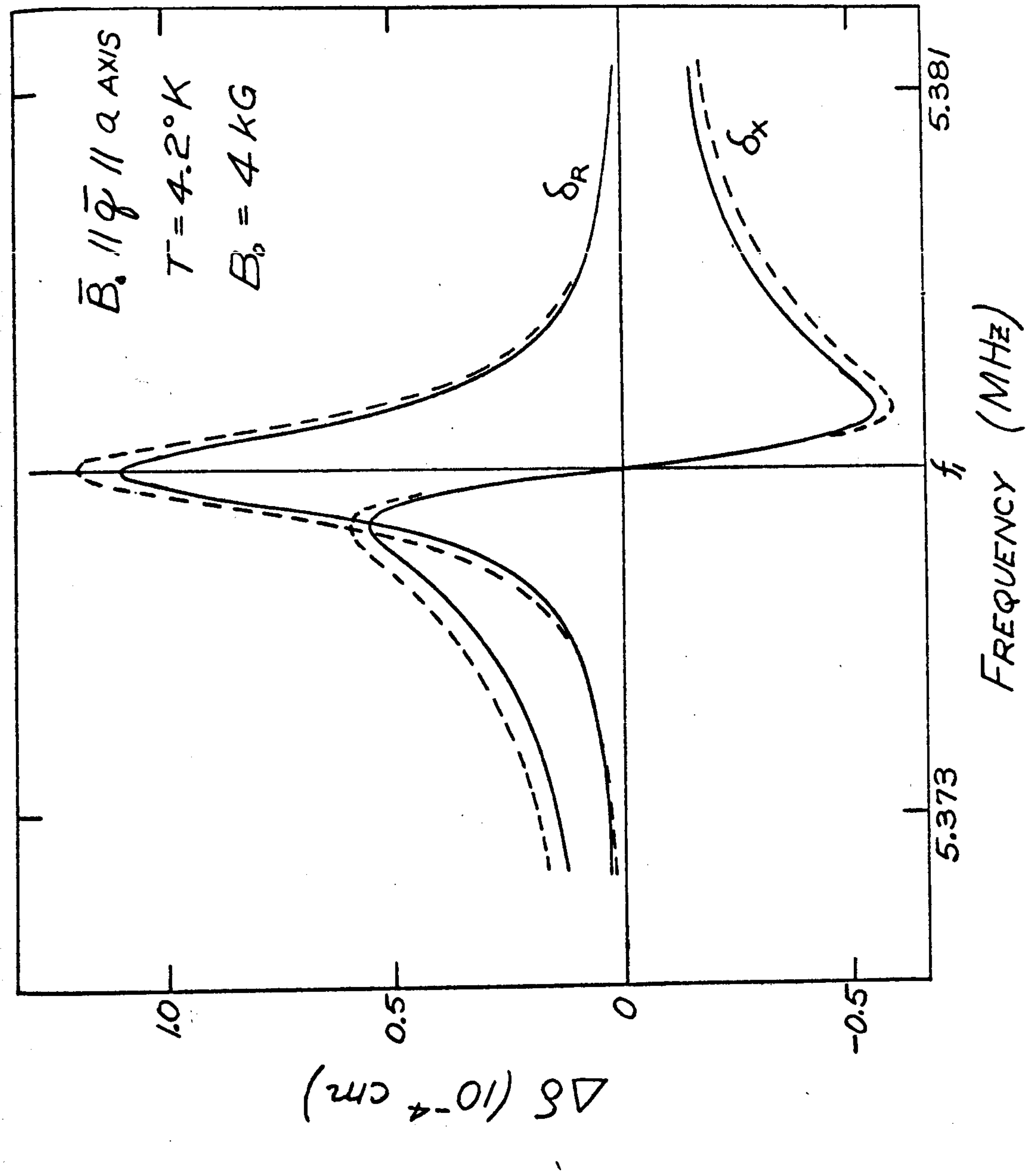

FIG. 4-3. ACOUSTIC RESONANCE IN THE SKIN DEPTH. EXPERIMENTAL (SOLID LINE) AND THEORETICAL (DASHED LINE).

than expected theoretically, possibly due to the fact that a small amount of acoustic energy was always coupled into other vibrational modes of the plate.

When the magnetic field is perpendicular to the plate, the background resistive skin depth increases almost quadratically with field. This effect, which was also observed with parallel magnetic fields for several crystal orientations in gallium (42), may be extremely large, the resistive skin depth increasing to fifty times its zero-field value (27) in a perpendicular field of 10 kG. A change in the background skin depth of this magnitude can change the coupling between the primary and secondary coils so as to appreciably affect the phase calibration of the detection apparatus (*). The result is that acoustic resonances superimposed on this background exhibit an apparent phase-shift, i.e., the detected δ_X and δ_R lineshapes become asymmetrical at high values of a perpendicular magnetic field. A second consequence of this large radio-frequency magnetoresistance is that the condition $\Delta/\lambda_s << 1$ may no longer hold, and the physical model which led to equation [2-15] may not be valid. This is also expected to result in a change in the resonance lineshapes, as suggested

---

(*) It was estimated in the previous chapter that the maximum skin depth change which could be recorded linearly by the detection apparatus at 7 MHz is $\Delta\delta_{max} \cong 2 \times 10^{-3}$ cm. This is approximately twenty times the zero-field skin depth in gallium (27).

in reference (17), but because of the experimental effect outlined above, it cannot be measured unambiguously. Resonances with $\vec{B}_0$ smaller than 4 or 5 kG, or inclined at an angle of more than 5 degrees from the normal, showed no measurable phase-shifts, and possessed the symmetrical Lorentzian lineshapes predicted by equation [2-15], as is illustrated in Fig. 4-3.

According to [2-15], the resonance amplitude is proportional to B_0^2, if $\vec{B}_0$ is fixed in direction and if the acoustic attenuation is independent of field. No deviations from this behaviour were observed for transverse waves (*), as is illustrated by the 4.2°K data of Fig. 4-4, obtained with the magnetic field perpendicular to the plate. This result is in agreement with the findings of others (†).

The theory also predicts that the resonance amplitude varies as $\cos^2\theta$, if the attenuation is independent of θ. A plot of amplitude versus θ at 4.2°K is shown in Fig. 4-5, where the reproducibility of the data corresponds approximately to the size of the circles in the figure. The deviations from the cosine-squared dependence (solid line) are associated with changes in the acoustic attenuation as the field is rotated. This was confirmed by the measurable changes in the resonance linewidth at the two discontinuities near 0° and 10°,

---

(*) A slight magnetic-field dependence of the longitudinal-wave attenuation at low temperatures is reported in section 6.3.

(†) See, for example, reference (43).

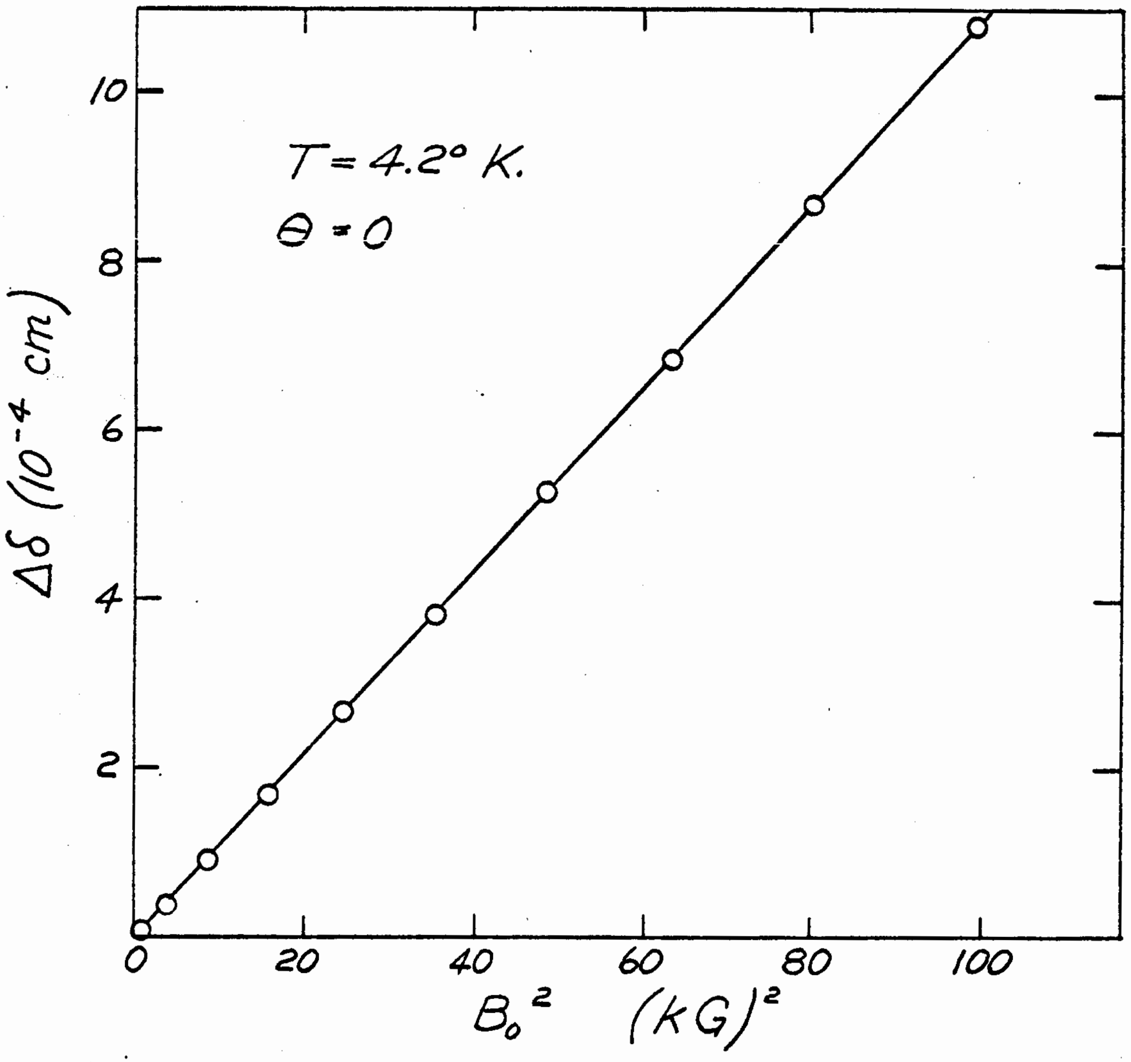

FIG. 4-4. VARIATION OF THE ACOUSTIC RESONANCE AMPLITUDE AS A FUNCTION OF B_0^2.

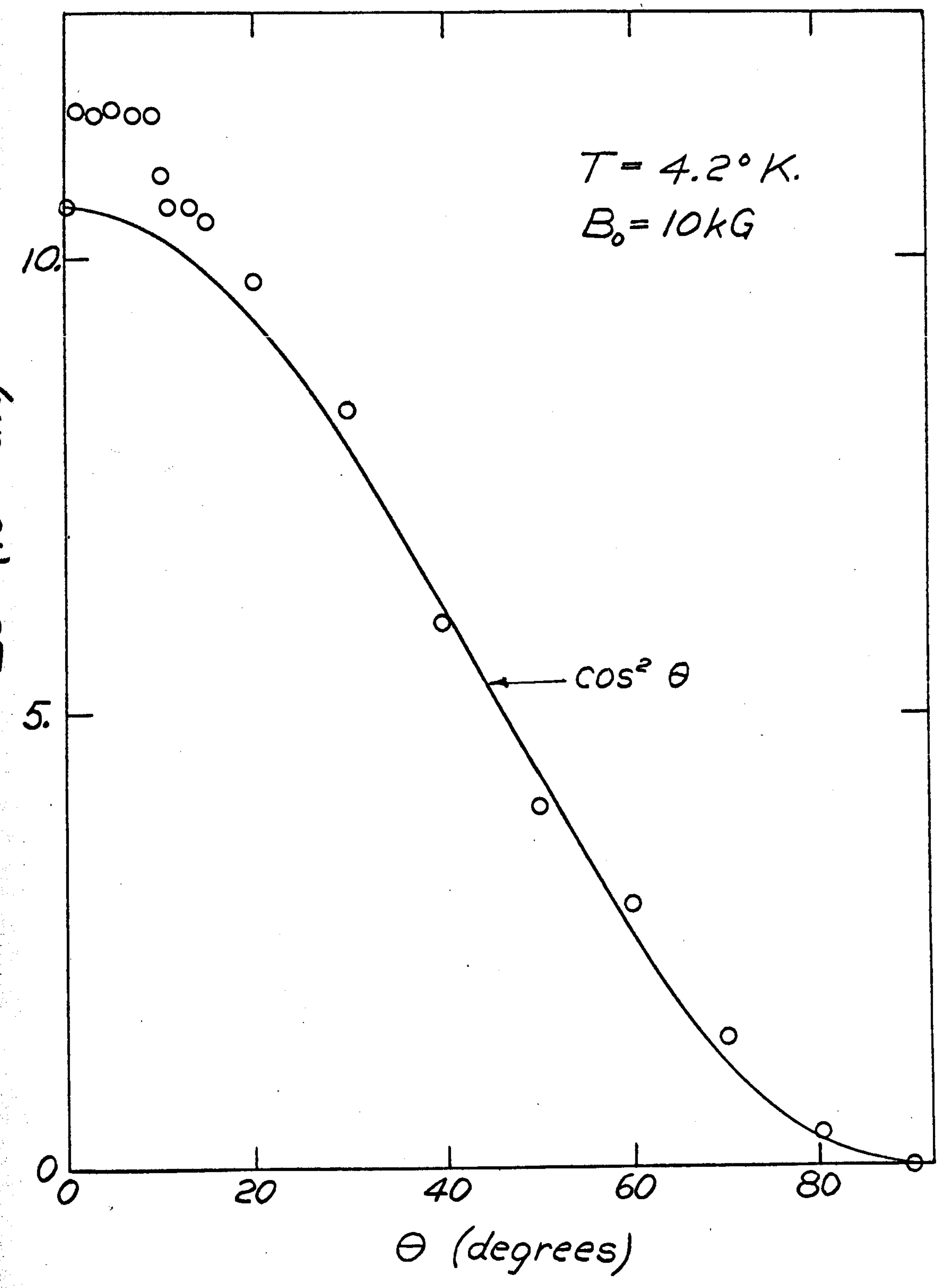

FIG. 4-5. VARIATION OF THE ACOUSTIC RESONANCE AMPLITUDE AS A FUNCTION OF θ.

corresponding to changes in the attenuation coefficient of approximately 0.001 cm^{-1}. No attempt has been made to correlate these deviations, which are not observed at higher temperatures, to properties of the Fermi surface of gallium.

The results presented thus far give us confidence in the correctness of the phenomenological model in predicting the electromagnetic-acoustic coupling at the surface of a metal. The Lorentzian lineshape and the absolute amplitude of the observed resonances in the skin depth, and the amplitude dependence on B_0^2 and on $\text{Cos}^2\theta$ are all in good agreement with the predictions of the model.

But one effect observed at temperatures below 4.2°K was not in accord with the theory. A study of the behaviour of the resonance amplitude and linewidth was carried out at temperatures between 1.2 K and 4.2 K using six .030 inch thick "on-axis" specimens. These specimens represented all of the possible orientations for which the crystal axes coincided with the axes of the rectangular plates. As the temperature was reduced from 4.2°K to 1.2°K, the acoustic attenuation and hence the linewidth of the transverse-wave resonances increased by as much as 2.5 times, although this factor varied with crystal orientation. According to [2.5], this increase in linewidth should be accompanied by a corresponding decrease in resonance amplitude. In four of the six crystals this behaviour was confirmed to within the accuracy of the measurement. In the remaining two crystals, however, (in each the lattice displacement was polarized along the a-axis), a behaviour was observed which is completely unexplained by the theory. In these crystals the resonance amplitude increased rapidly; in one specimen the amplitude at 1.5°K was ten times larger than that predicted. This "anomalous" behaviour is shown in Fig. 4-6. The open circles represent the measured amplitudes, and the solid circles the amplitudes calculated from equation [2-15] and the measured linewidths. Fig. 4-6 indicates that the measured amplitudes approximate the predicted amplitudes at temperatures down to 6°K, (*) but are greatly enhanced at lower temperatures. The resonance amplitude in this specimen at 1.5°K is plotted as a function of B_0^2 in Fig. 4-7. There is a marked deviation from the linear dependence predicted by [2-15], and observed in the other crystals (see Fig. 4-4).

We are unable to explain this drastic change in the acoustic generation at temperatures between 1.5°K and 6°K. That the effect is observed in only two of the six crystal orientations is presumably due to the anisotropic Fermi

---

(*) The discrepancy at temperatures above 6°K can be explained by the hypothesis that energy was coupled to several other resonant modes in this .030-inch thick plate; further, it is not known how much the absolute calibration of the apparatus changes at temperatures above 4°K.

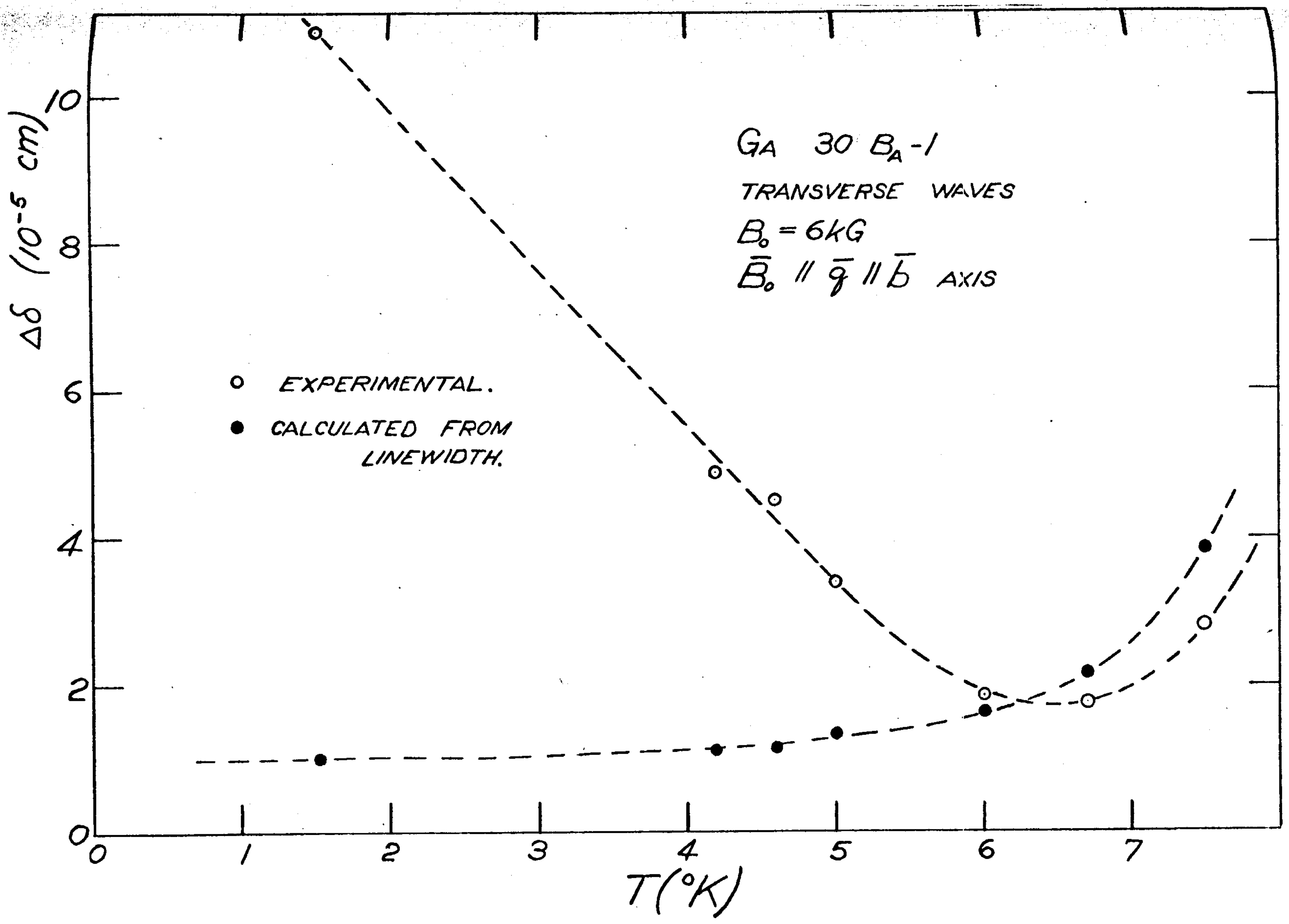

FIG. 4-6. ANOMALOUS EFFECT OBSERVED IN THE ACOUSTIC RESONANCE AT LOW TEMPERATURES. RESONANCE AMPLITUDE VERSUS TEMPERATURE.

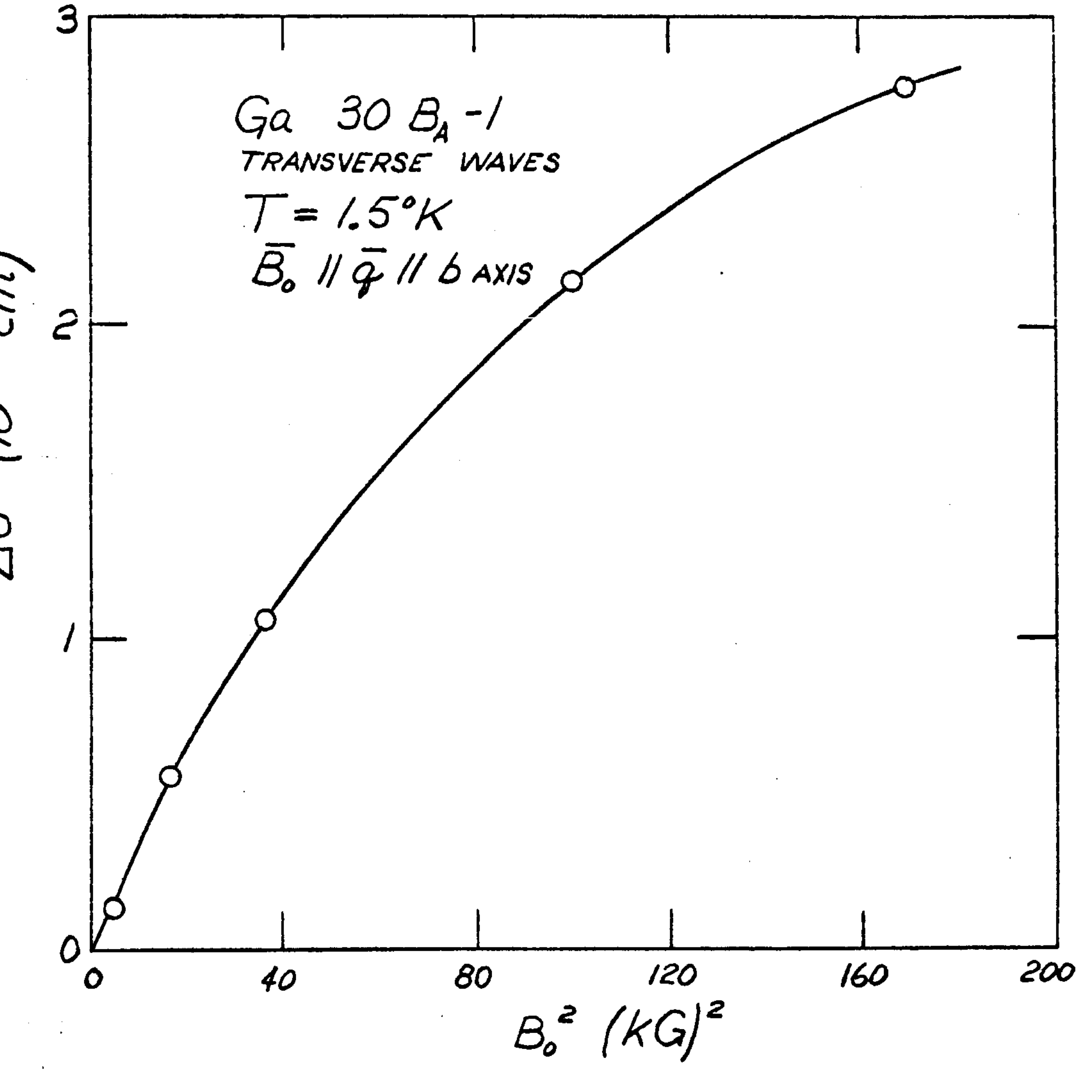

FIG. 4-7. ANOMALOUS EFFECT OBSERVED IN THE ACOUSTIC RESONANCE AT LOW TEMPERATURES. RESONANCE AMPLITUDE VERSUS B_o^2.

surface of gallium (*). There is evidence that this peculiar low-temperature behaviour is also present for the longitudinal wave resonances, although a complete study of the temperature variation in crystals of different orientations has not been carried out.

Acoustic resonances were observed at temperatures up to 273 K. The most striking feature of these results is the strong variation of the linewidth, γ, as a function of temperature. This variation is illustrated in Fig. 4-8, where the quality factor is

$$Q = \frac{\omega_n}{\gamma} .$$

These data, obtained from the transverse-wave resonance in a .030-inch specimen, are typical of the behaviour that was observed for both transverse and longitudinal waves. The maximum Q occurred at temperatures between 40°K and 50°K. The highest Q's (up to 3.5×10^5) were possibly limited by extrinsic damping; slightly sharper lines were observed when the specimen can was evacuated than when an exchange gas was present. These extremely sharp resonances were observable at fields as small as 10 gauss.

(*) In a recent paper, Reed (44) has calculated the band structure of gallium using a semiempirical pseudopotential method. The resulting Fermi surface consists of six closed electron sheets, one closed hole sheet, and a large multiply-connected hole sheet. Although much experimental data is explained by this model, apparently one or more small pieces of Fermi surface have been missed in the calculation.

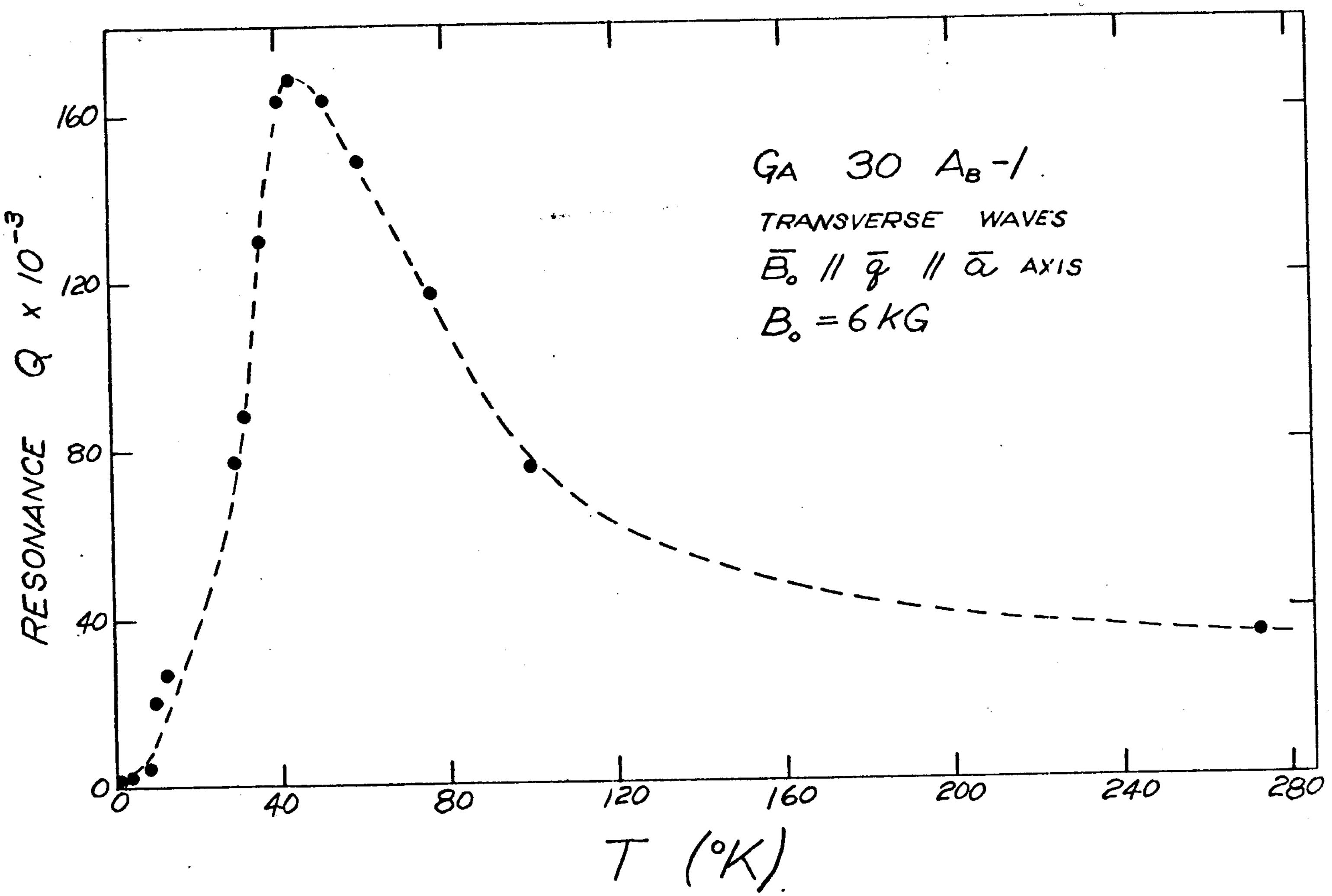

FIG. 4-8. VARIATION OF THE ACOUSTIC RESONANCE Q AS A FUNCTION OF TEMPERATURE.

It is interesting to note that non-parallelism of the plate does not spoil the quality factor of the resonances, but instead splits the line. In an experiment using a wedge-shaped plate of single-crystal aluminum, with $\Delta d/d$ estimated to be approximately 4%, two resonance lines were observed, with $\Delta f/f \cong 4\%$. Gantmakher (35) has similarly reported the splitting of radio-frequency size-effect lines in a wedge-shaped plate of indium.

CHAPTER 5. ELASTIC CONSTANTS OF GALLIUM

5.1 Introduction

According to the theory developed in Chapter 2 for an infinite metal plate immersed in a static magnetic field, singularities in the surface impedance of the plate occur at frequencies

$$f_n = \frac{nS}{2d} , \qquad [1]$$

where d is the plate thickness, S is the velocity of the acoustic wave which is present in the plate, and n is an odd integer. The resonant frequencies may thus be used to determine acoustic velocities in a metal. Since no velocity data for gallium have been published (*), we have used this continuous-wave resonance technique to obtain the acoustic velocities in single crystals of gallium at 4.2°K, 77°K, and 273°K, at low megahertz frequencies.

Determination of the nine elastic constants of orthorhombic gallium requires a minimum of nine velocity measurements at a given temperature; further measurements may be used to provide cross-checks of the data. From the elastic

---

(*) Measurements of unstated accuracy of the gallium elastic moduli at 273°K have been reported in a U.S. government document by Roughton and Nash (21). Their results are discussed briefly in section 5.3.

constants a Debye temperature, θ_D, may be calculated which is characteristic of the crystal. Since the Debye theory treats the solid as a continuum, it provides a good approximation at low temperatures, where only long-wavelength vibrational modes are excited, and the discrete nature of the crystal becomes unimportant. In fact, the Debye temperatures obtained from low temperature specific heat and ultrasonic velocity measurements have been found to agree for a large number of crystals (45).

In section 5.2, the elastic constants are defined, and their determination from velocity measurements is discussed. An approximate method of calculating θ_D from the constants following Anderson (46), is also included. The experimental results are presented in section 5.3, and in 5.4 the validity of the continuous-wave resonance technique is examined.

5.2 Theory

5.2.1 Wave propagation in elastic solids

In this section we develop the formalism which relates the acoustic velocities in a crystal to the elastic moduli, using the notation of Bhatia (47) and of Neighbours and Schacher (48). A more complete development may be found in these two references.

The forces acting on a volume element ($dx_1dx_2dx_3$) in a solid may be described by the nine stress components, σ_{ij}, $i,j = 1, 2, 3$ (Fig. 5-1). σ_{ij} is the component of force per unit area in the x_j direction which acts on the plane perpendicular to the x_i axis. For equilibrium, the torques about each axis must vanish, and therefore

$$\begin{aligned} \sigma_{12} &= \sigma_{21} \\ \sigma_{13} &= \sigma_{31} \\ \sigma_{23} &= \sigma_{32} \end{aligned} \qquad [2]$$

In writing equations [2], we assume that there are no interactions within the solid that produce torques in addition to those due to the stress components σ_{ij}.

Let $\xi_i(\vec{x})$ be the ith component of the displacement of the solid at a point $\vec{x}$. Then the equation of motion for free sound propagation is

$$\rho' \frac{\partial^2 \xi_i}{\partial t^2} = \frac{\partial \sigma_{ji}}{\partial x_j} , \qquad [3]$$

where ρ' is the density of the solid, which may be approximated by the density in the absence of wave propagation, ρ. In order to write the wave equation [3] in terms of the displacement $\vec{\xi}$, we define the strain, or deformation, components

$$\epsilon_{ij} = \frac{1}{2}\left\{\frac{\partial \xi_i}{\partial x_j} + \frac{\partial \xi_j}{\partial x_i}\right\}, \quad \epsilon_{ij} = \epsilon_{ji} . \qquad [4]$$

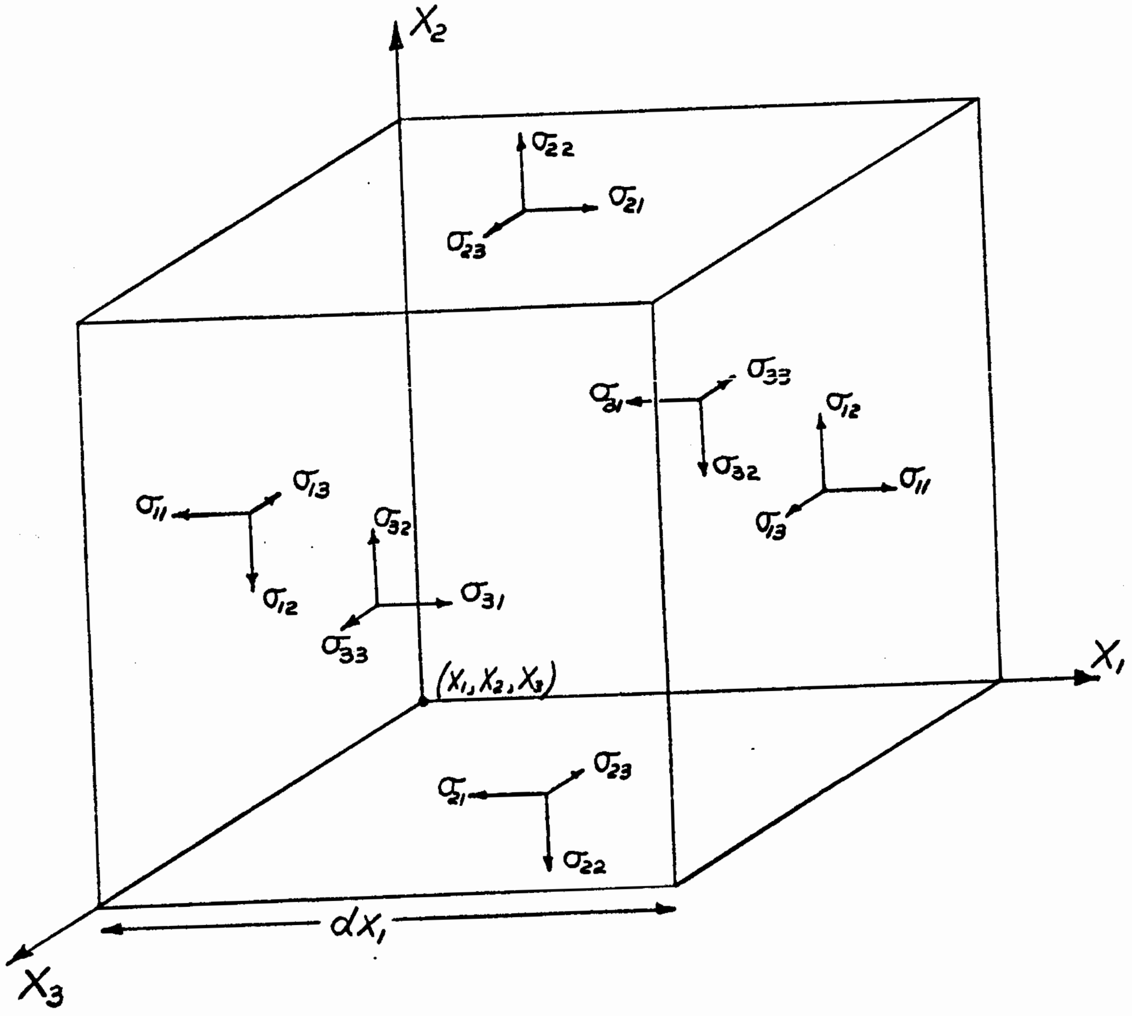

FIG. 5-1. COMPONENTS OF STRESS IN A CRYSTAL.

For small $(\partial\xi_i/\partial x_i \ll 1)$ displacements, the six quantities ε_{ij} completely describe the changes in the volume, V, and the shape of the solid. The fractional change in volume, or the dilation, is

$$\Delta = \frac{dV}{V} = \epsilon_{11} + \epsilon_{22} + \epsilon_{33} = \mathrm{div}\,\vec{\xi}, \qquad [5]$$

while ε_{23}, ε_{13}, and ε_{12} are the components of shear strain in the planes perpendicular to the X_1, X_2, and X_3 axes.

If Hooke's law is obeyed, each of the 6 strain components at a given point in the solid is linearly related to the 6 stress components at that point, and the 36 elastic stiffness constants, $C_{ijk\ell}$, are defined: (*)

$$\sigma_{ij} = C_{ijk\ell}\,\epsilon_{k\ell}\,. \qquad [6]$$

Similarly, the 36 elastic compliance constants, $S_{ijk\ell}$:

$$\epsilon_{ij} = S_{ijk\ell}\,\sigma_{k\ell}\,. \qquad [7]$$

A contracted notation is commonly used:

(*) Throughout this chapter, we use the summation convention:

$$C_{ijk\ell}\,\varepsilon_{k\ell} \equiv \sum_k \sum_\ell C_{ijk\ell}\,\varepsilon_{k\ell}.$$

$$\begin{aligned} \sigma_1 &= \sigma_{11} & \epsilon_1 &= \epsilon_{11} \\ \sigma_2 &= \sigma_{22} & \epsilon_2 &= \epsilon_{22} \\ \sigma_3 &= \sigma_{33} & \epsilon_3 &= \epsilon_{33} \\ \sigma_4 &= \sigma_{23} = \sigma_{32} & \epsilon_4 &= 2\epsilon_{23} = 2\epsilon_{32} \\ \sigma_5 &= \sigma_{13} = \sigma_{31} & \epsilon_5 &= 2\epsilon_{13} = 2\epsilon_{31} \\ \sigma_6 &= \sigma_{12} = \sigma_{21} & \epsilon_6 &= 2\epsilon_{12} = 2\epsilon_{21} \end{aligned}$$

$$\left.\begin{aligned} \sigma_m &= C_{mn}\epsilon_n \\ \epsilon_m &= S_{mn}\sigma_n \end{aligned}\right\} (m, n = 1, 2 \ldots 6).$$

From the requirement that the increase in the energy of the solid per unit volume, $dW = \sigma_m d\varepsilon_m$, be a single-valued function of the strain components, it follows that (47)

$$C_{mn} = C_{nm}, \qquad [9]$$

and the number of independent elastic stiffness constants is reduced from 36 to 21. This number is further reduced in crystals which possess rotational symmetry: crystals belonging to the orthorhombic system (e.g., gallium) have nine independent elastic constants. If the coordinate axes coincide with the three symmetry axes of the orthorhombic crystal, the nine elastic constants may be written as the array:

$$C_{mn} = \begin{pmatrix} C_{11} & C_{12} & C_{13} & 0 & 0 & 0 \\ C_{12} & C_{22} & C_{23} & 0 & 0 & 0 \\ C_{13} & C_{23} & C_{33} & 0 & 0 & 0 \\ 0 & 0 & 0 & C_{44} & 0 & 0 \\ 0 & 0 & 0 & 0 & C_{55} & 0 \\ 0 & 0 & 0 & 0 & 0 & C_{66} \end{pmatrix} . \qquad [10]$$

In crystals of cubic symmetry, the matrix is the same as above, but with

$$C_{11} = C_{22} = C_{33}$$
$$C_{12} = C_{13} = C_{23}$$
$$C_{44} = C_{55} = C_{66}$$

In elastically-isotropic crystals, the 3 independent constants of a cubic crystal are reduced to 2 by the relation

$$2C_{44} = C_{11} - C_{12} .$$

The equation of motion, [2], may now be rewritten in terms of the elastic stiffness constants, C_{mn}. From equations [3] and [8]:

$$\begin{aligned} \rho \frac{\partial^2 \xi_1}{\partial t^2} &= \frac{\partial \sigma_1}{\partial x_1} + \frac{\partial \sigma_6}{\partial x_2} + \frac{\partial \sigma_5}{\partial x_3} \\ \rho \frac{\partial^2 \xi_2}{\partial t^2} &= \frac{\partial \sigma_6}{\partial x_1} + \frac{\partial \sigma_2}{\partial x_2} + \frac{\partial \sigma_4}{\partial x_3} \\ \rho \frac{\partial^2 \xi_3}{\partial t^2} &= \frac{\partial \sigma_5}{\partial x_1} + \frac{\partial \sigma_4}{\partial x_2} + \frac{\partial \sigma_3}{\partial x_3} . \end{aligned} \qquad [11]$$

For the simplest case, that of an isotropic solid, these equations reduce to a single vector equation:

$$\rho \frac{\partial^2 \vec{\xi}}{\partial t^2} = (C_{12} + 2C_{44}) \vec{\nabla}(\vec{\nabla} \cdot \vec{\xi}) - C_{44} \vec{\nabla} \times (\vec{\nabla} \times \vec{\xi})$$

$$= C_\ell \vec{\nabla}(\vec{\nabla} \cdot \vec{\xi}) - C_t \vec{\nabla} \times (\vec{\nabla} \times \vec{\xi}). \qquad [12]$$

The irrotational (purely longitudinal) and isovoluminous (purely transverse) waves propagate independently through the isotropic solid with velocities $[(C_{12} + 2C_{44})/\rho]^{\frac{1}{2}}$ and $(C_{44}/\rho)^{\frac{1}{2}}$, respectively.

In an anisotropic crystal, the propagating waves will in general have neither a purely longitudinal, nor a purely transverse, character, and the equations which relate the experimentally observed velocities to the elastic constants of the crystal are complicated. The impure modes which propagate, however, are characterized by displacements which are nearly parallel (quasi-longitudinal) or nearly perpendicular (quasi-transverse) to the propagation direction, and for any direction in the crystal it is possible to measure 3 velocities which correspond to two pure or quasi-transverse modes and one pure or quasi-longitudinal mode. We now outline the procedure given by Neighbours and Schacher (48) to determine the elastic constants from sound-velocity measurements in crystals of general symmetry.

The equations [11] may be simplified by choosing a coordinate system (x_1', x_2', x_3') such that the wave propagation is along x_1'; derivatives with respect to x_2' and x_3' then vanish, and these equations become:

$$\rho \frac{\partial^2 \xi_1'}{\partial t^2} = C_{11}' \frac{\partial^2 \xi_1'}{\partial x_1'^2} + C_{16}' \frac{\partial^2 \xi_2'}{\partial x_1'^2} + C_{15}' \frac{\partial^2 \xi_3'}{\partial x_1'^2}$$

$$\rho \frac{\partial^2 \xi_2'}{\partial t^2} = C_{16}' \frac{\partial^2 \xi_1'}{\partial x_1'^2} + C_{66}' \frac{\partial^2 \xi_2'}{\partial x_1'^2} + C_{56}' \frac{\partial^2 \xi_3'}{\partial x_1'^2} \qquad [13]$$

$$\rho \frac{\partial^2 \xi_3'}{\partial t^2} = C_{15}' \frac{\partial^2 \xi_1'}{\partial x_1'^2} + C_{56}' \frac{\partial^2 \xi_2'}{\partial x_1'^2} + C_{55}' \frac{\partial^2 \xi_3'}{\partial x_1'^2} .$$

The primed notation C_{mn}' is used to distinguish these elastic constants, defined in the x_1', x_2', x_3' system, from the desired constants C_{mn}, defined in the coordinate system (x_1, x_2, x_3) which coincides with the symmetry axes of the crystal. (The C_{mn}'s are then obtained from the C_{mn}''s by means of transformations which are given, for orthorhombic crystals, in equations [16]). The secular equation which results from [13] is

$$\begin{vmatrix} (C_{11}' - \rho V^2) & C_{16}' & C_{15}' \\ C_{16}' & (C_{66}' - \rho V^2) & C_{56}' \\ C_{15}' & C_{56}' & (C_{55}' - \rho V^2) \end{vmatrix} = 0 . \qquad [14]$$

This equation possesses three roots corresponding to the velocities V of the one (quasi) longitudinal and two (quasi) transverse modes. It has been solved by means of a perturbation method by Neighbours and Schacher. The solution is:

$$C_{11}' = \rho V_1^2 - \left[\frac{C_{15}'^{\,2}}{C_{11}' - C_{55}'} + \frac{C_{16}'^{\,2}}{C_{11}' - C_{66}'} + \frac{2C_{15}'C_{16}'C_{56}'}{(C_{11}' - C_{55}')(C_{11}' - C_{66}')} + \cdots \right]$$

$$C_{66}' = \rho V_2^2 - \left[\frac{C_{16}'^{\,2}}{C_{66}' - C_{11}'} + \frac{C_{56}'^{\,2}}{C_{66}' - C_{55}'} + \frac{2C_{15}'C_{16}'C_{56}'}{(C_{66}' - C_{11}')(C_{66}' - C_{55}')} + \cdots \right] \qquad [15]$$

$$C_{55}' = \rho V_3^2 - \left[\frac{C_{15}'^{\,2}}{C_{55}' - C_{11}'} + \frac{C_{56}'^{\,2}}{C_{55}' - C_{66}'} + \frac{2C_{15}'C_{16}'C_{56}'}{(C_{55}' - C_{11}')(C_{66}' - C_{55}')} + \cdots \right] .$$

Finally, the unprimed constants are related to the primed constants by the cosines of the angles between the $(x_1'x_2'x_3')$ and $(x_1x_2x_3)$ coordinate systems. The positive direction cosines ℓ, m, and n specify the x'-axis orientation with respect to the x_1, x_2, and x_3 axes (e.g., the a, b, and c axes of gallium), and if we choose to let x_2' lie in the

$x_1 - x_2$ plane (x'_1 is the direction of wave propagation) the complete set of direction cosines may be presented in the form:

	x_1	x_2	x_3
x'_1	ℓ	m	n
x'_2	$-m\alpha^{-1}$	$\ell\alpha^{-1}$	0
x'_3	$-\ell n\alpha^{-1}$	$-mn\alpha^{-1}$	α

where $\alpha^2 = \ell^2 + m^2$, and we have assumed that the angles between x_1 and x'_1, x_2 and x'_2, and x_3 and x'_3 are all less than 90°. The transformation equations, written in terms of these direction cosines for the 6 primed elastic constants occurring in equation [15] are given, for all crystal classes, by Neighbours and Schacher. Reproduced below are the transformations appropriate for crystals of orthorhombic symmetry: (*)

$$C'_{11} = \ell^4 C_{11} + m^4 C_{22} + n^4 C_{33} + 4m^2n^2 C_{44} + 4\ell^2 n^2 C_{55}$$
$$+ 4\ell^2 m^2 C_{66} + 2\ell^2 m^2 C_{12} + 2\ell^2 n^2 C_{13} + 2m^2 n^2 C_{23} .$$

(*) Note that from [14] and [15], for sound waves propagating along the x' axis, the velocities are related only to the six primed constants C'_{11}, C'_{55}, C'_{66}, C'_{15}, C'_{16}, and C'_{56}, and therefore only transformation equations for these six constants are required.

$$C'_{55} = l^4 n^2 \alpha^{-2} C_{11} + m^4 n^2 \alpha^{-2} C_{22} + n^2 \alpha^2 C_{33} + m^2 \alpha^{-2} (1-2n^2)^2 C_{44}$$
$$+ l^2 \alpha^{-2} (1-2n^2)^2 C_{55} + 4l^2 m^2 n^2 \alpha^{-2} C_{66} + 2l^2 m^2 n^2 \alpha^{-2} C_{12}$$
$$-2l^2 n^2 C_{13} - 2m^2 n^2 C_{23} .$$

$$C'_{66} = l^2 m^2 \alpha^{-2} C_{11} + l^2 m^2 \alpha^{-2} C_{22} + l^2 n^2 \alpha^{-2} C_{44} + m^2 n^2 \alpha^{-2} C_{55}$$
$$+ \alpha^{-2} (l^2 - m^2)^2 C_{66} - 2l^2 m^2 \alpha^{-2} C_{12} .$$

$$C'_{15} = -l^4 n \alpha^{-1} C_{11} - m^4 n \alpha^{-1} C_{22} + n^3 \alpha C_{33} + 2m^2 n \alpha^{-1} (1-2n^2) C_{44}$$
$$+ 2l^2 n \alpha^{-1} (1-2n^2) C_{55} - 4l^2 m^2 n \alpha^{-1} C_{66} - 2l^2 m^2 n \alpha^{-1} C_{12}$$
$$+ l^2 n \alpha^{-1} (1-2n^2) C_{13} + m^2 n \alpha^{-1} (1-2n^2) C_{23} .$$

[16]

$$C'_{16} = -l^3 m \alpha^{-1} C_{11} + l m^3 \alpha^{-1} C_{22} + 2lmn^2 \alpha^{-1} C_{44}$$
$$-2lmn^2 \alpha^{-1} C_{55} + 2lm \alpha^{-1} (l^2 - m^2) C_{66}$$
$$+ lm \alpha^{-1} (l^2 - m^2) C_{12} - lmn^2 \alpha^{-1} C_{13} + lmn^2 \alpha^{-1} C_{23} .$$

$$C'_{56} = l^3 mn \alpha^{-2} C_{11} - lm^3 n \alpha^{-2} C_{22} + lmn \alpha^{-2} (1-2n^2) C_{44}$$
$$- lmn \alpha^{-2} (1-2n^2) C_{55} - 2lmn \alpha^{-2} (l^2 - m^2) C_{66}$$
$$- lmn \alpha^{-2} (l^2 - m^2) C_{12} - lmn C_{13} + lmn C_{23} .$$

It is seen that the C'_{mn}'s are linear functions of the C_{mn}'s, and equations [15] may be written in terms of the unprimed constants. For crystal directions in which pure modes propagate, the secular determinant [14] is diagonal, and the bracketed terms in [15] vanish. For directions in which impure modes propagate, the bracketed terms in [15] are present, but small compared to the ρV^2 terms, and these equations may be solved by the method of successive approximations. In practice, the calculations are eased by making as many pure-mode velocity measurements as possible. In the experiments described here, the six diagonal constants, C_{ii}, were first obtained from the velocities of pure transverse and longitudinal modes. Quasi-longitudinal modes were then propagated in the three "off-axis" crystals with $\ell = 0$, $m = 0$, and $n = 0$, respectively; in each of these cases two out of the three off-diagonal terms in the determinant [14] vanish, and the first of equations [15] yields the constants C_{23}, C_{13}, and C_{12} directly from the measured velocities. This procedure will be discussed in more detail in section 5.3.

5.2.2. The Debye temperature

The Debye theory of lattice specific heat is based on a model which replaces the atomic nature of the solid by an isotropic continuum through which acoustic excitations may propagate. This model leads to a quadratic frequency spectrum of vibrations up to a maximum frequency, ν_D, from which the Debye temperature, θ_D, is defined:

$$\theta_D = \frac{h\nu_D}{k} , \qquad [17]$$

where h and k are the Planck and Boltzmann constants. The theory yields a temperature-dependent lattice specific heat which is determined by the Debye temperature characteristic of a solid. At low temperatures, where only long-wavelength vibrations are excited in a crystal, the discrete nature of the lattice is least important, and the Debye model correctly predicts the observed T^3 dependence of the lattice specific heat. At temperatures $T < (\theta_D/10)$, the predicted specific heat is (49)

$$C_V = 1944 \left(\frac{T}{\theta_D}\right)^3 \text{ J/mole-degree} \qquad [18]$$

The elastic and thermal properties of solids are simply related according to the Debye theory, since the Debye temperature may also be determined from the velocity, v_m, of acoustic waves in the continuum (46):

$$\theta_D = \frac{h}{k}\left(\frac{3}{4\pi}\frac{\eta}{V_0}\right)^{1/3} v_m , \qquad [19]$$

where η is the number of atoms per unit cell, and V_0 is the volume of the unit cell. At low temperatures, then, the Debye temperature obtained by calorimetric measurements and equation [18] may be compared with that derived from acoustic-wave velocity measurements, if an appropriate mean velocity is used for the velocity v_m.

In an anistropic crystal, the velocity of elastic waves depends upon the propagation direction in the crystal, and in any direction there are three different velocities associated with the two (quasi) transverse, and one (quasi) longitudinal modes which may propagate. v_m in equation [19] must then be a velocity which is the average of these three velocities, v_i, in all crystal directions (46):

$$\frac{1}{v_m^3} = \frac{1}{3}\sum_{i=1}^{3}\int_{Vol.}\frac{1}{v_i^3}\frac{d\Omega}{4\pi} , \qquad [20]$$

where $d\Omega$ is an element of solid angle. Several numerical methods have been devised to evaluate v_m from equation [20], using the measured single crystal elastic constants (45, 50).

Anderson (46) has proposed and tested an alternative (to equation [20]) method of determining the mean sound velocity in anisotropic crystals. Equation [20] reduces to a very simple form for isotropic crystals, in which the transverse and longitudinal velocities, v_T and v_L, are invariant with respect to propagation direction:

$$v_m = \left[\frac{1}{3}\left(\frac{2}{v_T^3} + \frac{1}{v_L^3}\right)\right]^{-1/3}. \qquad [21]$$

Anderson suggested that in anisotropic crystals, average transverse and longitudinal velocities calculated from the elastic constants be used in equation [21] to arrive at an approximate mean sound velocity v_m (approx.). We now outline this method, called by Anderson the VRHG approximation after Voight, Reuss, Hill, and Gilvarry.

The VRGH approximation is based on relations between the isotropic bulk and shear moduli, K and G, of a polycrystalline solid and its single-crystal elastic constants. According to Anderson, Voight related these moduli to the stiffness constants:

$$K_V = \frac{1}{9}(C_{11} + C_{22} + C_{33}) + \frac{2}{9}(C_{12} + C_{23} + C_{13}) \qquad [22]$$

$$G_V = \frac{1}{15}(C_{11} + C_{22} + C_{33}) - \frac{1}{15}(C_{12} + C_{23} + C_{13}) + \frac{1}{5}(C_{44} + C_{55} + C_{66}). \qquad [23]$$

whereas Reuss expressed the moduli in terms of the compliance constants: (*)

$$\frac{1}{K_R} = (S_{11} + S_{22} + S_{33}) + 2(S_{12} + S_{23} + S_{13}) \qquad [24]$$

$$\frac{15}{G_R} = 4(S_{11} + S_{22} + S_{33}) - 4(S_{12} + S_{23} + S_{13}) + 3(S_{44} + S_{55} + S_{66}). \qquad [25]$$

Hill (51) proved that the Voight and Reuss approximations represent the upper and lower bounds to the true polycrystalline moduli, and suggested that the average between the two be used

---

(*) There is an error in sign in Anderson's form of equation [25] (46).

as a practical estimate:

$$K_H = \frac{K_V + K_R}{2}; \qquad G_H = \frac{G_V + G_R}{2} . \qquad [26]$$

The transverse and longitudinal velocities in the isotropic, polycrystalline solid are, using the Hill moduli:

$$\overline{v}_T = \left(\frac{G_H}{\rho}\right)^{1/2} \qquad [27]$$

and

$$\overline{v}_L = \left(\frac{K_H + \frac{4}{3}G_H}{\rho}\right)^{1/2}. \qquad [28]$$

Finally, the mean sound velocity, v_m (approx), computed by substituting $\overline{v}_T$ and $\overline{v}_L$ for v_T and v_L in equation [21], may be used to determine the Debye temperature using [19]. A similar method was used by Gilvarry to approximate the Debye temperature of sodium (52).

Anderson has compared the VRHG approximate mean velocity with that calculated numerically from equation [20], using elastic constant data from 223 crystals belonging to 6 crystal classes. He found that in all but a very few cases, the difference in the two mean velocities was less than the probable error in the experimental data (46).

5.3 Experiment and results

Acoustic resonances in the frequency spectrum of the skin depth were observed in rectangular plates of single-crystal gallium, with nominal dimensions 2.35 cm × 0.8 cm × 0.08 cm. The ten crystals which were used for these measurements are listed in Table 5-1. The crystal axes in the first seven specimens coincide with the rectangular axes of the plates; in specimen A_B, for example, the gallium a-axis lies along the plate normal, and the b-axis is parallel to the long dimension of the plate. The last three specimens are oriented as shown in Fig. 5-2. All of the crystals are oriented to within ± 1°.

Thickness measurements, made at room temperature using three quality micrometers of different makes, were in agreement to within ± .0001 inch, which was the measurement precision in each case. It should be noted that the thickness uncertainties listed in Table 5-1 were obtained from the thickness variations measured over the entire lengths of the plates, whereas the thicknesses over the central areas covered by the secondary coil were, in every specimen except A_C-5, uniform to within the measurement accuracy of ± 0.3 %.

The velocities of pure longitudinal and pure transverse waves, with propagation vectors lying along the crystal axes, are sufficient to obtain only six of the nine elastic constants of gallium. The determination of the remaining three constants requires a measurement of the velocity of three impure modes. These measurements were provided by propagating quasi-longitudinal waves in the [101], [011], and [110] specimens, whose direction cosines are given in Table 5-2. (l, m, and n

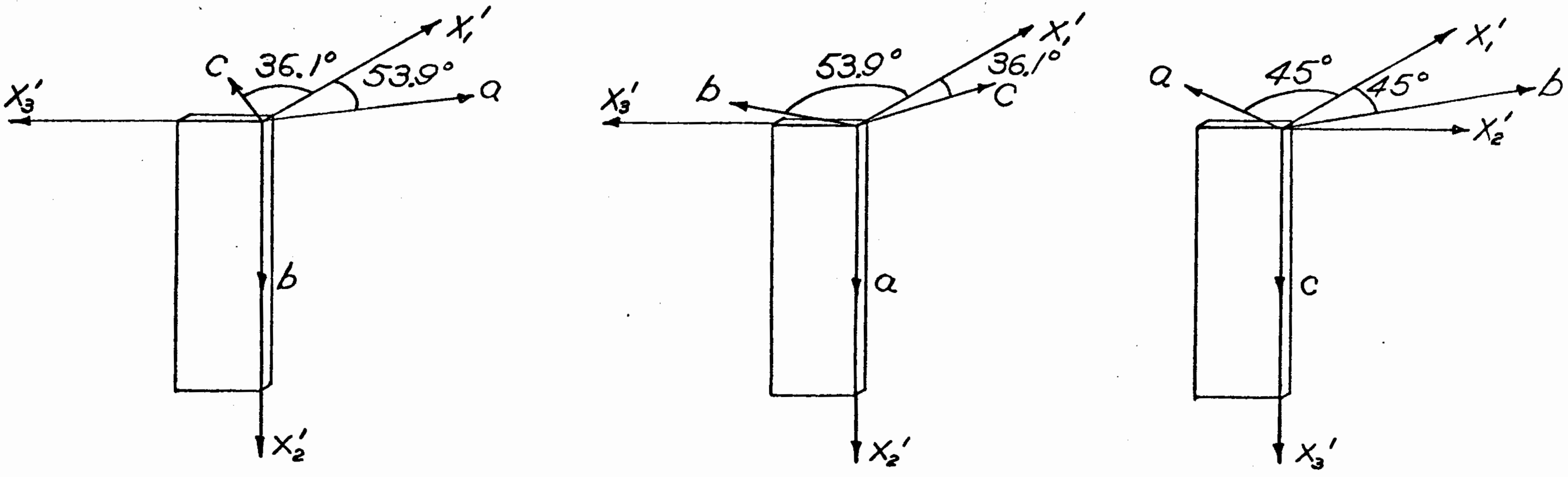

[101] [011] [110]

FIG. 5-2. ORIENTATIONS OF THE THREE OFF-AXIS CRYSTALS.

CRYSTAL	THICKNESS (300°K) (10^{-2} cm)
30 A_B - 1	8.090 ± .3%
30 A_B - 2	8.141 ± .5%
30 A_C - 5	8.026 ±1.0%
30 A_C - 6	8.115 ± .3%
30 B_A - 1	8.065 ± .3%
30 B_C - 5	8.128 ± .3%
30 C_A - 1	8.090 ± .5%
30 [101] - 2	8.090 ± .3%
30 [011] - 2	8.103 ± .3%
30 [110] - 1	8.090 ± .3%

TABLE 5-1.

GALLIUM CRYSTALS USED IN THE VELOCITY MEASUREMENTS.

are the cosines of the angles formed between the a, b, and c crystal axes and the propagation direction, or plate normal). The orientations of these crystals were chosen for computational simplicity: for wave propagation in directions perpendicular to the plates, two of the three off-diagonal terms in [14] are zero. As a result, the quasi-longitudinal velocities each involve, in addition to the previously measured diagonal elastic constants, only one off-diagonal constant. Also, pure transverse waves, with displacement polarized along the long dimensions of the plates, may be propagated in these specimens. The velocities of these pure transverse modes are each determined by only two diagonal constants, and their measurement provides a useful cross-check of the data obtained using the "on-axis" crystals.

CRYSTAL	ℓ	m	n	ℓ^2	m^2	n^2
30[101] - 2	.5892	0	.8080	.3472	0	.6529
30[011] - 2	0	.5892	.8080	0	.3472	.6529
30[110] - 2	.7071	.7071	0	.5000	.5000	0

TABLE 5-2. DIRECTION COSINES FOR THE THREE OFF-AXIS GALLIUM CRYSTALS.

As an example of this procedure we consider the measurements obtained using the 30 [011] - 2 crystal. In this case, $\ell = 0$, and from [16], $C'_{56} = C'_{16} = 0$. The solutions [15] to the secular equation are:

$$C_{11}' = \rho V_1^2 - \frac{C_{15}'^{\,2}}{C_{11}' - C_{55}'} + \ldots \qquad \text{(quasi-longitudinal)}$$

$$C_{66}' = \rho V_2^2 \qquad \text{(pure-transverse)}$$

$$C_{55}' = \rho V_3^2 - \frac{C_{15}'^{\,2}}{C_{55}' - C_{11}'} + \cdots \qquad \text{(quasi-transverse)}$$

The measurement of the quasi-longitudinal mode velocity V_1 directly yields C_{23}, since this is the only elastic constant which appears in the expressions for C_{11}', C_{15}', and C_{55}', when $\ell = 0$. The measurement of the pure transverse mode velocity V_2 (with displacement vector along the long dimension of the plate), directly yields C_{66}', which is a combination of C_{55} and C_{66} and thus provides a cross-check of these earlier-obtained elastic constants (see Table 5-6). The velocity V_3 of the quasi-transverse mode, polarized ~ 90° from the pure transverse wave, was not measured in our experiments, but would have provided another measurement of C_{23}.

The fundamental (n = 1 in equation [1]) longitudinal-wave resonances were observed at frequencies between 2.4 MHz and 2.9 MHz and the transverse-wave resonances between 1.5 MHz and 1.8 MHz, for various crystal directions. Resonances corresponding to n = 1, 3, and 5 were observed in many instances. Static magnetic field strengths of 6 kG were normally used, although fields as large as 14 kG were applied to increase the signal-to-noise ratio of some resonances (*). Specimen

---

(*) Magnetic fields of this magnitude will change the sound velocity by only a few parts in a million and hence will not affect our results appreciably (see section 6.2).

temperatures of 4.2°K, 77°K, or 273°K were obtained by filling the can which surrounded the specimen holder with helium gas, and immersing it in liquid helium, liquid nitrogen, or an ice-water mixture.

The measured velocities are presented in Tables 5-3, 4 and 5. They have been calculated from equation [1], using plate thicknesses corrected for thermal expansion using the X-ray diffraction data of Barrett (53). In those instances where a group of peaks, rather than a single resonance, was observed in the frequency spectrum of the skin depth, the velocities were obtained from the data by taking for the value of f_n the center frequency of the group, and the uncertainty assigned to f_n was the approximate half-width of the frequency distribution of the group. This frequency uncertainty was in every case less than 0.2%, i.e., smaller than the uncertainty in the plate thicknesses. The sum of these two uncertainties represents the total error in a particular measurement, and is shown in column five of Tables 5-3, 4 and 5. The results of the cross-checks in the data are shown in column seven of these tables, and in Table 5-6, which compares the measured pure transverse wave velocities in the off-axis crystals with the appropriate combinations of previously measured diagonal elastic constants. Considering all of this data, we estimate the error in the velocity measurements to be ± 0.3%. A discussion of a further possible error which may arise due to the presence of extraneous coupled vibrational modes in the plates is reserved for the next section.

NUMBER	CRYSTAL	MODE	DIRECTION OF PARTICLE MOTION	VELOCITY (10^5 cm-sec^{-1})	WEIGHTED MEAN (10^5 cm-sec^{-1})	DEVIATION FROM MEAN (%)
1	A_B - 1	long.	A	4.326 ± .3%		.09
2	A_B - 2	"	A	4.319 ± .6%	4.322	.07
3	A_C - 6	"	A	4.318 ± .8%		.09
4	B_A - 1	"	B	4.081 ± .7%		.01
5	B_C - 5	"	B	4.080 ± .3%	4.080	.01
6	C_A - 1	"	C	4.970 ± .7%		
7	B_C - 5	shear	C	2.575 ± .3%		
8	C_A - 1	"	A	2.750 ± .5%	2.748	.07
9	A_C - 6	"	C	2.747 ± .3%		.04
10	A_B - 1	"	B	2.810 ± .3%		.01
11	A_B - 2	"	B	2.810 ± .3%	2.810	.01
12	B_A - 1	"	A	2.809 ± .3%		.02
13	(101) - 2	quasi-long.	in AC plane	4.689 ± .4%		
14	(011) - 2	"	in BC plane	4.561 ± .4%		
15	(110) - 1	"	in AB plane	4.523 ± .4%		
16	(101) - 2	shear	B	2.654 ± .4%		
17	(011) - 2	"	A	2.756 ± .5%		
18	(110) - 1	"	C	2.658 ± .3%		

TABLE 5-3. VELOCITIES MEASURED AT 4.2°K

NUMBER	CRYSTAL	MODE	DIRECTION OF PARTICLE MOTION	VELOCITY (10^5 cm-sec^{-1})	WEIGHTED MEAN (10^5 cm-sec^{-1})	DEVIATION FROM MEAN (%)
19	A_C - 6	long.	A	4.294 ± .3%		.09
20	A_C - 5	"	A	4.296 ±1.0%	4.297	.02
21	A_B - 1	"	A	4.304 ± .4%		.16
22	B_C - 5	"	B	4.077 ± .3%	4.073	.10
23	B_A - 1	"	B	4.064 ± .7%		.22
24	C_A - 1	"	C	4.957 ± .6%		
25	B_C - 5	shear	C	2.561 ± .3%		
26	C_A - 1	"	A	2.745 ± .5%	2.742	.11
27	A_C - 6	"	C	2.740 ± .3%		.07
28	B_A - 1	"	A	2.788 ± .4%	2.789	.02
29	A_B - 1	"	B	2.789 ± .3%		.02
30	(101) - 2	quasi-long.	in AC plane	4.682 ± .4%		
31	(011) - 2	"	in BC plane	4.567 ± .4%		
32	(110) - 1	"	in AB plane	4.521 ± .5%		
33	(101) - 2	shear	B	2.637 ± .4%		
34	(011) - 2	"	A	2.743 ± .4%		
35	(110) - 1	"	C	2.646 ± .3%		

TABLE 5-4. VELOCITIES MEASURED AT 77°K

NUMBER	CRYSTAL	MODE	DIRECTION OF PARTICLE MOTION	VELOCITY (10^5 cm-sec^{-1})	WEIGHTED MEAN (10^5 cm-sec^{-1})	DEVIATION FROM MEAN (%)
36	A_B - 1	long.	A	4.158 ± .4%	4.151	0.17
37	A_C - 6	"	A	4.146 ± .3%		0.12
38	B_C - 5	"	B	3.950 ± .5%	3.948	0.05
39	B_A - 1	"	B	3.946 ± .4%		0.05
40	C_A - 1	"	C	4.823 ± .6%		
41	B_C - 5	shear	C	2.453 ± .3%		
42	C_A - 1	"	A	2.670 ± .5%	2.663	0.26
43	A_C - 6	"	C	2.658 ± .4%		0.19
44	A_B - 1	"	B	2.639 ± .3%	2.641	0.08
45	B_A - 1	"	A	2.643 ± .3%		0.08
46	(101) - 2	quasi-long.	in AC plane	4.554 ± .4%		
47	(011) - 2	"	" BC "	4.422 ± .5%		
48	(110) - 1	"	" AB "	4.353 ± .5%		
49	(101) - 2	shear	B	2.513 ± .4%		
50	(011) - 2	"	A	2.642 ± .4%		
51	(110) - 1	"	C	2.555 ± .3%		

TABLE 5-5. VELOCITIES MEASURED AT 273°K.

CRYSTAL	EQUATIONS FOR CROSS-CHECKING	DIFFERENCE (%) BETWEEN CALCULATED & OBSERVED VALUES		
		4.2°K	77°K	273°K
30[101] - 2	$\rho V^2 = n^2C_{44} + \ell^2C_{66}$	0.38	0.42	0.57
30[011] - 2	$\rho V^2 = n^2C_{55} + m^2C_{66}$	1.00	1.14	1.02
30[110] - 1	$\rho V^2 = m^2C_{44} + \ell^2C_{55}$	0.37	0.54	0.41

TABLE 5-6. CROSS-CHECK USING PURE SHEAR MODES PROPAGATING IN OFF-AXIS CRYSTALS.

Where two or more measurements in different crystals yield the same elastic constant, a weighted mean velocity was used in the elastic constant calculations. This mean was obtained by weighting the individual velocities in inverse proportion to their estimated uncertainties. The elastic constants, calculated from the velocities using equations given in the previous section, are presented in Table 5-7;

	4.2°K	77°K	273°K
C_{11}	11.18	11.04	10.18
C_{22}	9.96	9.92	9.21
C_{33}	14.78	14.69	13.75
C_{44}	3.97	3.92	3.56
C_{55}	4.52	4.49	4.19
C_{66}	4.72	4.65	4.12
C_{12}	4.44	4.44	4.44
C_{13}	2.83	2.72	2.75
C_{23}	2.33	2.30	2.40

TABLE 5-7. THE ADIABATIC ELASTIC CONSTANTS OF GALLIUM (IN 10^{11} DYNE-CM^{-2}).

the diagonal constants are plotted as a function of temperature in Figs. 5-3 and 5-4. The densities used in these calculations are those obtained from the X-ray diffraction data of Barrett (53) (*).

The final accuracies of the elastic constants may be considered by summing the estimated errors from various sources: errors in the frequency and thickness measurements and in the crystal orientation, and, in the case of the off-diagonal constants, errors compounded in the computation.

For the diagonal constants, C_{ii}, the errors arising from crystal misorientations are small: a 1° misalignment results in a maximum error of only a few hundredths of one percent in these constants. Thus the total error originates in the velocity measurement as discussed above, and is estimated to be ± 0.6%.

The off-diagonal constants, C_{ij}, on the other hand, are subject to much larger errors. In the computation of these constants, errors arise from the compounding of the ± 0.6% uncertainties in the C_{ii}'s which occur in the calculations. These errors may be as large as ± 12.7% for C_{13}, ± 15.9% for C_{23}, and ± 5.4%

(*) These densities are: $\rho(4.2°K) = 5.9836$ g-cm^{-3},
$\rho(77°K) = 5.977$ g-cm^{-3},
$\rho(273°K) = 5.91$ g-cm^{-3}.

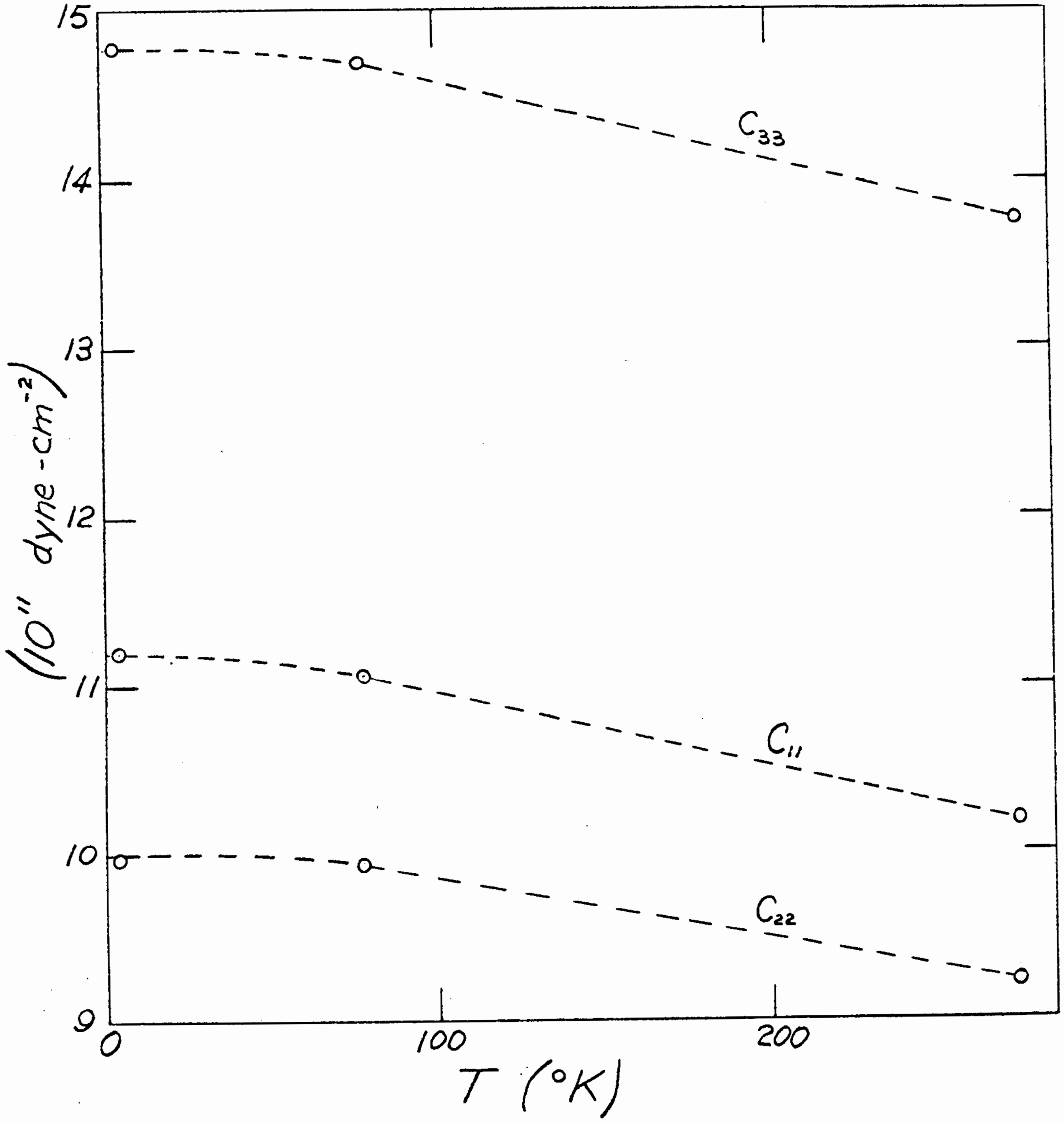

FIG. 5-3. TEMPERATURE DEPENDENCE OF C_{11}, C_{22}, AND C_{33}.

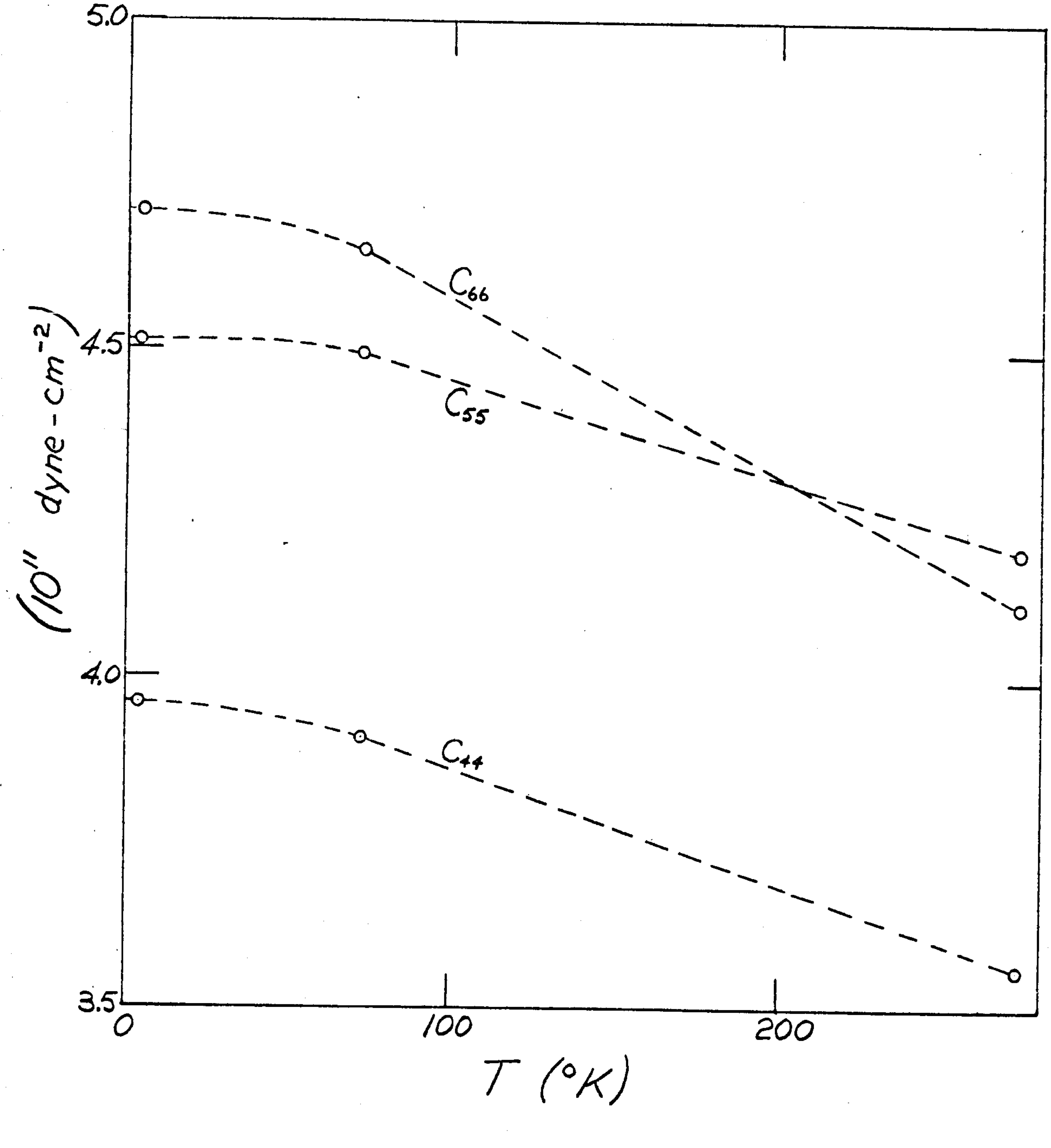

FIG. 5-4. TEMPERATURE DEPENDENCE OF C_{44}, C_{55}, AND C_{66}.

for C_{12}. In addition, these constrants are extremely sensitive to certain alignment errors, as can be seen by calculating the sound velocities for various small rotations of the crystal axes within the plates. In particular, small rotations about the long dimensions of the [101], [011], and [110] specimens produce large errors in the constants: an alignment error of ± ½° about the a-axis in the [011] specimen causes an error of ± 6.2% in C_{23}. The orientation accuracy of the three specimens in these important directions is ± .5°, and the total errors estimated for the three off-diagonal constants are ± 16% for C_{13}, ± 22% for C_{23}, and ± 6% for C_{12}. It should be emphasized that these figures represent the maximum possible errors, and that it is very improbable that the actual errors in the results are this large. In any case, one can conclude that the off-diagonal elastic constants of gallium are temperature independent, within our experimental accuracy.

The 273°K elastic constants measured by Roughton and Nash using the ultrasonic pulse-echo technique are (in units of 10^{11} dyne-cm^{-2}): $C_{11} = 9.8$; $C_{22} = 8.76$; $C_{33} = 13.32$; $C_{44} = 3.42$; $C_{55} = 4.2$; $C_{66} = 3.92$; $C_{12} = 3.26$; $C_{23} = 4.23$; and $C_{13} = 2.76$ (21). No accuracies for these constants were estimated by the authors. The diagonal constants are lower by 0% to 4.9% than the values presented here. It seems likely that the off-diagonal constants were calculated from the measured velocities using incorrect expressions; many errors have appeared in the literature (48).

The mean sound velocity, v_m (approx.), calculated by means of the VRHG approximation method from the 4.2°K elastic constants is 2.965×10^5 cm-sec^{-1}. Substituting this velocity, $\eta = 8$, and $V_0 = 1.547 \times 10^{-22}$ cm^3 (53) into equation [19] yields a Debye temperature,

$$\theta_D = 328.8 \pm 3.3\,°K,$$

which is in good agreement with that obtained by Phillips from specific heat measurements at low temperatures (20),

$$(\theta_D)_{S.H.} = 324.7 \pm 2°K.$$

The uncertainty in our value was found simply by changing the elastic constants one at a time and recalculating θ_D, which fortunately is relatively insensitive to the large errors in C_{13} and C_{23}. It should be noted that the VRHG approximation almost always yields values of v_m (approx.), and hence θ_D, that are slightly higher than those obtained by numerically solving equation [20] (46). In the case of the other orthorhombic metal uranium, for example, v_m (approx.) is 0.86% higher than v_m. Such a correction would further improve the agreement between the two measured Debye temperatures.

5.4 Discussion

The electromagnetic generation of acoustic waves in metals provides a simple method for making ultrasonic velocity measurements, by means of the continuous-wave resonance technique. The question which must ultimately be answered, however, relates to the accuracy of this technique: to what extent does the sound velocity S in equation [1], derived for an infinite metal plate, approach the ordinary sound velocity in the bulk metal? The problem arises because of the large number of vibrational modes which are coupled, in a rectangular plate, to the fundamental transverse or longitudinal modes in which we are interested, and it is possible that these extraneous modes may significantly affect the velocity measurements. In the first place, a group of several resonances may often be observed, replacing the single resonance which is desired for an unambiguous measurement of the velocity. The measurement precision is then limited by the frequency-spread of this group (although as we have seen in the previous section, this limitation does not exceed ± 0.2% in our measurements). Secondly, the resonance group may not be centered about the desired pure resonance frequency, but may be shifted by the coupling to the extraneous modes. We will now discuss this latter uncertainty.

Theoretical investigations of the resonant vibrations in single-crystal plates have been motivated largely by the practical importance of piezoelectric resonators as electrical circuit elements. A recent review, with particular reference to the vibrations which couple to the thickness-shear modes in quartz plates, has been given by Spencer (54). The many modes which exist in an infinite plate -- thickness-shear, thickness-twist, extension, face-shear, and flexure -- are all coupled by the presence of the two sets of boundaries in a rectangular plate, resulting in an exceedingly complex spectrum of resonances. For the special anisotropy of AT-cut quartz plates, Mindlin and Spencer (55) have computed the frequencies of a few of the strongest resonances which surround the fundamental thickness-shear mode, and identified these resonances experimentally. In the words of these authors, however, "The resulting frequency scan of a quartz plate produces many more resonances than can be accounted for by present mathematical solutions.... The abundance of resonances in quartz plates might lead one to believe that any theory could be verified by making frequency measurements alone."

Because of this complexity, a theoretical analysis seems to offer little hope of confirming the validity of this velocity measurement technique. We turn now to empirical evidence which at least provides an upper limit for any systematic error in the data which was presented in the previous section.

This empirical evidence takes the form of two internal and two external checks of the data.

Internal checks

1) The transverse-wave velocities measured by this method in .8 mm and .27 mm thick plates are in

agreement (at all three temperatures) to within the accuracy of the latter measurement: ± 1%.

2) The velocities of transverse and longitudinal waves obtained by measuring the first, third and fifth harmonics ($n = 1, 3, 5$ in equation [1]) are in agreement to within 0.15%, in all cases in which these two or three harmonics were observed.

These two internal checks are significant, since any shift of the frequency of the nth harmonic resonance from the value given by [1], due to coupling of extraneous vibrations, is expected to be a function of the width-to-thickness ratio of the plate, and of the order of the harmonic (54).

External checks.

1) The velocities measured by this method in a single-crystalline .27 mm-thick plate of pure aluminum at 4°K, 77°K, and 300°K, are in agreement with the values published by Kamm and Alers (56), to within the accuracy of our measurements: ± 1%. The velocities reported by Kamm and Alers for aluminum have an estimated accuracy of ± .25%.

2) The 4.2°K velocity of longitudinal waves propagating along the b-axis in gallium has been measured by Neuringer and Shapira (57). Their value, 4.07×10^5 cm-sec^{-1} ± 1.2%, is in good agreement

with the velocity obtained in the present experiment, 4.080×10^5 cm-sec^{-1}.

Although these four empirical checks place an upper limit of ± 1% on the systematic error in our data, it seems probable that the error is indeed much less than this, and that the absolute accuracies are, in fact, those estimated in the previous section, i.e., ± 0.3%.

An authoritative comparison of this technique with conventional transducer methods must await a more unambiguous settlement of the problem which has been discussed above. It should be noted, however, that an ultrasonic measurement survey by Einspruch and Truell (58) has indicated that most velocity measurements probably contain errors of ± .3%, although the estimated accuracies may be much higher than this. Also, according to these authors, "... it seems doubtful whether the quality and reproducibility of available materials justify the considerable efforts required to make <u>absolute</u> velocity measurements to much better than 0.1%. ... it appears at this time that perfection of techniques for obtaining reliable <u>relative</u> measurements in the accuracy range of one part in 10^4 or 10^5 is of greater significance in the study of the solid state by means of physical acoustics than would be further improvement of absolute velocity measurement schemes". We shall turn to the measurement of small velocity changes in the next chapter.

CHAPTER 6. FURTHER APPLICATIONS TO ULTRASONIC MEASUREMENTS

6.1 Quantum oscillations

6.1.1 Introduction

Oscillations in many transport properties of pure metals at low temperatures have as their origin the quantization of electronic energies by an external magnetic field. The application of a magnetic field $\vec{B}_0$ in the z-direction quantizes the electron motion in the x-y plane; only those orbits are allowed which contain an integral multiple (apart from a phase factor, γ) of the fundamental flux quantum, $2\pi \hbar c/e$ gauss-cm^2. The result of this real-space quantization is to constrain the electron energies to lie on cylinders in k-space whose axes are parallel to the direction of $\vec{B}_0$, and whose areas in the k_x-k_y plane are given by

$$\mathcal{A}_n = \frac{2\pi e B_0}{\hbar c}(n+\gamma) \qquad \text{cm}^{-2},\ n=1,2,3... \qquad [1]$$

As B_0 is increased, these cylinders enlarge, and are swept through the Fermi surface, causing the energy of the electron assembly to oscillate with a frequency

$$F = \frac{\hbar c S_0}{2\pi e} \quad \text{gauss}, \qquad [2]$$

where S_0 is an extremal area of the Fermi surface in the k_x - k_y plane, measured in units of cm^{-2}.

The appearance of these oscillations in the low temperature magnetic susceptibility is known as the de Hass - van Alphen effect; related quantum oscillations have been observed in the electrical and thermal conductivities, thermoelectric power, surface impedance, and other transport properties of pure metals. A review of the theoretical and experimental aspects of the de Haas - van Alphen effect, with references to these associated quantum oscillations, has recently been given by Gold (59).

Since the propagation of acoustic waves in a metal is coupled to the conduction electrons, quantum oscillations may also be expected in the ultrasonic attenuation and velocity at low temperatures. Quantum oscillations in the attenuation have been observed in a large number of metals (*); velocity oscillations have been reported in bismuth (61), gold (62), beryllium (63), aluminum and copper (64), tin (65), and, in magnetic fields over 50 kG, in gallium (57).

We have observed several oscillation frequencies in both the ultrasonic attenuation and velocity of gallium at fields as low as a few kilogauss, by measuring the change in linewidth and frequency of the acoustic resonance in the skin depth. Although we have not made a comprehensive study of these oscillations in various crystal directions, quantitative

---

(*) A review of experimental studies of various types of magnetoacoustic oscillations is given by Roberts(60).

data pertaining to one particular oscillation were obtained which may be compared to theoretical predictions by Rodriguez and Quinn (66,67), and to experimental measurements of this same oscillation at high fields by Neuringer and Shapira (57).

6.1.2 Experiment and results

Since the frequency of the acoustic resonance in the skin depth of a metal plate is virtually independent of the magnitude of $\vec{B}_0$ (*), the magnetic field may be swept while the oscillator frequency remains at resonance. Such field sweeps of the reactive skin depth, with $\vec{B}_0$ lying in the plane of the specimen and parallel to the rf-coil axis, are shown in Fig. 6-1. For this crystal (Ga 30 A_B - 1) and geometry, $\vec{B}_0$ was parallel to the b-axis, and longitudinal waves, propagating along the a-axis, were generated. In Fig. 6-1(a) the oscillator frequency was set so that no resonance effects were observed, and in (b) the field was swept with the frequency set at the center of the acoustic resonance. Although, at higher gains, quantum oscillations may be seen in the skin depth in the absence of acoustic wave resonance (see Fig. 3-9), Fig. 6-1 shows that these oscillations are greatly enhanced by the acoustic resonance. The reason for this enhancement in the observability of the oscillations is that the measurement indicated by Fig. 6-1(b) is extremely sensitive to small changes in acoustic velocity,

---

(*) See section 6.2.

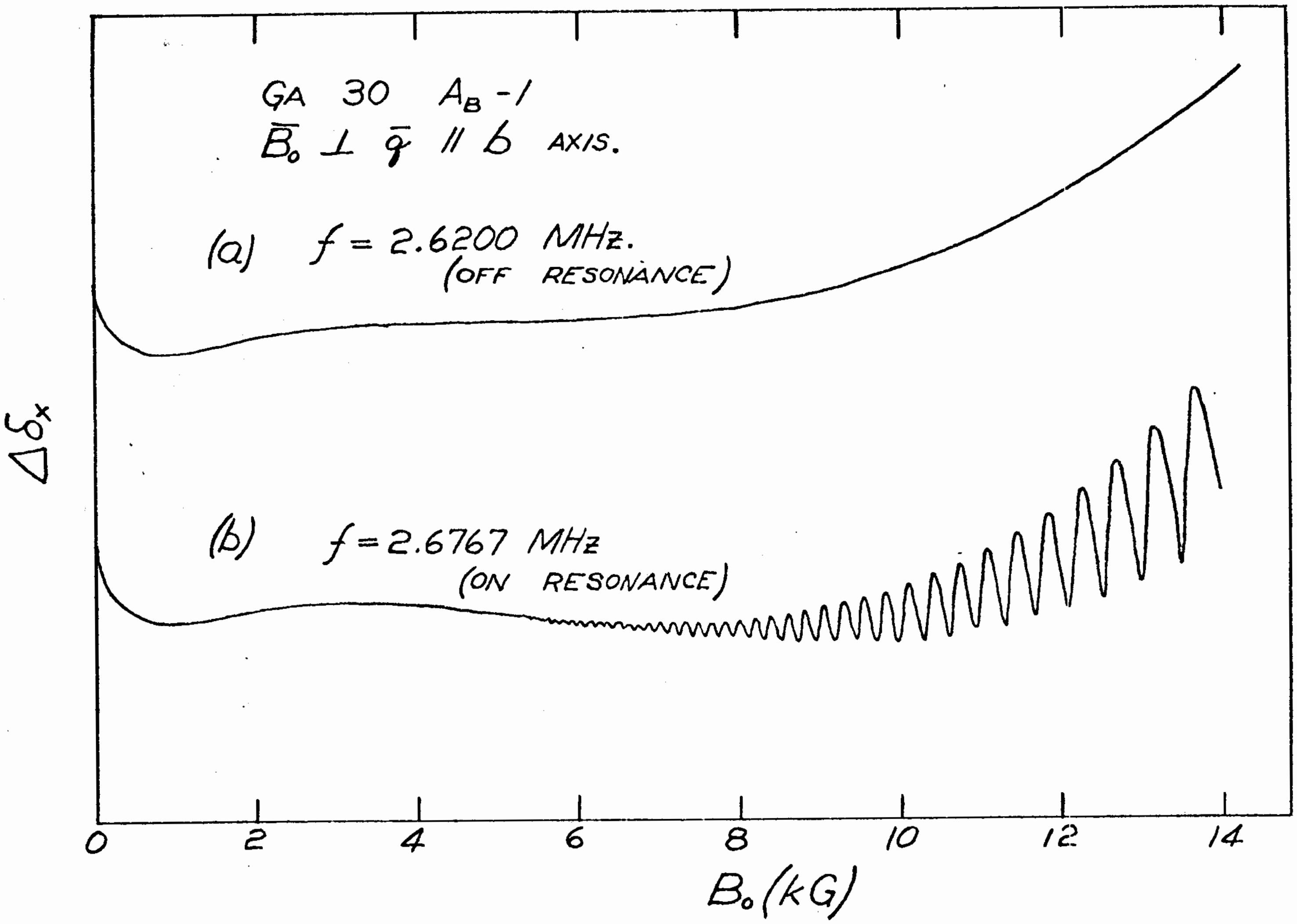

FIG. 6-1. MAGNETIC FIELD SWEEPS OF THE REACTIVE SKIN DEPTH WITH THE OSCILLATOR FREQUENCY (a) OFF, AND (b) ON, THE ACOUSTIC RESONANCE.

S_ℓ: a change in resonant frequency amounting to a small fraction of the line-width results in an easily detectable change in the reactive skin depth. This effect has recently been reported in tin, by Gaidukov, Perov, et.al. (65).

The measured frequencies of three quantum oscillations, with $\vec{B}_0$ lying along the a, b, and c-axes, are listed in Table 6-1; each of these three oscillations was observed in the velocity of both longitudinal and transverse waves. Our frequencies are seen to be in good agreement with those obtained from the de Haas - van Alphen measurements of Goldstein and Foner (68) and Shoenberg (69), and from the magnetoacoustic attenuation measurements of Shapira and Lax (70). The frequencies of the .338 MG, $\vec{B}_0 \parallel b$ oscillation which were obtained from longitudinal and transverse-wave resonances in three different specimens were in agreement to within 0.5%.

Fig. 6-2 shows a recorder trace similar to Fig. 6-1(b) but with higher amplifier gain; $\vec{B}_0$ is perpendicular to the propagation direction of the longitudinal waves. Since the oscillation in the resonance frequency is a small fraction of the line-width, the sound velocity oscillations are reproduced essentially linearly by changes in the reactive skin depth, and the ordinate of Fig. 6-2 is proportional to $\Delta S_\ell/S_\ell$. The recorder traces of Fig. 6-3 were obtained by sweeping the oscillator frequency with the magnetic field set equal to the values indicated by the two arrows in Fig. 6-2. From such traces the amplitudes of the attenuation and velocity oscillations

$\vec{B}_0$ ALONG	THIS WORK	GOLDSTEIN & FONER[(a)]	SHOENBERG[(b)]	SHAPIRA & LAX[(c)]
a	.509 ± .005[(d)]	.495 .505 .500	.50	
b	.338 ± .001[(d,e)]	.345 .335 .342	.33	.336
c	.220 ± .005[(f)]	.220 .225 .232	.232	.22

(a) Reference (69).
(b) Reference (70).
(c) Reference (68).
(d) measured from longitudinal-wave velocity oscillation.
(e) measured from transverse-wave velocity oscillation.
(f) measured from skin-depth oscillation in the absence of acoustic resonance.

TABLE 6-1. COMPARISON OF DE HAAS-VAN ALPHEN FREQUENCIES IN GALLIUM.

(UNITS OF 10^6 GAUSS).

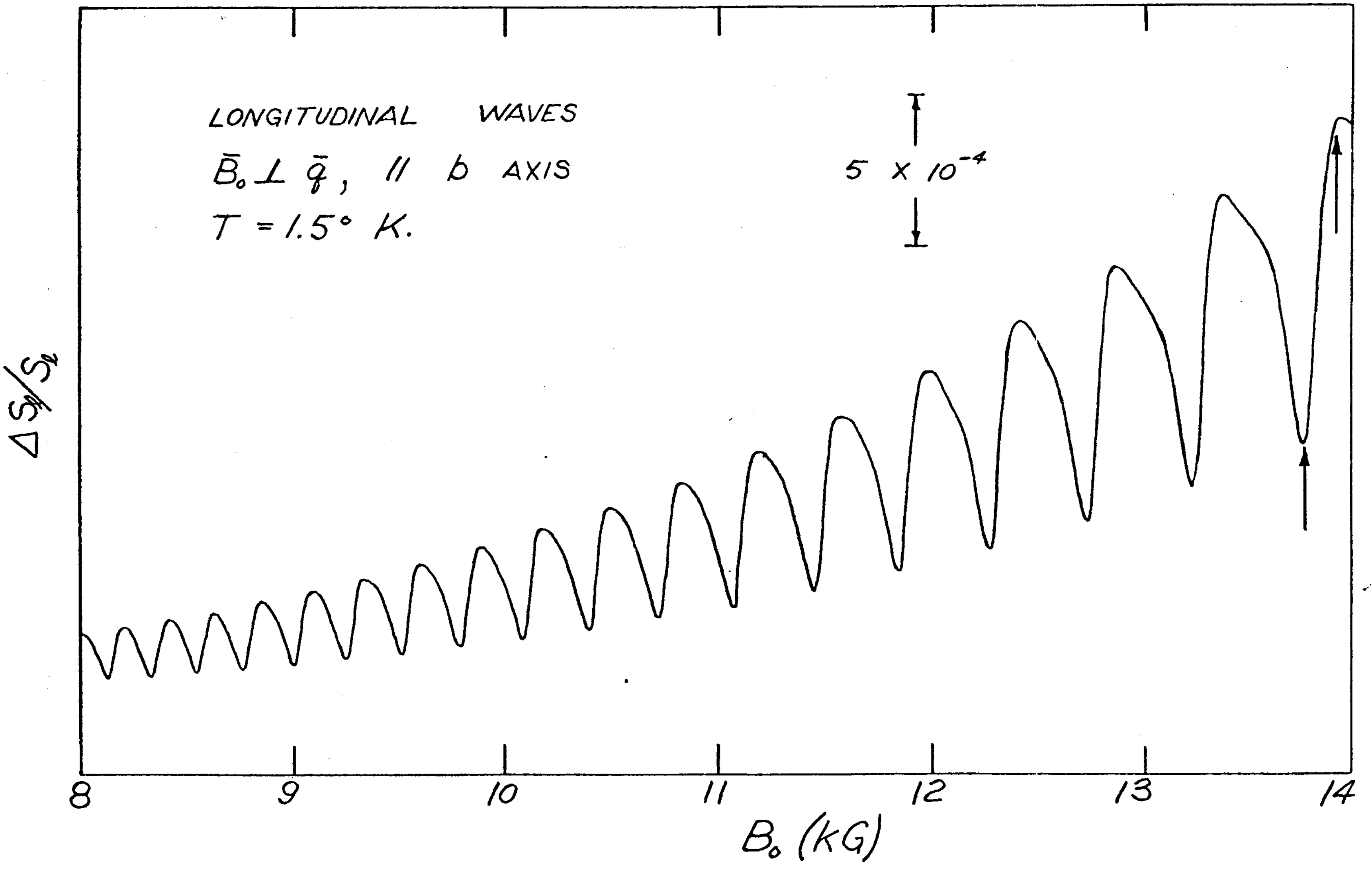

FIG. 6-2. QUANTUM OSCILLATIONS IN THE LONGITUDINAL SOUND VELOCITY.

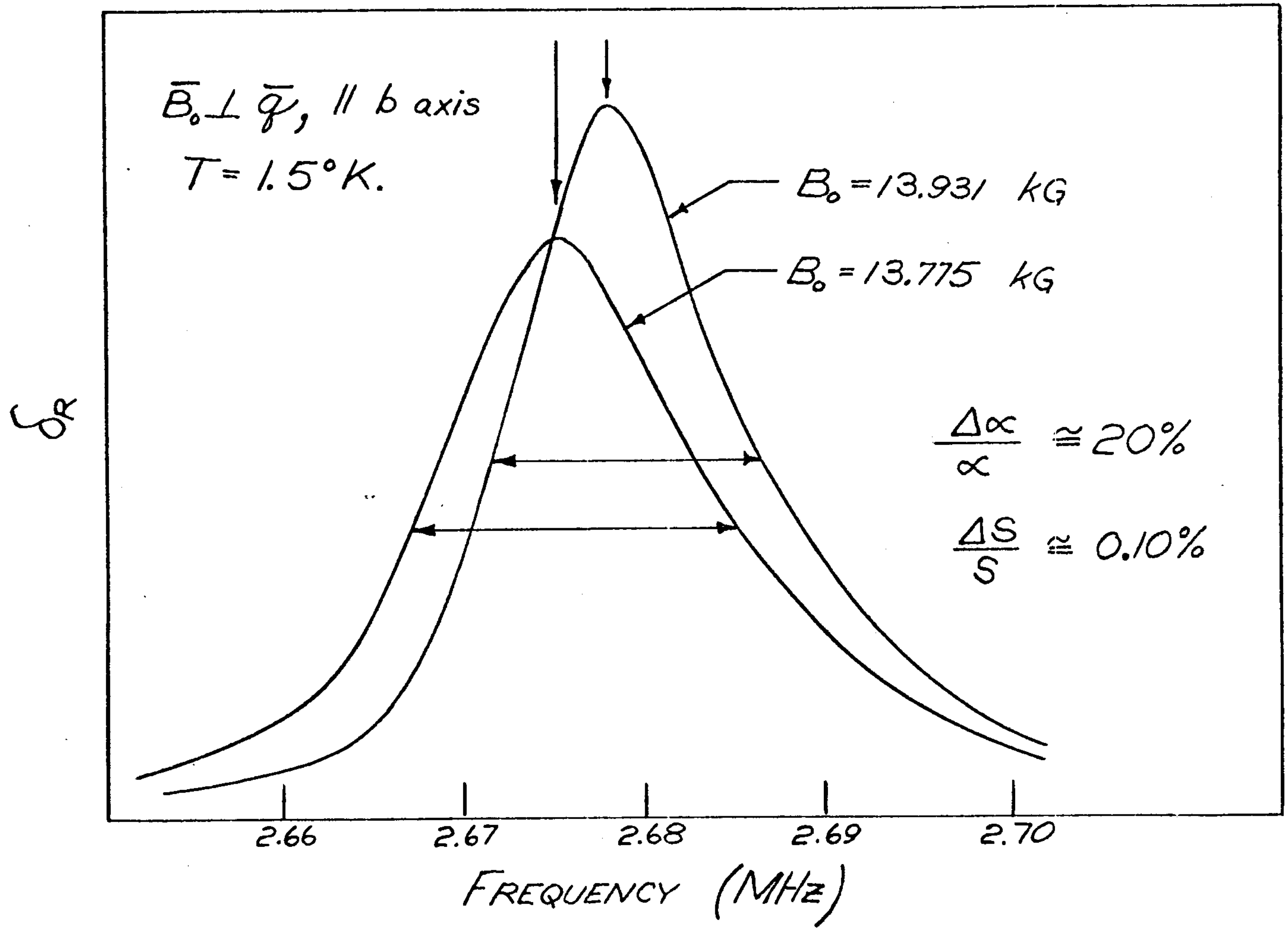

FIG. 6-3. FREQUENCY SWEEPS OF THE RESISTIVE SKIN DEPTH SHOWING THE AMPLITUDES OF THE QUANTUM OSCILLATIONS IN THE ULTRASONIC VELOCITY AND ATTENUATION.

may be determined directly, and compared with the theoretical predictions. It can be seen from Fig. 6-3 that the acoustic attenuation passes through a maximum when the velocity is at a minimum.

6.1.3 Discussion

Rodriguez (66) has derived an expression which predicts the amplitude of the quantum oscillations in the velocity of longitudinal sound waves which propagate at right angles to an applied magnetic field in a metal. This derivation considers the oscillations which arise in the bulk modulus, and hence in the longitudinal sound velocity, due to the thermodynamic relationship between the bulk modulus, K, and the Hemholtz free energy, A, in an isotropic solid:

$$K = V\left(\frac{\partial^2 A}{\partial V^2}\right)_T . \qquad [3]$$

For oscillations arising from a group of electrons which can be described by a parabolic dispersion law and an effective mass, m*, Rodriguez' result (equation [29] of reference (66)) may be written:

$$-\frac{\Delta S_l}{S_l} = \frac{4}{9}\frac{E_F^2 (m^*)^{3/2} kT}{\hbar^3 \rho S_l^2 (\hbar\omega_c)^{1/2}} \sum_{\nu=1}^{\infty} (-1)^{\nu} \nu^{1/2} \frac{\cos\left[\frac{\nu\hbar c S_0}{eB_0} - \frac{\pi}{4}\right] \cos\left[\frac{g\pi\nu m^*}{2m}\right]}{\sinh\left[\frac{2\pi^2 \nu kT}{\hbar\omega_c}\right]} , \qquad [4]$$

where E_F is the Fermi energy, and g is the spectroscopic splitting factor. The above approximations are not strictly valid for the case of gallium, which has a complicated Fermi surface and anisotropic elastic properties.

Fig. 6-4 shows a plot of equation [4], with $T = 1.5°K$, $g = 2$, $E_F = 10.5$ eV (*), $S_\ell = 4.322 \times 10^5$ cm-sec^{-1} (velocity of longitudinal wave propagating along the a-axis), $m^* = .051\ m$ (effective mass appropriate to this oscillation, $\vec{B}_0 \| $b-axis (71)), and $\nu\hbar S_0 c/(eB_0) = 2\pi\nu F/B_0$, where $F = 0.338$ MG is the measured frequency of the oscillation. The first ten terms in the sum in equation [4] were included in the calculation. There is quite striking agreement between the experimental and theoretical line-shapes shown in Figs. 6-2 and 6-4. The amplitudes are in agreement to within an order of magnitude (Table 6-2), although the amplitude of the experimentally observed oscillations increases more rapidly with magnetic field than is predicted by Rodriguez' theory.

It is interesting to note that the predicted magnetic field dependence can be adjusted to agree with the data by making a correction for the broadening of the Landau-levels. This correction consists of multiplying each term in the series in [4] by a factor $\exp[-2\pi^2\nu kT_D/(\hbar\omega_c)]$, where T_D is the Dingle temperature (59). Fig. 6-5 shows the predicted oscillation for $T_D = 3.5°K$. The magnetic field dependence obtained from this plot is compared to the observed dependence in Fig. 6-6, where

---

(*) This is the free-electron Fermi energy calculated assuming 3 conduction electrons per atom, and a spherical Fermi surface.

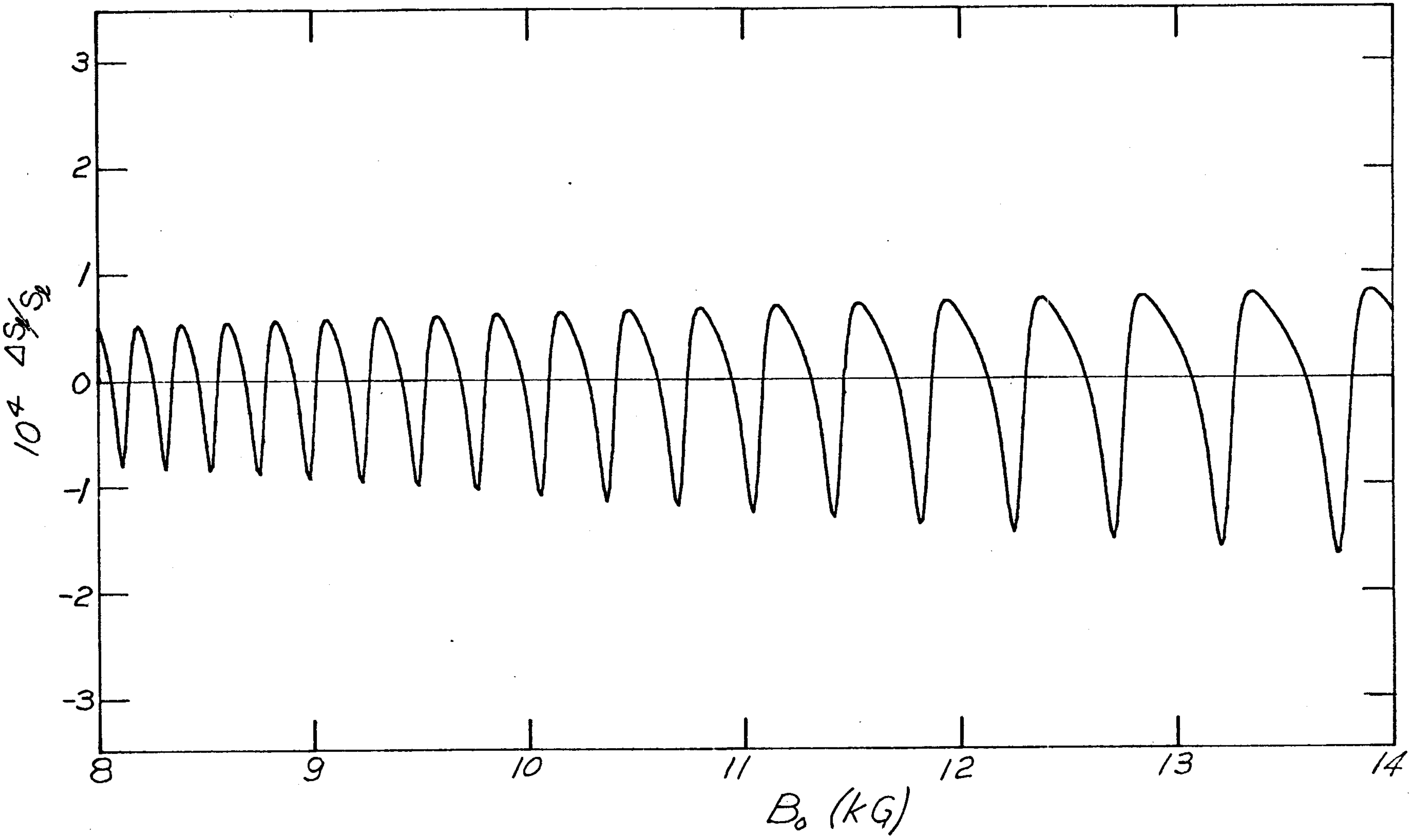

FIG. 6-4. QUANTUM OSCILLATIONS IN THE LONGITUDINAL SOUND VELOCITY: FREE-ELECTRON THEORY.

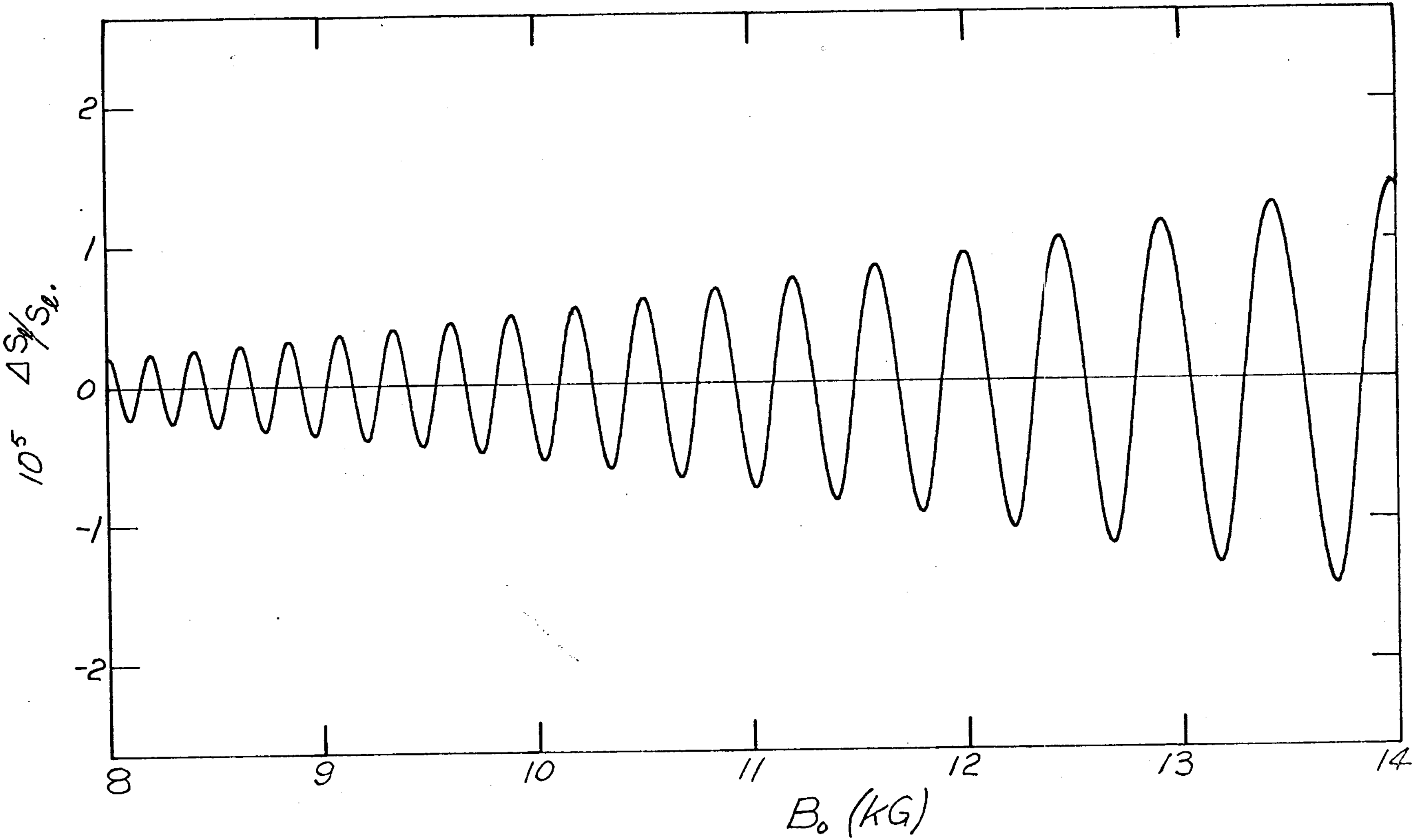

FIG. 6-5. QUANTUM OSCILLATIONS IN THE LONGITUDINAL SOUND VELOCITY: FREE-ELECTRON THEORY WITH T_D = 3.5°K. CORRECTION.

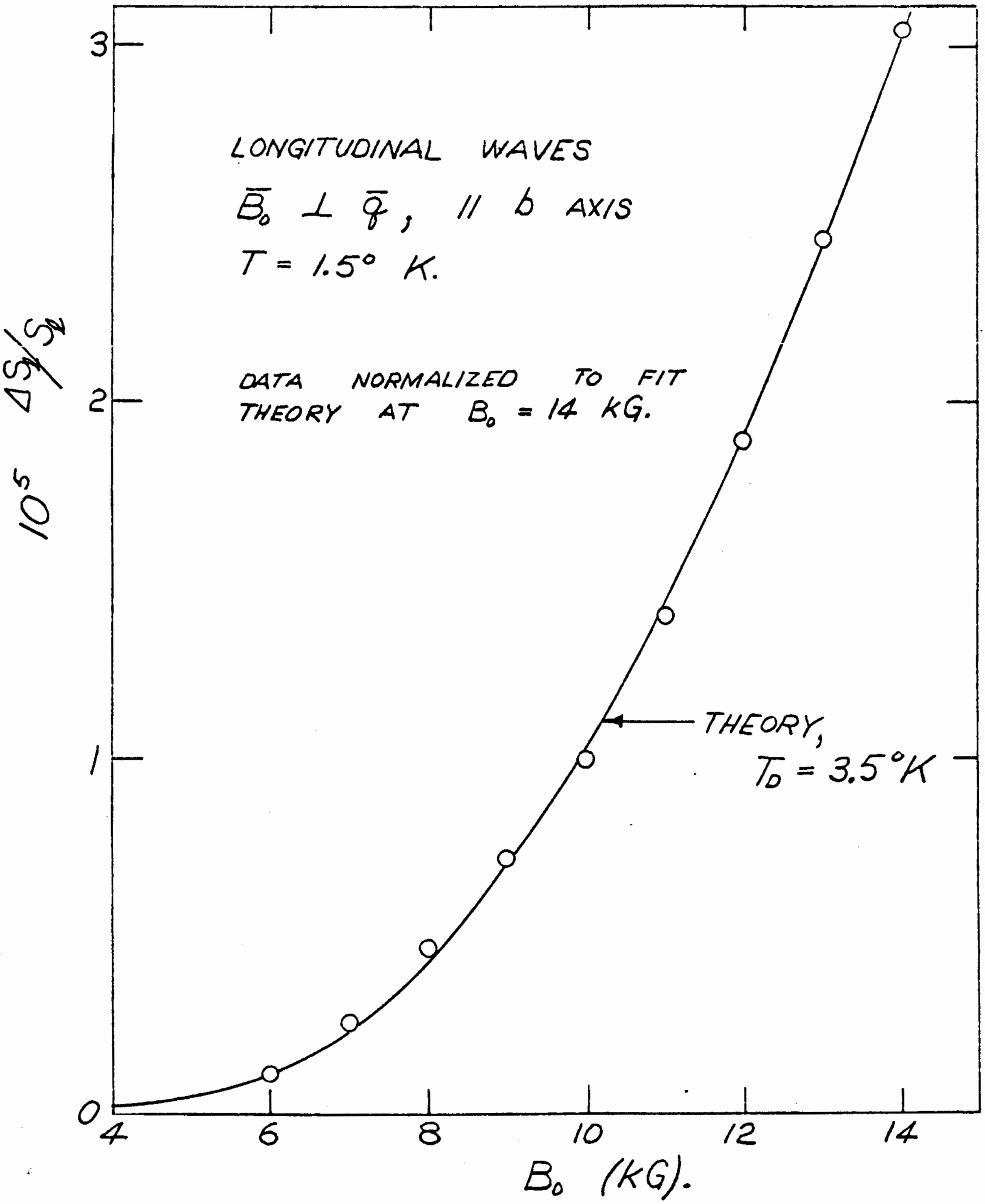

FIG. 6-6. AMPLITUDE OF THE QUANTUM OSCILLATIONS IN THE LONGITUDINAL SOUND VELOCITY.

B_0	$\Delta S_\ell / S_\ell$	
	THEORY$^{(a)}$	EXPERIMENT
8 kG	1.3×10^{-4}	1.5×10^{-4}
14 kG	2.6×10^{-4}	10.5×10^{-4}

(a): equation [4].

TABLE 6-2. AMPLITUDES OF THE QUANTUM OSCILLATIONS IN THE LONGITUDINAL SOUND VELOCITY.

the experimental points have been normalized to agree with the theoretical curve at $B_0 = 14$ kG. A comparison of Figs. 6-2, 4, and 6 shows that the Dingle temperature correction lowers the predicted amplitude of the oscillations by an order of magnitude, and considerably worsens the absolute agreement with the experimental results. Further, the line-shape agreement is destroyed by the Dingle term, and it must be concluded that the free-electron theory fails to predict quantitatively all of the observed features of the quantum oscillations in the sound velocity in gallium.

Neuringer and Shapira (57) have measured the amplitude of quantum oscillations in the velocity of sound in gallium for magnetic fields between 50 kG and 140 kG. In their experiment, $\vec{B}_0$ was also applied along the b-axis, but was parallel to the sound propagation. Equation [4] is claimed to be valid for this case also (66). In addition to the 0.338 MG oscillation discussed above, they observed a second oscillation frequency at 0.725 MG, which complicated the interpretation of their results. Although their measured value for $\Delta S_\ell/S_\ell$ ($\cong$ 0.1%) is in order-of-magnitude agreement with the prediction of Rodriguez' theory (*), they found no measurable change in the amplitude of the oscillations with magnetic field, in the interval between 50 kG and 140 kG.

Beattie (64) has compared his measurements of $\Delta S_\ell/S_\ell$ in aluminum and copper to the Rodriguez theory, and also found order-of-magnitude agreement. He corrected the theory for Landau-level broadening by using Dingle temperatures (0.9°K for aluminum and 0.5°K for copper) which were obtained from the observed magnetic field dependence of the oscillations.

Rodriguez and Quinn (66,67) have derived an expression for the amplitude of the quantum oscillations appearing in the acoustic attenuation. Combining equation [23] of reference (66)

(*) Neuringer and Shapira's results are in approximate agreement with the theory only if the free-electron Fermi energy, E_F = 10.53 eV is used in [4], and not the effective free-electron Fermi energy E_F = 0.076 eV, which was used by Neuringer and Shapira. That this change should be made was pointed out by Beattie (64), who claims that by using $m^* = 0.051$ m, and E_F = 0.076 eV in [4], Neuringer and Shapira have accounted twice for the size of the electron pocket which is involved in these oscillations. Accordingly, we have used the free-electron value, E_F = 10.53 eV, in the above calculations.

and equation [21] of reference (67), we can write for the oscillatory part of the longitudinal wave attenuation, with $\vec{B}_0$ perpendicular to the direction of propagation,

$$\alpha_{\text{osc.}} = \frac{\pi z \omega^2 \tau k T}{M S_\ell^{\,3}} \left(\frac{\hbar \omega_c}{2E_F}\right)^{1/2} \times \sum_{\nu=1}^{\infty} (-1)^\nu \nu^{1/2} \frac{\cos\left[\frac{\nu \hbar c S_0}{e B_0} - \frac{\pi}{4}\right] \cos\left[\frac{g \pi \nu m^*}{2m}\right]}{\sinh\left[\frac{2\pi^2 \nu k T}{\hbar \omega_c}\right]} \ \text{cm}^{-1}. \qquad [5]$$

where z is the number of electrons per atom and M is the ionic mass. The appearance of the electronic relaxation time, τ, which is not known for our gallium specimen, presents a difficulty in comparing this expression to our experimental results. If we assume that at 1.5°K, $\tau = 10^{-8}$ sec, (*) the calculated amplitude of $\alpha_{\text{osc.}}$ at 14 kG is 1.31×10^{-5} cm^{-1}, which is almost 300 times smaller than the observed value of 3.6×10^{-3} cm^{-1}. Although this is the first comparison of the Rodriguez-Quinn theory to experimental results in gallium (†), Beattie found that the observed oscillation amplitudes in copper and aluminum were over three orders of magnitude larger

---

(*) The value $\tau = 10^{-8}$ sec is consistent with a Fermi velocity of 10^8 cm-sec^{-1} and an electron mean free path of 1 cm, as estimated by Yaqub and Cochran (41). Relaxation-time measurements in gallium at helium temperatures also yield values of this order of magnitude (72,73).

(†) The attenuation measurements of Shapira and Lax (70) were obtained with $\vec{B}_0 \parallel \vec{q}$, and the above theory is not applicable to this case.

than theoretically predicted. Our results substantiate Beattie's conclusion that this theory does not predict the correct amplitude for quantum oscillations in the attenuation of metals.

6.2 Small changes in the ultrasonic velocity

6.2.1 Introduction

The measurements described in the previous section revealed oscillations in the low-temperature velocity as small as one part in 10^6, simply by recording changes in the reactive skin depth at the acoustic resonance frequency of the plate. At higher temperatures, where the acoustic resonance lines may be a thousand times narrower than those discussed above, the measurement of extremely small velocity changes becomes possible without any modification of the technique. A comprehensive review of the measurement of very small velocity changes and their use in the study of solids has been given by Alers (74).

One origin of small velocity changes in a metal is the application of a static magnetic field. Consider the geometry discussed in Chapter 2: a transverse wave, polarized along the y-axis, propagates in the z-direction parallel to the external magnetic field, $\vec{B}_0$. The effect of the field on the sound velocity is due to the Lorentz interaction between $\vec{B}_0$ and the ac Hall current which flows in the x-direction. According to equation [2-16], this transverse current in the metal is

$$j_x(z) = \frac{c^2 q^2 B_0 \xi_y(z)}{4\pi} \quad \text{esu},$$

and the Lorentz force density is

$$F_y(z) = -\frac{j_x(z) B_0}{c}$$

$$= -\frac{q^2 B_0^2 \xi_y(z)}{4\pi} \quad \text{dyne-cm}^{-2}.$$

The equation of motion of the ions in the interior of the metal may then be written

$$\frac{\partial^2 \xi_y(z)}{\partial t^2} = S_t^2(0) \frac{\partial^2 \xi_y(z)}{\partial z^2} - \frac{q^2 B_0^2 \xi_y(z)}{4\pi\rho},$$

or

$$\omega^2 = q^2\left(S_t^2(0) + \frac{B_0^2}{4\pi\rho}\right),$$

where $S_t(0)$ is the transverse sound velocity in the absence of a magnetic field. For transverse waves propagating parallel to an applied magnetic field, therefore,

$$S_t(B_0) = S_t(0)\left(1 + \frac{B_0^2}{4\pi\rho S_t^2(0)}\right)^{1/2}$$

$$\cong S_t(0)\left(1 + \frac{B_0^2}{8\pi\rho S_t^2(0)}\right).$$

This simple argument is correct, of course, only in the approximation that equations [2-10] and [2-16] correctly describe the transverse electric field and current which exist in the metal due to the passage of the acoustic wave, and is therefore subject to the same conditions as the phenomenological model presented in Chapter 2.

Alpher and Rubin (75) were the first to present a macroscopic theory for this effect. Rodriguez (23) has treated the problem microscopically, using the formulation which we have reproduced in Chapter 2. In the regime where $\omega\tau << 1$, $q\ell << 1$, and $\omega_c\tau << 1$, the results may be obtained directly from the dispersion relation [2-32]:

$$S_\ell(B_0) = S_\ell(0)\left[1 + \frac{B_0^2 \sin^2\theta}{8\pi\rho S_\ell^2(0)(1 + 4q^4\delta_0^4)}\right] \qquad [6]$$

$$S_t(B_0) = S_t(0)\left[1 + \frac{B_0^2 \cos^2\theta}{8\pi\rho S_t^2(0)(1 + 4q^4\delta_0^4)}\right], \qquad [7]$$

where S_ℓ and S_t are the longitudinal and transverse sound velocities, and θ is the angle between $\vec{B}_0$ and the direction of wave propagation. It should be remembered that these predictions are based on the model of a free-electron gas embedded in an isotropic background of positive charge. In this approximation the metal conductivity enters equations [6] and [7] only through the term $4(q\delta_0)^4$, which is negligible for good conductors at megahertz frequencies.

The most comprehensive experimental study of this effect has been carried out by Alers and Fleury (76) who measured the sound velocity changes in single crystals of the cubic metals Cu, Ag, Au, Al, Ta, and V in external fields of up to 21 kG. They found excellent agreement with the theory for high-conductivity metals where the term $4(q\delta_0)^4$ is unimportant, and only slight disagreement for those metals in which this term is not negligible. Their results at 4.2°K in high-purity copper indicate that for some field directions, corresponding to the open-orbit directions in copper, the expressions [6] and [7] no longer apply.

6.2.2 Results and discussion

We have observed frequency shifts in the acoustic resonance lines at 77°K in a single crystal of gallium (specimen 30 A_B-1) as a function of magnetic field for parallel and perpendicular fields of up to 14 kG. These shifts were obtained by measuring the frequency of a resonance line at a low magnetic field (2 kG) and then at successively higher fields.

The velocity (and hence resonance frequency) changes predicted by [6] and [7] are of the order of a few parts per million (ppm) for an external field of 10 kG, and hence we must be able to measure the frequency shifts with a precision of approximately 0.1 ppm. Since the sound velocity depends on temperature with a coefficient of approximately 500 ppm per Kelvin degree (see Figs. 5-3 and 5-4), temperature drifts must be kept to less than 0.001°K over the time taken for a measurement. It was found that immersing the specimen can, filled with helium gas, in liquid nitrogen provided sufficiently stable temperatures: the resonance frequency changed by only a few ppm from one day to the next, and the temperature drift corrections which were applied to the velocity shifts were less than 0.5 ppm.

Some typical results are shown in Fig. 6-7. These data were obtained from the fundamental ($n = 1$) resonance with the magnetic field parallel to the specimen; this geometry corresponds to the generation of longitudinal acoustic waves. Six fairly strong peaks in the resistive skin depth were grouped within 0.1% of this longitudinal resonance frequency (Fig. 6-8), and the frequency shift of the strongest of these peaks, indicated by an arrow in Fig. 6-8, was measured.

It can be seen from Fig. 6-7 that the fractional velocity (frequency) shifts are proportional to B_0^2, as predicted by equation [6]. The circular data points drawn in this figure have a diameter which corresponds to ± 0.1 ppm, which is approximately the scatter exhibited by the results. The slope of the experimental straight line, however, is not in agreement with that calculated from [6] using $\theta = 90°$, and the velocity for longitudinal sound propagating in this (a-axis) crystal direction. The predicted behaviour is represented by the solid line in Fig. 6-7. The velocity shifts of resonating transverse waves ($\vec{B}_0$ perpendicular to the plate, $\theta = 0°$) were similarly

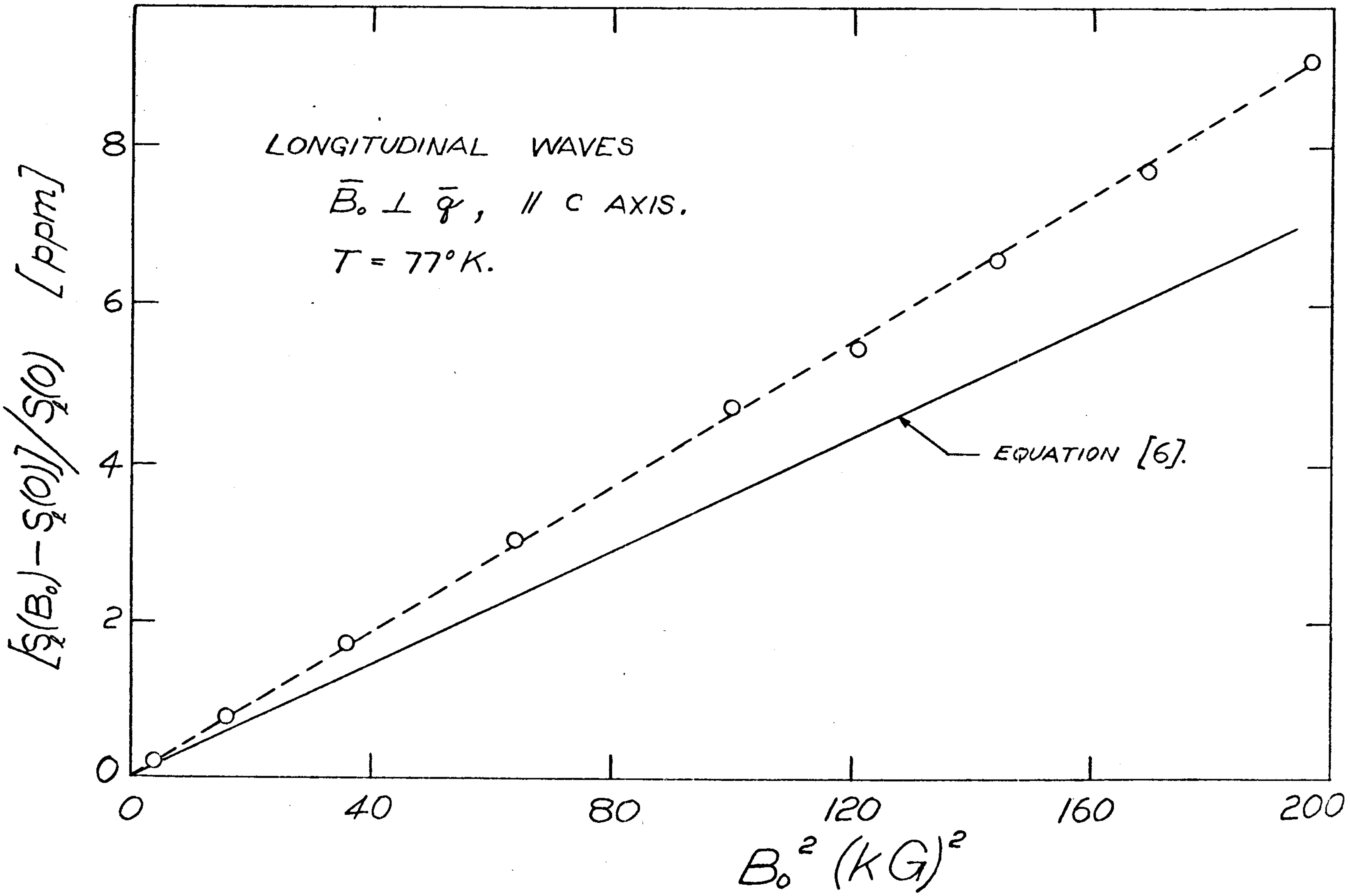

FIG. 6-7. ULTRASONIC VELOCITY SHIFT WITH AN APPLIED MAGNETIC FIELD.

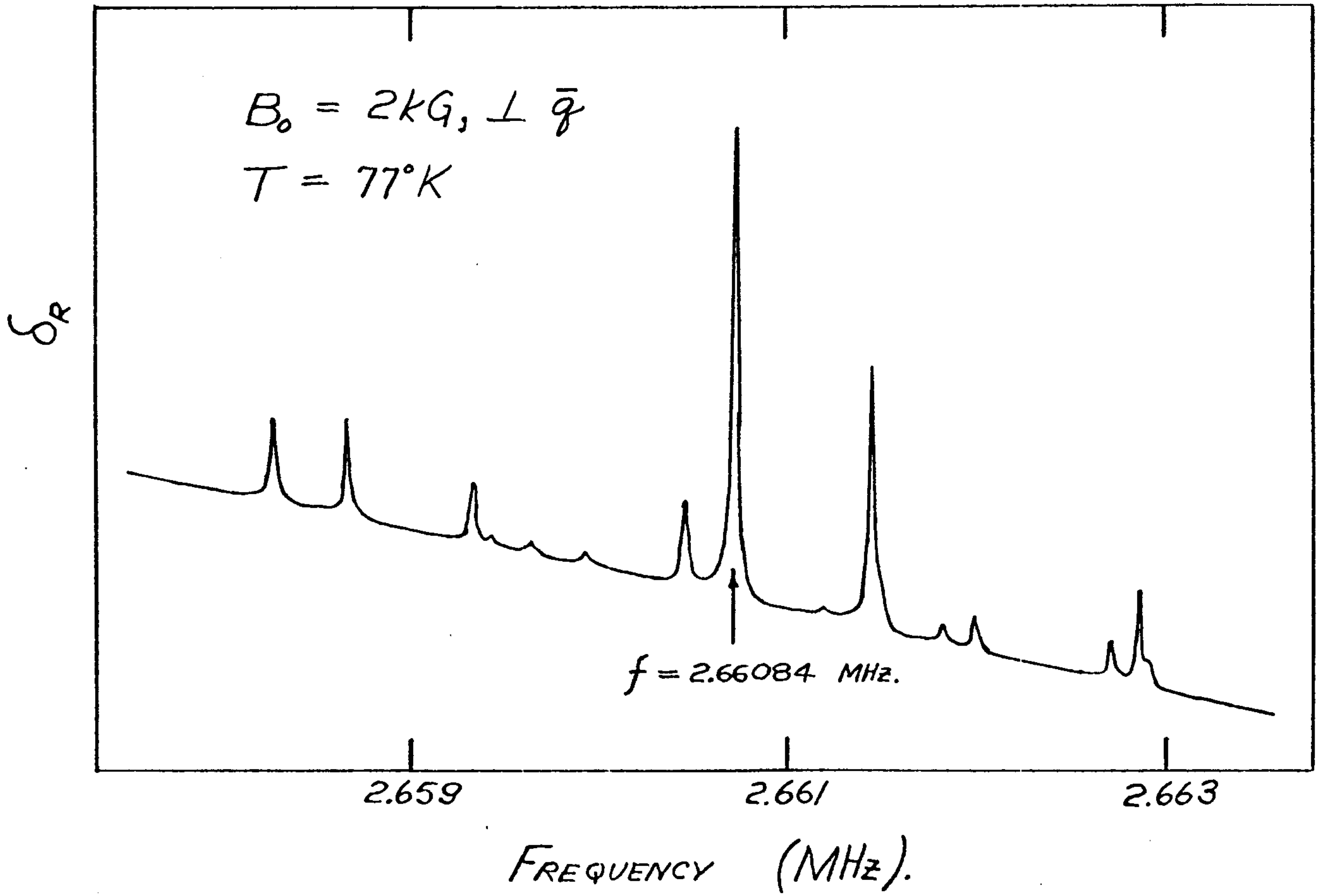

FIG. 6-8. ACOUSTIC SINGULARITIES IN THE RESISTIVE SKIN DEPTH.

proportional to B_0^2 with slopes in disagreement with [7]. In this case, the observed shifts were less than those predicted by the theory. Although the reasons for these apparent discrepancies between experiment and theory are not understood, it should be noted that these results represent the first measurement of the field-dependence of the sound velocity in a non-cubic metal.

The precision of ± 0.1 ppm in the measurement of ultrasonic velocity displayed by Fig. 6-7 is as high as any that has previously been reported (74). This precision is due in part to the extremely low acoustic attenuation in gallium, but it should be emphasized that the technique is considerably more simple than other methods. Most precision velocity-change measurements have been made using the pulse sing-around technique developed by Forgacs (77) which involves complex pulse circuitry. Beattie (64) has used a continuous-wave resonance method (78) in which the specimen, transducer, and bound form a composite oscillator which exhibits strong impedance variations at the acoustic resonances of the system. Continuous-wave phase comparison methods have been used by Blume (79) and by Beattie and Uehling (80,81).

The transducerless resonance technique described above could be further improved by some refinement of the rather crude data-taking process, such as by digitalizing the frequency and voltage data while slowly sweeping the frequency through an acoustic resonance. Although such refinements may well make precision measurements possible in higher-attenuation specimens, an appreciable increase in the precision beyond ± 0.1 ppm may be frustrated by the difficulty in stabilizing the temperature of the sample.

Observations of singularities or oscillations in the sound velocity as a function of a variable such as magnetic field are not as susceptible to small temperature drifts, and may be made with extreme sensitivity. A singularity with an amplitude of 1 part in 10^9 would result, with the present apparatus, in a detectable change in the reactive skin depth at one of the 77°K acoustic resonances in gallium. Measurements of such sensitivity, however, would require an oscillator having a very stable frequency.

6.3 Absolute ultrasonic attenuation

The method of determining the acoustic attenuation by measuring the quality factor, Q, of mechanical resonances in plates or rods is well known (78,1). We have not carried out a systematic study of the ultrasonic attenuation in gallium, but discuss here some observations that were made during the accumulation of the data presented in this thesis.

The data shown in Fig. 4-8 for the variation of the Q of a transverse-wave resonance with temperature may be inverted to obtain the attenuation coefficient, α, from the relation

$$\alpha = \frac{\gamma}{2S} = \frac{\pi f}{S}\left(\frac{1}{Q}\right) . \qquad [8]$$

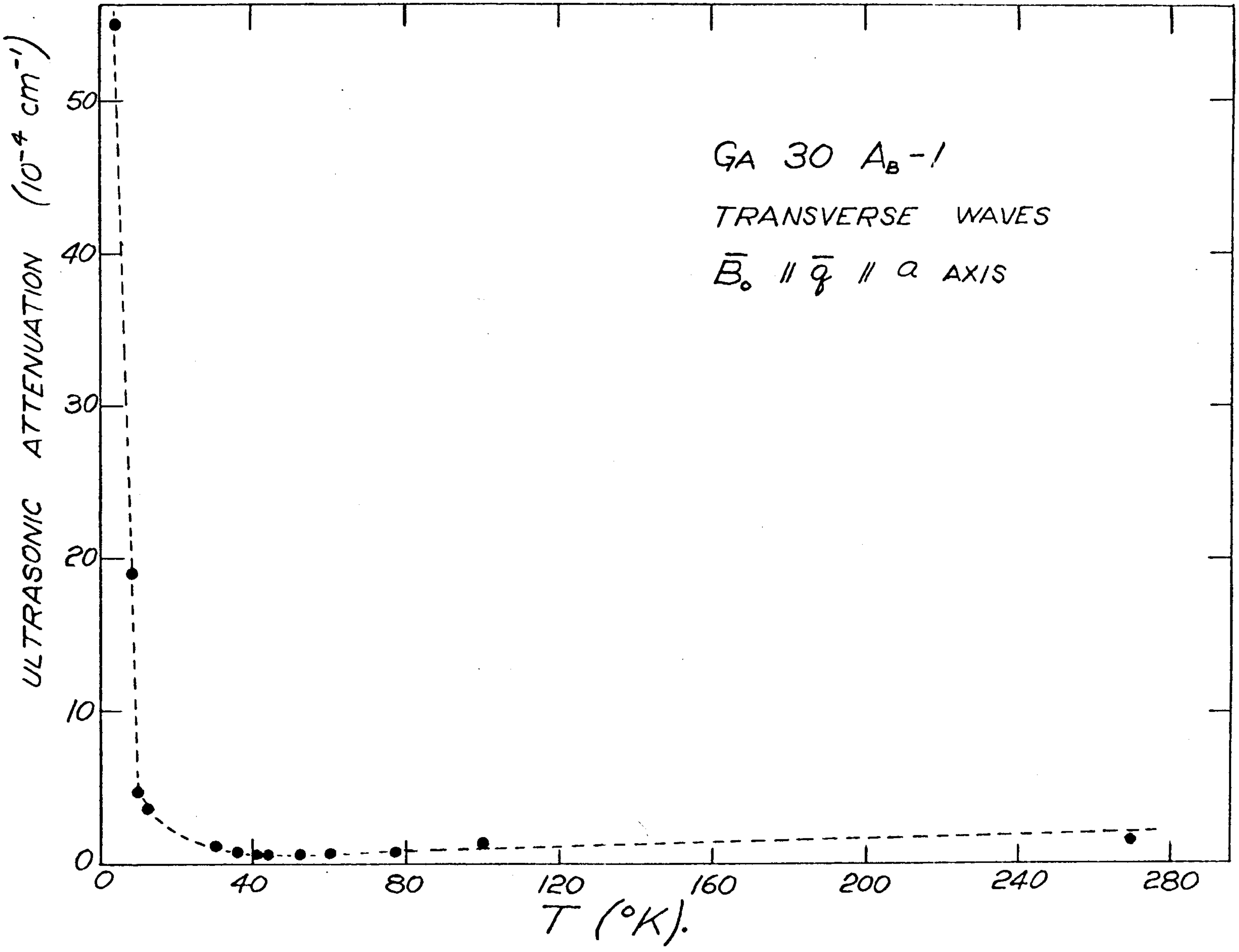

FIG. 6-9. VARIATION OF THE ACOUSTIC ATTENUAION COEFFICIENT AS A FUNCTION OF TEMPERATURE.

The resulting plot of α vs. T, shown in Fig. 6-9, exhibits the general characteristics that were observed for both transverse and longitudinal waves in many specimens:

1. a sharp decrease in attenuation as the temperature is increased from 1.5°K, corresponding to a decrease in the electrical conductivity.

2. a minimum in the attenuation in the neighbourhood of 50°K.

3. a very slow, possibly linear, increase in the attenuation as T is increased from 50°K.

In single metal crystals, most of the acoustic absorption at low megahertz frequencies and at temperatures above ~ 50°K is due to extended faults called dislocations (47). The most remarkable feature of our attenuation vs. temperature data is the extremely small contribution of this non-electronic damping. At helium temperatures the absorption is almost entirely due to the conduction electrons; at room temperature the observed attenuation of $\sim 2 \times 10^{-4}$ cm^{-1} is orders of magnitude smaller than the attenuation in many other metals, e.g., aluminum (82), and copper (83). This result is consistent with the findings of Hikata and Elbaum (84), who have reported the only other absolute attenuation measurements in gallium. These authors investigated the room-temperature acoustic attenuation of longitudinal waves propagating in the three principal directions as a function of frequency, amplitude, and plastic deformation.

The main conclusion of their experiments was that dislocation damping does not contribute appreciably to the attenuation in gallium, although they do not comment specifically on the extremely low attenuations observed. The room-temperature measurements obtained by Hikata and Elbaum at 200 MHz, extrapolated to 5 MHz assuming a frequency-squared dependence, yield attenuations of 10^{-5} to 10^{-4} cm^{-1} which are of the same orders of magnitude as those observed at 273°K in our experiments.

The measured attenuations at 4.2°K were slightly higher for longitudinal waves ($\alpha = .050$ to $.095\ \text{cm}^{-1}$) than for transverse waves ($\alpha = .003$ to $.037\ \text{cm}^{-1}$). No variation of attenuation with magnetic field was observed for transverse waves, for fields between 2 kG and 14 kG. For longitudinal waves, in the one orientation that was examined ($\vec{B}_0 \parallel$ a-axis; $\vec{q} \parallel$ b-axis), the attenuation was found to increase slightly with magnetic field strength, showing an approximately linear variation between $.059\ \text{cm}^{-1}$ at 4 kG and $.073\ \text{cm}^{-1}$ at 13 kG. The 4.2°K longitudinal attenuations obtained using two crystals of similar orientation (Ga 30 A_B - 1 and Ga 30 A_B - 2) differed by 30%, an indication that the electronic attenuation depends strongly on slight differences in crystal orientation or purity.

CHAPTER 7. CONCLUSIONS

The experimental results obtained using gallium single crystals lead us to believe that the phenomenological model of Turner, Lyall, and Cochran (17) provides the correct description for the electromagnetic - acoustic coupling in thin metal plates, within a limited range of frequency and magnetic field. The observed singularities in the surface resistance and reactance, arising from electromagnetically-excited acoustic resonances, displayed the Lorentzian lineshapes predicted by the theory. The resonance amplitudes at high temperatures varied as B_0^2 and $\cos^2\theta$, in agreement with [2-13]; deviations from this behaviour at helium temperatures are due to the complicated magnetic field dependence of the electronic attenuation of the acoustic wave. The absolute amplitude of the surface impedance singularity arising from the transverse-wave resonance at 4.2°K was found to be in good agreement with the amplitude predicted by the model. The origin of the anomalously high resonance amplitudes which were observed for transverse waves in two crystals as the temperature was reduced from 4.2°K, however, is not understood.

The acoustic velocities measured by the continuous-wave resonance technique in single crystal gallium plates have an estimated uncertainty of ± 0.3%, and the elastic stiffness constants calculated directly from these velocities, an uncertainty of ± 0.6%. Although much higher uncertainties must be assigned to the indirectly measured elastic constants, the low temperature data yield a value for the Debye temperature of gallium, $\theta_D = 328.8 \pm 3.3°K$, which is in agreement with that obtained from the low temperature specific heat measurements of Phillips (20), $(\theta_D)_{S.H.} = 324.7 \pm 2°K$. This is the first comparison between the Debye temperatures obtained from low temperature ultrasonic and specific heat data for a metal with orthorhombic crystal symmetry.

The three measured frequencies of quantum oscillations which were observed in the ultrasonic velocity and attenuation of gallium are in excellent agreement with those obtained from de Haas-van Alphen (68, 69) and magnetoacoustic attenuation measurements (70). In a magnetic field of 14 kG perpendicular to the propagation direction of longitudinal waves, the amplitude of the velocity oscillations is approximately 0.1% of the ultrasonic velocity, whereas the apparatus is capable of detecting low-temperature oscillations as small as one part in 10^6. The amplitude of the quantum oscillations in the velocity is in agreement to within an order of magnitude with that predicted by the free-electron theory derived by Rodriguez (66). The theoretical magnetic field dependence, however, is not observed. The oscillation in the attenuation is more than two orders of magnitude larger than that predicted by Rodríguez and Quinn (66,67). Other comparisons of theories with measurements in aluminum and copper (64) and in gallium (57) have led to similar discrepancies. The conclusion from these results must be that the amplitudes of the quantum oscillations are sensitive to properties of the Fermi surface which are not accounted for in the free-electron theories.

Measurements of the surface impedance resonance linewidths reveal a large electronic contribution to the attenuation of both longitudinal and transverse ultrasonic waves at temperatures below 40°K. At higher temperatures, the extremely small absolute attenuations ($\cong 10^{-4}$ cm^{-1}) result in resonance linewidths as narrow as 12 hertz at a frequency of 5 megahertz. Small changes in the ultrasonic velocity are easily detectable as frequency shifts of these narrow resonance lines. Our measurements at 77°K indicate that the velocity shift varies as the square of an applied magnetic field, with a scatter in the data of one part in 10^7. The functional form of this magnetic field dependence of the velocity is in agreement with the theory (75), but a discrepancy between the size of the observed shifts and those predicted by the theory is not understood.

The results presented in this thesis demonstrate that the electromagnetic generation of acoustic waves at the surface of a metal offers a new and powerful tool for the study of ultrasonic effects in metals. When this method is used to excite resonant acoustic modes in thin plates, large signals may be observed in the surface impedance, especially in metals which are characterized by a low acoustic attenuation. The advantages inherent in such a technique over conventional methods employing piezoelectric transducers are several. The most notable, especially for low temperature work, is that the ultrasonic properties of a metal specimen may be investigated without the need for making any physical contact to its surface. Further, the amplitude of the generated acoustic wave can be simply calculated if the intensities of the electromagnetic and static magnetic fields applied to the specimen surface are known. Measurements may be made on very small specimens, and the instrumentation required is extremely simple. It is anticipated that these advantages will stimulate future applications of the electromagnetic-acoustic interaction to ultrasonic studies, not only in pure metal plates, but in alloys, superconductors, semiconductors, and liquid metals.

APPENDIX A. ELECTROMAGNETIC GENERATION OF ACOUSTIC WAVES IN METALS

A Chronological Bibliography, 1962-1969

G. AKRAMOV, "Resonance Damping of Sound in Metals in a Magnetic Field," Fiz. Tver. Tela 5, 1310-1315 (1962). English transl.: Soviet Phys. Sol. St. 5, 995-958 (1963).

E. A. KANER and V. G. SKOBOV, "Theory of Resonance Excitation of Weakly Decaying Electromagnetic Waves in Metals," Zh. Eksperim. i Teor. Fiz. 45, 610-630 (1963). English trans.: Soviet Phys. JETP 18, 419-432 (1964).

V. G. SKOBOV and E. A. KANER, "Theory of Coupled Electromagnetic and Acoustic Waves in Metals in a Magnetic Field," ZH. Eksperim, i Teor. Fiz. 46, 273-286 (1964). English transl.: Soviet Phys. JETP 19, 189-198 (1964).

D. N. LANGENBERG and J. BOK, "Helicon-Phonon Interaction in Solids," Phys. Rev. Letters 11, 549-552 (1963).

J. J. QUINN and S. RODRIGUEZ, "Helicon-Phonon Interaction in Metals," Phys. Rev. Letters 11, 552-554 (1963); Phys. Rev. 133, A1589-A1594 (1964).

C. C. GRIMES and S. J. BUCHSBAUM, "Interaction between Helicon Waves and Sound Waves in Potassium," Phys. Rev. Letters 12, 357-360 (1964).

M. I. KAGANOV and V. B. FIKS, "Excitation of a Sound by Current in Metal Films," Fiz. metal. metalloved. 19, 489-494 (1965). English transl.: Phys. Metals Metall. 19, No. 4, 8-12 (1965).

V. F. GANTMAKHER and V. T. DOLGOPOLOV, "Excitation of Standing Sound Waves in Bi by an Electromagnetic Method," Zh. Eksperim. i Teor. Fiz. Pis'ma 5, 17-20 (1967). English transl.: Soviet Phys. JETP Letters 5, 12-14 (1967).

P. K. LARSEN and K. SAERMARK, "Helicon Excitation of Acoustic Waves in Aluminum," Phys. Letters 24A, 374-375 (1967).

K. SAERMARK and P. K. LARSEN, "Helicons and Acoustic Shear Waves in Aluminum," Phys. Letters 24A, 668-669 (1967).

K. B. VLASOV and V. G. KULEYEV, "Transformation of Electromagnetic to Elastic Waves, and vice versa, on the Boundaries of Magnetically Polarized Metals," Fiz. metal. metalloved. 25, 15-27 (1968). English transl.: Phys. Metals Metall. 25, No. 1, 12-22 (1968).

J. R. HOUCK, H. V. BOHM, B. W. MAXFIELD, and J. W. WILKINS, "Direct Electromagnetic Generation of Acoustic Waves," Phys. Rev. Letters 19, 224-227 (1967).

J. J. QUINN, "Electromagnetic Generation of Acoustic Waves and the Surface Impedance of Metals," Phys. Letters 25A, 522-523 (1967).

B. ABELES, "Electromagnetic Excitation of Transverse Microwave Phonons in Metals," Phys. Rev. Letters 19, 1181-1183 (1967).

A. G. BETJEMANN, H. V. BOHM, D. J. MEREDITH, and E. R. DOBBS, "R.F. - Ultrasonic Wave Generation in Metals," Phys. Letters 25A, 753-754 (1967).

M. I. KAGANOV, V. B. FIKS, and N. I. SHIKINA, "Sound Excitation by an Electromagnetic Wave at the Surface of a Metal," Fiz. metal. metalloved. 26, 11-17 (1968). English transl.: Phys. Metals Metall. 26, No. 1, 8-16 (1968).

V. Ya. KRAVCHENKO, "Electromagnetic Excitation of Sound in a Metallic Plate," Zh. Eksperim. i Teor. Fiz. 54, 1494-1509 (1968). English transl.: Soviet Phys. JETP 27, 801-808 (1968).

R. L. THOMAS, G. TURNER, and H. V. BOHM, "Circularly Polarized Ultrasonic Shear Waves in Metals," Phys. Rev. Letters 20, 207-208 (1968).

P. K. LARSEN and K. SAERMARK, "Electromagnetic Excitation of Elastic Modes in Aluminum," Phys. Letters 26A, 296-297 (1968).

G. S. WEISBARTH, "Frequency Dependence of the Electromagnetic Generation of Transverse Microwave Phonons in Metals," Phys. Letters 27A, 230-231 (1968).

D. J. MEREDITH, R. J. WATTS-TOBIN, and E. ROLAND DOBBS, "Electromagnetic Generation of Ultrasonic Waves in Metals," J. Acoust. Soc. Am. 45, 1393-1401 (1969).

W. D. WALLACE, J. R. HOUCK, R. BOWERS, B. W. MAXFIELD, and M. R. GAERTTNER, "Transducerless Method for Ultrasonic Flaw Testing in Metals," Rev. Sci. Instr. 39, 1863-1864 (1968).

P. D. SOUTHGATE, "An Approximate Theory of Skin-Effect Acoustic Generation in Conductors," J. Appl. Phys. 40, 22-29 (1969).

R. C. ALIG, "Direct Electromagnetic Generation of Transverse Acoustic Waves in Metals," Phys. Rev. 178, 1050-1058 (1969).

Yu. P. GAIDUKOV and A. P. PEROV, "Electromagnetic Excitation of Sound in Tin," Zh. Eksperim. i Teor. Fiz. Pis. Red. 8, 666-668 (1968). English transl.: Soviet Phys. JETP Letters 8, 412-414 (1969).

R. W. COHEN, "Microwave Excitation of Phonons in Superconductors," Phys. Letters 29A, 85-86 (1969).

Yu. P. GAIDUKOV, A. P. PEROV, and I. F. VOLOSHIN, "Singularities in the Behaviour of the Surface Impedance of Tin upon Establishment of a Standing Sound Wave, and Quantum Oscillations in the Speed of Sound," Zh. Eksperim. i Teor. Fiz. Pis. Red. 9, 585-590 (1969). English transl.: Soviet Phys. JETP Letters 9, 356-360 (1969).

M. R. GAERTTNER, W. D. WALLACE, and B. W. MAXFIELD, "Experiments Relating to the Theory of Magnetic Direct Generation of Ultrasound in Metals," Phys. Rev. 184, 702-704 (1969).

K. R. LYALL and J. F. COCHRAN, "Electromagnetic Excitation of Acoustic Waves in Metal Plates," Phys. Letters 29A, 626-627 (1969).

R. TURNER, K. R. LYALL, and J. F. COCHRAN, "Generation and Detection of Acoustic Waves in Metals by Means of Electromagnetic Radiation," Can. J. Phys. 47, 2293-2301 (1969).

V. F. GANTMAKHER and V. T. DOLGOPOLOV, "Electromagnetic Excitation of Sound Waves in Tin and Bismuth," to be published in Zh. Eksperim. i Teor. Fiz.

R. L. THOMAS, G. TURNER, and D. HSU, "Electromagnetic Generation of Ultrasonic Shear Waves in the Non-Local Limit," Phys. Letters 30A, 316-317 (1969).

APPENDIX B. INDIUM-TIN ALLOY SPECIMENS

The rectangular plates of indium - 3% tin alloy used to calibrate the rf detection system were prepared using a molding technique developed by Mr. D. Gabel. The apparatus is shown in Fig. B-1. Indium and tin metal were placed in the top glass funnel, and were heated by means of two electrical resistance tapes: one wrapped around the funnel, and the other around the body of the mold. The entire process of melting and crystallization was carried out within the Bell jar of a vacuum system, at a pressure of 10^{-4} to 10^{-5} torr. Flat, smooth surfaces were obtained by molding the specimens against mica wafers; upon removal of the plate from the mold, the mica was easily stripped off, leaving only an extremely thin mica layer on the surface. The mold itself was held together by clamps and screws, and was easily disassembled.

The three plates produced by this technique, measuring 0.8 cm by 3.8 cm, and having thicknesses of approximately 0.26 mm, 0.40 mm, and 0.80 mm, displayed surfaces which appeared mirror-smooth. X-ray back-reflection Laue photographs showed that one of the plates was in fact a single crystal and the other two consisted of only a few crystallites, even though no particular care had been taken in the heating and cooling of the mold. It seems likely that smooth-surface, oriented single crystals of low-melting-point metals and alloys may be grown in this manner, if a seed crystal is placed at the bottom of the mold, and a more controlled

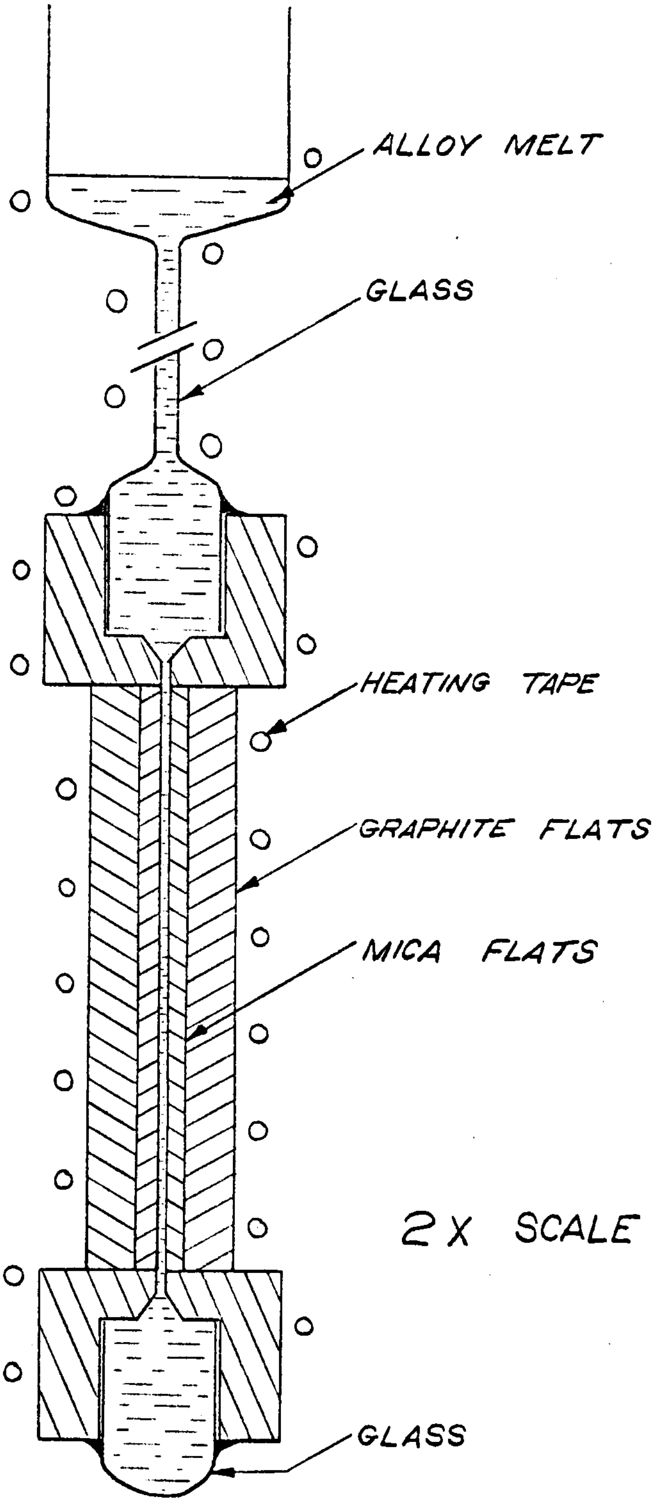

FIG. B-1. MOLD FOR IN-SN ALLOY SPECIMENS.

heating technique is used.

Each rectangular alloy plate was accompanied from the mold by a 4 cm - long, 2 mm - diameter wire, obtained by dissolving the top glass funnel with hydrofluoric acid. The room- and helium-temperature resistivities of these wire specimens were measured using the standard four-terminal method. Measurements of the resistivities of different segments along the wire yielded identical results, indicating that the alloys are homogeneous. Also, the resistivities of the three specimens were equal to within a few percent, which was the uncertainty in the alloy composition. The following measured parameters are typical, and were obtained using the wire which was grown together with the 0.26 mm plate:

wire diameter: $d = 0.233$ cm ± 0.9%
wire length: $\ell = 3.82$ cm ± 0.5%
resistance at 4.2°K: $R_{4.2} = 1.046 \times 10^{-4}\ \Omega \pm 0.5\%$
resistivity at 4.2°K: $\rho_{4.2} = 1.17 \times 10^{-6}\ \Omega\text{-cm} \pm 2.8\%$
resistance at 300°K: $R_{300} = 7.41 \times 10^{-4}\ \Omega$
resistivity at 300°K: $\rho_{300} = 8.30 \times 10^{-6}\ \Omega$ - cm.

The calculated classical skin depth at 4.2°K and 7 MHz is then

$$\delta_{\ell} = \left(\frac{c^2}{8\pi\omega\sigma_0}\right)^{1/2} \text{ cm}$$

$$= 1.03 \times 10^{-3} \text{ cm} \pm 1.5\%$$

where

$$\sigma_0 = \frac{9 \times 10^{11}}{\rho_{4.2}} \text{ esu.}$$

The residual-resistivity ratio, $\rho_{300}/\rho_{4.2}$, is 7.1. The measured resistance ratio in pure indium is 1.65×10^4, and the estimated electron mean free path, ℓ, in that material is 5×10^{-2} cm (Appendix C). Since we expect ℓ to be inversely proportional to the residual resistance, the mean free path in the alloy is

$$\ell_A = \frac{7.1 \times 5 \times 10^{-2}}{1.65 \times 10^4} = 2.2 \times 10^{-5} \text{ cm.}$$

Thus $\ell_A/\delta_{C\ell} = 2.1 \times 10^{-2} << 1$, and the condition for the validity of the classical-skin-effect theory is satisfied.

APPENDIX C. THE ANOMALOUS SKIN DEPTH IN PURE INDIUM

C.1 Introduction

The theory of the skin effect for free electrons has been given by Reuter and Sondheimer (85). Their results for the anomalous limit, $|\delta|/\ell << 1$, where ℓ is the electronic mean free path, are

$$\delta_x = \sqrt{3}\,\delta_R = \left[\frac{9c^2}{64\pi^2\omega(\sigma_0/\ell)}\right]^{1/3} \qquad [1]$$

for diffuse scattering (p=0) of the electrons at the metal surface, and

$$\delta_x = \sqrt{3}\,\delta_R = \left[\frac{8c^2}{81\pi^2\omega(\sigma_0/\ell)}\right]^{1/3} \qquad [2]$$

for specular scattering (p=1).

Pippard (86,87) has generalized the anomalous-skin-effect theory to include metals having an arbitrary Fermi surface. He has shown that the anomalous limit is characterized by the following three properties:

(i) $\delta_x/\delta_R = \sqrt{3}$

(ii) δ_x, δ_R are proportional to $\omega^{-1/3}$

(iii) δ_x, δ_R are independent of the purity of the metal.

We have been motivated to measure the anomalous skin depth in pure polycrystalline indium for two reasons. In the first place, a measurement of the ratio δ_x/δ_R provides, through the property (i) above, a convenient test of the phase calibration of the rf detection apparatus. Secondly, skin-depth measurements at low radio-frequencies (88), and at microwave frequencies (89) are not in agreement with prediction (ii), and a measurement at an intermediate frequency was felt to be worthwhile. It should be noted that the frequency dependence (ii) has been shown to hold over a frequency range of 7 decades in tin (88, 90).

In the following sections we present the details of the preparation of pure indium polycrystalline specimens, and discuss the results of the measurements of the reactive and resistive skin depths at frequencies of 7.00 MHz and 5.38 MHz.

C.2 Specimens

Polycrystalline indium plates were prepared by rolling and electropolishing 99.9999% pure indium metal (*). A .36 mm thick sheet was first rolled, in one direction only, between layers of mylar film, and was then etched so that the polycrystalline structure could be examined. This sheet was then electropolished to a final thickness of 0.260 mm ± .005 mm, following the procedure outlined in reference (91). The etching solution was made up of 400 cc ethanol, 20 cc hydrochloric acid, and 4 g picric acid. Finally, two 0.8 cm x

---

(*) 99.9999% pure indium, in the form of ¼-inch-diameter wire, was obtained from the Consolidated Mining and Smelting Company of Canada, Limited, Montreal, Quebec.

2.35 cm plates were spark-cut from the sheet, their long dimensions parallel and perpendicular to the direction of rolling .

The surfaces of the finished specimens were examined microscopically, and except for small pock marks were smooth to much better than 1 μ. The electropolishing process produced a slight waviness in the surface, with deviations from flatness amounting to approximately 1 μ over a lateral distance of 100 μ. The average grain diameter in the polycrystalline sheet after rolling and etching was estimated to be approximately 1 mm, with a few grains having a length of up to 4 mm. No preferred orientation was visibly apparent, although no quantitative measurement to determine grain orientation was made.

The ratio of the room-temperature and helium-temperature resistivities of a 1 mm-wide strip, spark-cut from the electropolished sheet, was measured and found to be 1.65×10^4. This is in agreement with the value obtained in this laboratory in an earlier experiment, using a different batch of indium from the same source. The electronic mean free path of that material was estimated to be approximately 5×10^{-2} cm at 4°K (88).

C.3 Results and discussion

Transitions between the superconducting and normal states of the pure indium specimens were induced by switching on a static magnetic field in a direction parallel to the plate. A small correction for the normal-state magnetoresistance, amounting to approximately 1% for a 300 G magnetic field, was applied to the data, which then agreed with the results obtained by warming the specimen through the transition. A typical recorder trace is shown in Fig. C-1.

The experimental results are presented in Table C-1. Specimens A and B have their long dimensions perpendicular and parallel, respectivley, to the direction in which the polycrystalline sheet was rolled. The predicted ratio of the reactive and resistive skin depths, $\tan^{-1}(\delta_x/\delta_R) = 60°$, is obtained in each measurement, within the estimated ± 1.5° phase uncertainty. Confidence in the phase calibration of the detection apparatus is thus reinforced.

FREQUENCY (MHz)	SPECIMEN	δ_x (10^{-4} cm)	δ_x/δ_R	$\tan^{-1}(\delta_x/\delta_R)$ (degrees)
7.000	A	1.65	1.66	58.9
	B	1.72	1.71	59.7
5.377	A	1.80	1.64	58.6
	B	1.87	1.70	59.5

TABLE C-1. REACTIVE AND RESISTIVE SKIN DEPTHS IN INDIUM

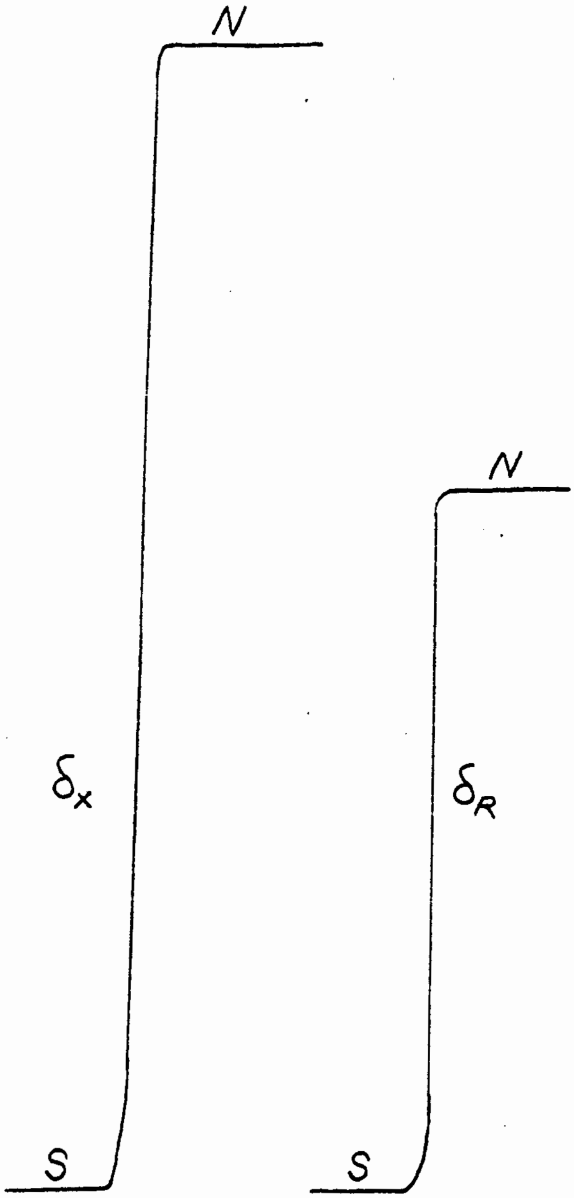

FIG. C-1. S-N TRANSITION IN PURE, POLYCRYSTALLINE INDIUM.

In Fig. C-2 the reactive skin depths are compared with those obtained at 10^3 - 10^4 Hz by Lyall and Cochran (88) and at 3×10^9 Hz by Dheer (89). In each case straight lines have been drawn whose slopes, $S_x = \delta_x / f^{-1/3}$, should be equal according to the anomalous-skin-effect theory. Two lines are drawn for the low-frequency data of Lyall and Cochran: line (a) has the slope of the actual data taken at frequencies between 10^3 Hz and 2×10^4 Hz, and line (b) has the slope obtained by fitting this data to the free-electron theory (85,92) and extrapolating to the extreme anomalous limit (88). This extrapolation is based on the assumption of diffuse electron scattering at the metal surface; the assumption of specular scattering leads to a line just slightly steeper than line (b).

It is interesting to note that the measured skin depths of the two specimens A and B differ by less than the absolute uncertainty of ± 3% assigned to the data, although Table C-1 does indicate a slight systematic difference between the two plates. Since the low-frequency data of reference (88) have an uncertainty which is indicated by the separation of the lines (a) and (b), they are in agreement with the present results.

According to [1] and [2], the measurement of the anomalous skin depth yields, for free electrons, a characteristic property of the metal:

$$\left(\frac{\sigma_0}{\ell}\right) = \frac{n_0 e^2}{p_F} , \qquad [3]$$

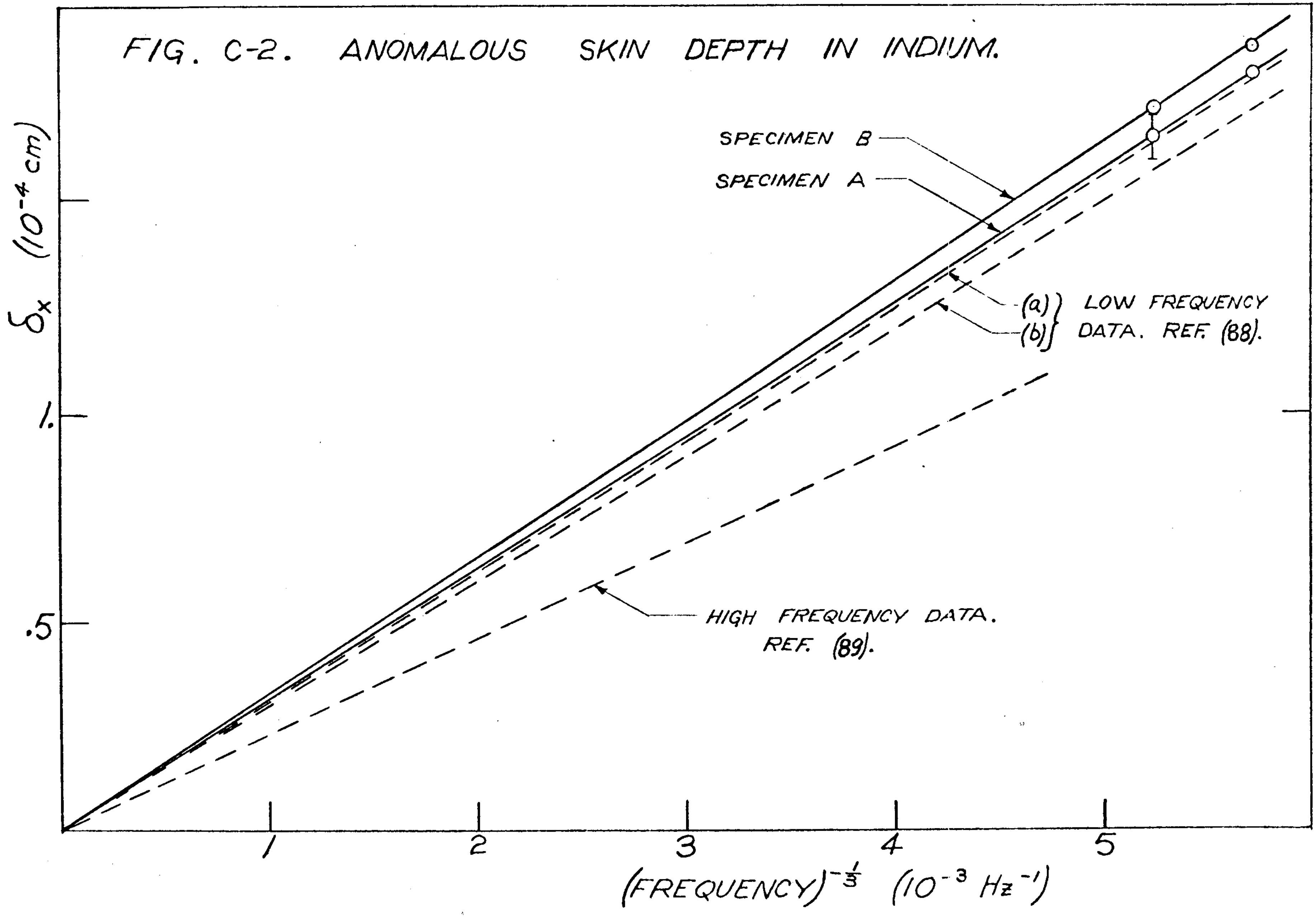
FIG. C-2. ANOMALOUS SKIN DEPTH IN INDIUM.

where n_0 is the density of charge carriers with charge (-e), and p_F is their Fermi momentum. The values of σ_0/ℓ calculated from skin-effect measurements are compared with the dc size-effect data in Table C-2, where all values were obtained under the assumption of diffuse electron scattering at the metal surface. The value listed for the low-frequency experiment (reference 88) corresponds to the extrapolated data (line (b) of Fig. C-2).

It should be noted that Dheer's value is the result of averaging single-crystal measurements over various orientations, and that the discrepancy between his value and ours may be due to some preferred crystal orientation in our specimens. Judging, however, from the rather close agreement between the measurements taken on the two specimens cut at 90° out of the same sheet, and between the very low-frequency results (88) and those presented here, this explanation is considered to be unlikely. The relative ease with which quantitative measurements may be made at low frequencies suggests that, for very pure metals, investigations of the anomalous skin effect should be carried out at low megahertz frequencies rather than in the microwave range.

The temperature dependence of the reactive part of the measured quantity $[\delta_N - \delta_S(T)]$ yields, in principle, values for both δ_N and $\delta_S(0)$. In the anomalous-skin-effect regime, δ_N is independent of temperature, and the variation of $\delta_S(T)$

METHOD	σ_0/ℓ ($10^{10}\ \Omega^{-1}$ - cm^{-2})	INVESTIGATOR
ASE,(a) 7×10^6 Hz		This work
Specimen A	7.2 ± .6	
Specimen B	6.4 ± .6	
ASA, $10^3 - 10^4$ Hz	9.0 ± 1.6	Lyall and Cochran(b)
ASE, 3×10^9 Hz	18.0 ± 1.1	Dheer(c)
dc size effect	7.41	Aleksandrov(d)
Eddy-current size effect	7.88	Cotti(e)
Theoretical(f)	18.9	

(a) Anomalous Skin Effect
(b) Reference (88)
(c) Reference (89)
(d) Reference (93)
(e) Reference (94)
(f) Calculated assuming 3 conduction electrons per atom and a spherical Fermi surface.

TABLE C-2. VALUES OF σ_0/ℓ FOR PURE INDIUM, OBTAINED USING VARIOUS METHODS.

can be approximated by (95)

$$\delta_s(t) = \frac{\delta_s(0)}{(1-t^4)^{1/2}} , \qquad [4]$$

where $t = T/T_c$, and $T_c = 3.407°K$ (95) is the critical temperature. In Fig. C-3 the temperature dependence of the data is compared with the relation [4], using the values of $\delta_s(0)$ which have been measured by Dheer (curve (a)) (89), and by Lock (curve (b)) (96). It is clear that our results are compatible with the superconducting penetration depth given by Dheer, $\delta_s(0) = 4.3 \times 10^{-6}$ cm, but not with the value obtained by Lock, 6.4×10^{-6} cm. The scatter of the experimental points, however, prevents us from obtaining a more definitive value for $\delta_s(0)$.

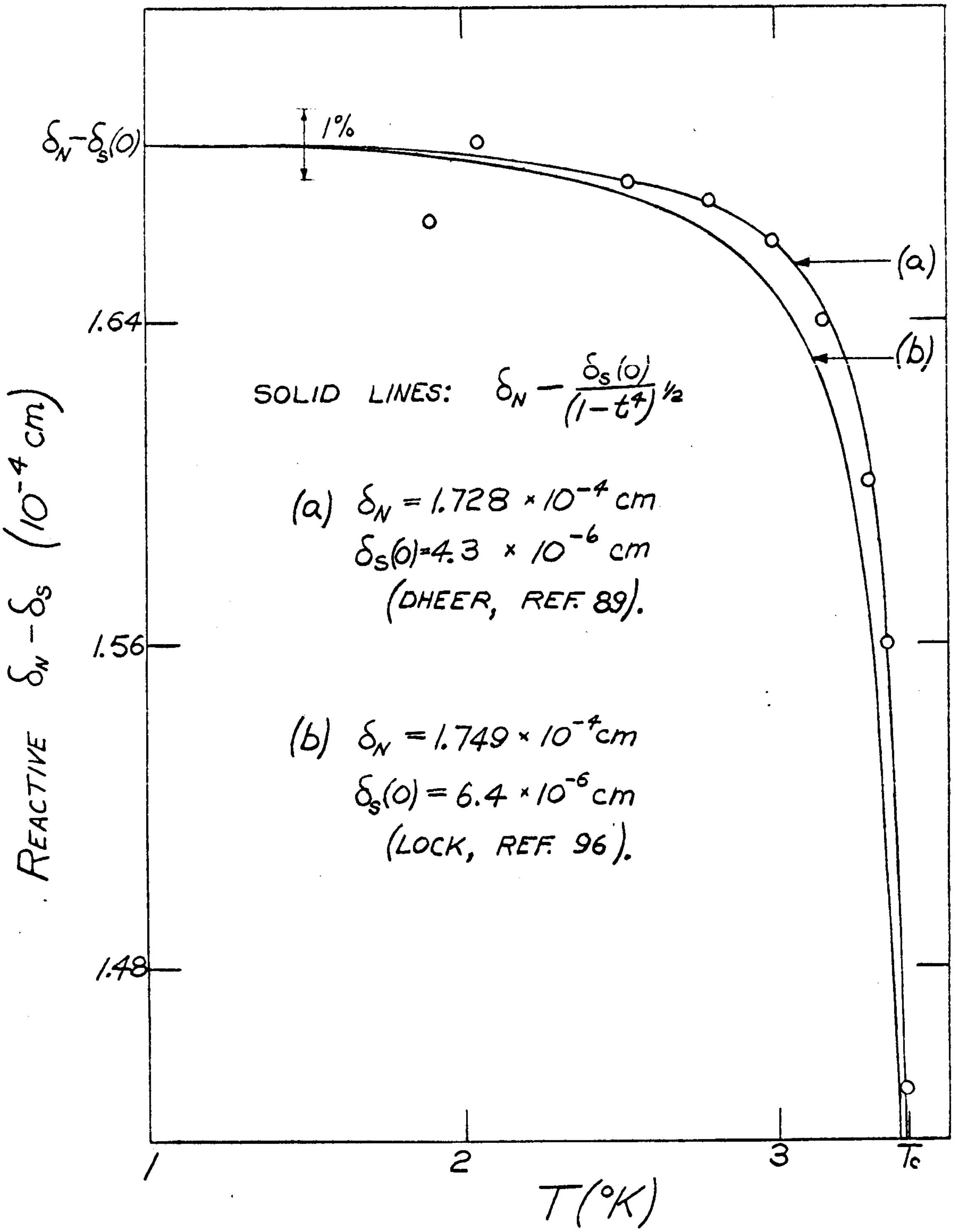

FIG. C-3. TEMPERATURE DEPENDENCE OF $(\delta_N - \delta_s)_x$ IN PURE INDIUM.

REFERENCES

1. R.H. Randall, F.C. Rose, and C. Zener, Phys. Rev. 56, 343 (1939).
2. D.P. Morgan, Phys. Stat. Sol. 24, 9 (1967).
3. V.G. Skobov and E.A. Kaner, Zh. Eksperim. i Teor. Fiz. 46, 273 (1964). English transl.: Soviet Phys. - JETP 19, 189 (1964).
4. D.N. Langenberg and J. Bok, Phys. Rev. Letters 11, 549 (1963).
5. J.J. Quinn and S. Rodriguez, Phys. Rev. Letters 11, 552 (1963); Phys. Rev. 133, A1589 (1964).
6. C.C. Grimes and S.J. Buchsbaum, Phys. Rev. Letters 12, 357 (1964).
7. V.F. Gantmakher and V.T. Dolgopolov, Zh. Eksperim. i Teor. Fiz. Pis'ma 5, 17 (1967). English transl.: Soviet Phys. - JETP Letters 5, 12 (1967).
8. P.K. Larsen and K. Saermark, Phys. Letters 24A, 374 (1967).
9. J.R. Houck, H.V. Bohm, B.W. Maxfield, and J.W. Wilkins, Phys. Rev. Letters 19, 224 (1967).
10. J.J. Quinn, Phys. Letters 25A, 522 (1967).
11. A.G. Betjemann, H.V. Bohm, D.J. Meredith, and E.R. Dobbs, Phys. Letters 25A, 753 (1967).
12. D.J. Meredith, R.J. Watts-Tobin, and E.R. Dobbs, J. Acoust. Soc. Am. 45, 1393 (1969).
13. P.D. Southgate, J. Appl. Phys. 40, 22 (1969).
14. B. Abeles, Phys. Rev. Letters 19, 1181 (1967).
15. G.S. Weisbarth, Phys. Letters 27A, 230 (1968).
16. R.W. Cohen, Phys. Letters 29A, 85 (1969).
17. R. Turner, K.R. Lyall, and J.F. Cochran, Can. J. Phys. 47, 2293 (1969).
18. Yu. P. Gaidukov and A.P. Perov, Zh. Eksperim. i Teor. Fiz. Pis. Red. 8, 666 (1968). English transl.: Soviet Phys. - JETP Letters 8, 412 (1969).

19. V. Ya. Kravchenko, Zh. Eksperim. i Teor. Fiz. 54, 1494 (1968). English transl.: Soviet Phys. - JETP 27, 801 (1969).

20. N.E. Phillips, Phys. Rev. 134, A385 (1964).

21. H.A. Roughton and H.C. Nash, U.S. Office of Naval Res. Tech. Rep. No. 6 (1962).

22. M.H. Cohen, M.J. Harrison, and W.A. Harrison, Phys. Rev. 117, 937 (1960).

23. S. Rodriguez, Phys. Rev. 130, 1778 (1963).

24. D.C. Mattis and G. Dresselhaus, Phys. Rev. 111, 403 (1958).

25. V.M. Kontorovich, Zh. Eksperim. i Teor. Fiz. 45, 1638 (1963). English transl.: Soviet Phys. - JETP 18, 1125 (1964).

26. R. Goldman, Ultrasonic Technology (Reinhold Publishing Corporation, New York, 1962).

27. P.H. Haberland, J.F. Cochran, and C.A. Shiffman, Phys. Rev. 184, 655 (1969).

28. J.A. Carruthers, J.F. Cochran, and K. Mendelssohn, Cryogenics 2, 160 (1962).

29. M. Strongin and E. Maxwell, Rev. Sci. Instr. 34, 590 (1963).

30. G.L. Salinger and J.C. Wheatley, Rev. Sci. Instr. 32, 872 (1961).

31. J.W. Hansen, C.C. Grimes, and A. Libchaber, Rev. Sci. Instr. 38, 895 (1967).

32. R. Morrison, Shielding and Grounding for Instrumentation Systems (pamphlet published by the Dynamics Instrumentation Co., 583 Monterey Pass Road, Monterey, Calif., n.d.).

33. A.B. Pippard, Proc. Roy. Soc. (London) A216, 547 (1953).

34. A.B. Pippard, Phil. Trans. Roy. Soc. London A248, 97 (1955).

35. V.F. Gantmakher, in Progress in Low Temperature Physics, edited by C.J. Gorter (North-Holland Publishing Co., Amsterdam, 1967) Vol. V.

36. W.M. Walsh, in Solid State Physics: Vol. I, Electrons in Metals, edited by J.F. Cochran and R.R. Haering (Gordon and Breach Science Publishers, Inc., New York, 1968).

37. D.E. Gabel, Simon Fraser University, private communication.

38. J.F. Koch and T.K. Wagner, Phys. Rev. 151, 467 (1966).

39. R.F. Frindt and A. Stuart, Rev. Sci. Instr. 39, 782 (1968).

40. E.J. Walker, Rev. Sci. Instr. 30, 834 (1959).

41. M. Yaqub and J.F. Cochran, Phys. Rev. 137, A1182 (1965).

42. K.R. Lyall and J.F. Cochran, Magnetic Field Dependence of the Skin Depth in Gallium, Paper presented at the Pacific Metal Physics Conference, Vancouver, B.C., 1968. Unpublished.

43. P.K. Larsen and K. Saermark, Phys. Letters 26A, 296 (1968).

44. W.A. Reed, Phys. Rev. 188, 1184 (1969).

45. G.A. Alers and J.R. Neighbours, Rev. Mod. Phys. 31, 675 (1959).

46. O.L. Anderson, J. Phys. Chem. Solids 24, 909 (1963).

47. A.B. Bhatia, Ultrasonic Absorption (Oxford University Press, London, 1967).

48. J.R. Neighbours and G.E. Schacher, J. Appl. Phys. 38, 5366 (1967).

49. E.S.R. Gopal, Specific Heats at Low Temperatures (Plenum Press, New York, 1966).

50. R.A. Robie and J.L. Edwards, J. Appl. Phys. 37, 2659 (1966).

51. R. Hill, Proc. Phys. Soc. (London) 65, 350 (1952).

52. J.J. Gilvarry, Phys. Rev. 103, 1701 (1956).

53. C.S. Barrett, in Advances in X-ray Analysis, edited by W.M. Mueller (Plenum Press, New York, 1962) Vol. 5.

54. W.J. Spencer, in Physical Acoustics, edited by W.P. Mason (Academic Press, New York, 1968) Vol. V.

55. R.D. Mindlin and W.J. Spencer, J. Acoust. Soc. Am. 42, 1268 (1967).

56. G.N. Kamm and G.A. Alers, J. Appl. Phys. 35, 327 (1964).

57. L.J. Neuringer and Y. Shapira, Phys. Rev. 165, 751 (1968).

58. N.G. Einspruch and R. Truell, J. Appl. Phys. 33, 3087 (1962).

59. A.V. Gold, in Solid State Physics: Vol. I, Electrons in Metals, edited by J.F. Cochran and R.R. Haering (Gordon and Breach Science Publishers, Inc., New York, 1968).

60. B.W. Roberts, in Physical Acoustics, edited by W.P. Mason (Academic Press, New York, 1968) Vol. IV - Part B.

61. J.G. Mavroides, B. Lax, K.J. Button and Y. Shapira, Phys. Rev. Letters 9, 451 (1962).

62. G.A. Alers and R.T. Swim, Phys. Rev. Letters 11, 72 (1963).

63. L.R. Testardi and J.H. Condon, Bull. Am. Phys. Soc. 14, 400 (1969).

64. A.G. Beattie, Phys. Rev. 184, 668 (1969).

65. Yu. P. Gaidukov, A.P. Perov, and I.F. Voloshin, Zh. Eksperim. i Teor. Fiz. Pis. Red. 9, 585 (1969). English transl.: Soviet Phys.-JETP Letters 9, 356 (1969).

66. S. Rodriguez, Phys. Rev. 132, 535 (1963).

67. J.J. Quinn and S. Rodriguez, Phys. Rev. 128, 2494 (1962).

68. A. Goldstein and S. Foner, Phys. Rev. 146, 442 (1966).

69. D. Shoenberg, Phil. Trans. Roy. Soc. (London) A245, 1 (1952).

70. Y. Shapira and B. Lax, Phys. Rev. 138, A1191 (1965).

71. T.W. Moore, Phys. Rev. 165, 864 (1968).

72. T.W. Moore, Phys. Rev. Letters 16, 581 (1966).

73. P.H. Haberland and C.A. Shiffman, Phys. Rev. Letters 19, 1337 (1967).

74. G.A. Alers, in Physical Acoustics, edited by W.P. Mason (Academic Press, New York, 1966). Vol. IV - Part A.

75. R.A. Alpher and R.J. Rubin, J. Acoust. Soc. Am. 26, 452 (1954).

76. G.A. Alers and P.A. Fleury, Phys. Rev. 129, 2425 (1963).

77. R.L. Forgacs, IRE Trans. Instr. 9, 359 (1960).

78. D.I. Bolef and J. de Klerk, IEEE Trans. Ultrasonics Eng. UE-10, 19 (1963).

79. R.J. Blume, Rev. Sci. Instr. 34, 1400 (1963).

80. A.G. Beattie and E.H. Uehling, Phys. Rev. 148, 657 (1966).

81. A.G. Beattie, Phys. Rev. 174, 721 (1968).

82. E.Y. Wang and K.A. McCarthy, Phys. Rev. 183, 653 (1969).

83. G.A. Alers and D.O. Thompson, J. Appl. Phys. 32, 283 (1961).

84. A. Hikata and C. Elbaum, Phys. Rev. 153, 740 (1967).

85. G.E.H. Reuter and E.H. Sondheimer, Proc. Roy. Soc. (London) A195, 336 (1948).

86. A.B. Pippard, Proc. Roy. Soc. (London) A224, 273 (1954).

87. A.B. Pippard, The Dynamics of Conduction Electrons (Gordon and Breech Science Publishers, Inc., New York, 1965).

88. K.R. Lyall and J.F. Cochran, Phys. Rev. 159, 517 (1967).

89. P.N. Dheer, Proc. Roy. Soc. (London) A260, 333 (1961).

90. E. Fawcett, Proc. Roy. Soc. (London) A232, 519 (1955); also The Fermi Surface, edited by W.A. Harrison and M.B. Webb (John Wiley & Sons, Inc., New York, 1960), p. 197.

91. W.J. McG. Tegart, The Electrolytic and Chemical Polishing of Metals, 2d ed., rev. (Pergamon Press, London, 1959).

92. R.B. Dingle, Physica 19, 311 (1953).

93. B.N. Aleksandrov, Zh. Eksperim. i Teor. Fiz. 43, 399 (1962). English transl.: Soviet Phys.-JETP 16, 286 (1963).

94. P. Cotti, Phys. Kondensierten Materie 3, 40 (1964).

95. E.A. Lynton, Superconductivity, 2d ed. (John Wiley & Sons, Inc., New York, 1964).

96. J.M. Lock, Proc. Roy. Soc. (London) A208, 391 (1951).